Performance Scaling of a Novel Modular Hybrid Propulsion System for Aircraft Flight Performance Flexibility and Enhancement

by

David Yang

B.S., University of Texas (2012)
S.M., Massachusetts Institute of Technology (2014)

MIT LIBRARIES
JUL 0 1 2019
RECEIVED
ARCHIVES

Submitted to the Department of Aeronautics and Astronautics
in partial fulfillment of the requirements for the degree of

Doctor of Philosophy

at the

MASSACHUSETTS INSTITUTE OF TECHNOLOGY

June 2019

© Massachusetts Institute of Technology 2019. All rights reserved.

Author ..... Signature redacted .....
Department of Aeronautics and Astronautics
March, 2019

Certified by ..... Signature redacted .....
Choon S. Tan
Senior Research Engineer, MIT
Thesis Supervisor

Accepted by ..... Signature redacted .....
Sertac Karaman
Chairman, Department Committee on Graduate Theses

Performance Scaling of a Novel Modular Hybrid Propulsion System for Aircraft Flight Performance Flexibility and Enhancement

by

David Yang

Submitted to the Department of Aeronautics and Astronautics
on March, 2019, in partial fulfillment of the
requirements for the degree of
Doctor of Philosophy

Abstract

A novel propulsion system concept, the Modular Hybrid Propulsion System (MHPS) is introduced that has the potential to enable a step-change in aircraft performance and flexibility over traditional carbon-fuel propulsion systems. The MHPS describes a hybrid propulsion system where the electrical components are interchangeable on a mission-to-mission basis. Scale-agnostic performance relationships are developed for the MHPS concept for a conventional takeoff and landing (CTOL) aircraft. Takeoff, climb, cruise, and payload performance metrics are formulated in terms of hybridity (proportion of electric power output and energy storage) and modularity levels (proportion of total aircraft mass that is interchangeable). For takeoff, increasing the power hybridization value decreases takeoff distance when the electric motor (EM) specific power is greater than the carbon-fuel (CF) engine specific power for a parallel hybrid configuration. For a ratio of EM specific power to CF specific power of 3, increasing the power hybridization from 0 to 1 decreases takeoff distance by 73%. Cruise scaling indicates that the relationship between energy hybridization and cruise time is dependent on the battery to fuel specific energy ratio and EM to CF engine efficiency ratio. Specifically, the product of the two ratios controls whether or not increasing energy hybridization will lead to an increase in cruise time. When the product of ratios is less than 1, increases in energy hybridization decrease cruise time. If the product of ratios is greater than 1, behavior is dependent on battery and fuel mass proportion, there is either an optimum energy hybridization value for cruise time or increases in energy hybridization increase cruise time monotonically. The delineation between the two trends is dependent on the relative amount of energy storage (battery + fuel) mass on the aircraft. Specifically, the usage of carbon-fuel reduces aircraft mass in-flight which is an added benefit when maximizing cruise time. This results in carbon-fuel usage being more beneficial than battery usage even when the product of the battery to CF specific energy ratio and EM to CF efficiency is equal to 1. It is found that the greater the potential fuel mass, the larger the product

Thesis Supervisor: Choon S. Tan
Title: Senior Research Engineer, MIT

Acknowledgments

This thesis would not have been possible without the assistance of many people throughout my journey at MIT. To describe all of their support would require an entirely separate thesis in itself. Here I recognize just a trickle of the ocean of help that I received to get me to this point. Outside of singular persons, I would like to give a special thanks to the Northrup Grumman Corporation and the people there for supporting this research under contract number 40006592 and giving me the freedom to shape the research described in this thesis. In particular, Drew Telford, Rob Talbert and Bob Gamache were instrumental in making this possible.

First, I give my gratitude to Dr. Choon Tan, who lent his time to help shape my thesis into what is presented in this document. His wealth of experience provided a path forward in many foggy situations that I encountered over the course of my research. Furthermore, his empathy and flexibility throughout this research project helped me manage the stress that so often comes about in graduate school. This last point is something that I am forever grateful for.

Next, I give my appreciation to Professor Zoltán Spakovszky, whose mentor-ship guided me through my Masters research and transformed a newly-minted graduate student into a researcher capable of developing his own research project. Throughout this process he has helped show me where to best put my efforts and time. His unparalleled ability to pinpoint and clarify the crux of nascent research efforts was greatly valued.

Thirdly, I give my thanks to the members of my graduate committee, Drew Telford, Professor Wai-Cheng, and Dr. Ming Dao. Without their guidance and support, I may still be lost in research. In particular, they helped me stay grounded in reality and offered a dose of practicality that anchored the research. The ideas they offered often were poignant and are littered throughout this thesis.

For the readers of this thesis, Dr. David Hall and Dr. Phil Hammar, I give my thanks for taking the time to pour over this document and offer insightful comments for improvement. Without their assistance, this thesis would be sorely lacking in

clarity.

I would also like to add a special note of thanks to the staff in the GTL, particularly to Robin and Jimmy, who were always there when I needed help with things outside my expertise. Many stresses were alleviated with their assistance.

For my parents, I can only offer a pittance of the gratitude they deserve here. They have molded me into the man that I am today, and supported me in all the ways that I needed at all times, no matter what. I could not have wished for better parents and am forever grateful for all they have given me.

Throughout my time in research wonderland, I've had the good fortune to meet a great group of friends that have gotten me through this trip down the rabbit hole. Sébastien has always provided the perfect mix of levity and seriousness during my time in the GTL while teaching me about the power of openness. His willingness to share is something I strive for. Irene was always there to fill the caffeine need and share gossip; the lightheartedness was essential at times. Remí was always there to help tap my silliness and reminded me to keep perspective in life when I was down in the weeds. Steven reminded me about the power of bluntness and was always there to remind me of the greatness of home (Texas). Julie was there to push me to enjoy myself when it was time to, always helping to push me out of my comfort zone. Marc was always there to listen to my musings and remind me that it's okay to be whimsical and to wax philosophical at times. Margaret was there to show me the importance of standing one's ground about one's convictions, something that is easily lost on me at times. Clifton showed me the joys of pursuing one's hobbies and introduced me to the nuance of ice cream, something that has given me great joy kept me sane through this work. Andrew helped keep me abreast of the world outside of MIT and was there to remind me to keep an open mind. Louis helped coin a new verb among our group and always had the wit to make light of situations that I may have stressed out about. Dan showed me the joy of having a dog and always reminded me to chill out and keep my head in check. Finally, Bobby was there to remind me to savor life's little moments as they come. His devotion to his friends is something that I'll try to emulate for the rest of my life.

Last but certainly not least, to Daphne, to whom no words here will do justice. Her love and support through this whole process were truly something I could not have done without. I cannot think of anyone else with whom I would have rather shared this time.

O and to Chase, my silly, ridiculous puppy who slowed me down, taught me practical reinforcement learning and kept me laughing the short time that I've known him.

This doctoral thesis has been examined and certified by the following committee members:

Zoltán Spakovszky .....
Thesis Committee Member
Professor, Director, Gas Turbine Laboratory, MIT
Department of Aeronautics and Astronautics

Wai Cheng ..... Signature redacted .....
Thesis Committee Member
Professor, Director, Sloan Automotive Laboratory, MIT
Department of Mechanical Engineering

Ming Dao ..... Signature redacted .....
Thesis Committee Member
Director, Nanomechanics Laboratory MIT
Department of Materials Science and Engineering

Drew Telford ..... Signature redacted .....
Thesis Committee Member
Technical Fellow, Northrup Grumman Corporation

Contents

1 Introduction **26**

1.1 Background 26

1.1.1 Aircraft Propulsion Systems 26

1.1.2 Propulsion System Sizing and Design 27

1.2 Motivation 29

1.3 Literature Review 30

1.3.1 Electrical propulsion systems for aircraft 30

1.3.2 Hybrid propulsion systems for aircraft and automobiles 33

1.4 Technical Innovation: A Modular Hybrid Propulsion System 42

1.5 Research Objectives 43

1.6 Original Contributions 44

1.7 Thesis Organization 45

2 Technical Approach **46**

2.1 Introduction 46

2.2 Hybrid propulsion system performance 50

2.2.1 Scope of research 51

2.3 Propulsion system modularity 52

2.4 Operational considerations 53

2.5 Summary 57

3 Modular Hybrid Propulsion System Modeling and Large UAV Retrofit **59**

3.1 Introduction 59
3.2 Aircraft hybrid configurations 60
3.3 Propulsion system performance modeling 62
3.3.1 A model for takeoff performance estimation 62
3.3.2 A model for climb performance estimation 64
3.3.3 A model for cruise time estimation 67
3.4 Assessment of hybrid configurations 71
3.4.1 Hybrid configuration mass comparison 71
3.4.2 Hybrid configuration fuel consumption evaluation 73
3.4.3 Configuration integration flexibility 74
3.4.4 Transmission requirements 75
3.4.5 Hybrid configuration performance evaluation 77
3.5 Large UAV retro-fit comparison analysis 78
3.5.1 Large UAV retro-fit performance evaluation 81
3.6 Summary 83

4 Functional dependence of MHPS performance on hybridization and modularity levels **85**

4.1 Introduction 85
4.2 Hybrid propulsion system performance relationships 85
4.2.1 Takeoff performance relationship for hybrid propulsion systems 86
4.2.2 Climb rate performance relationship for hybrid propulsion systems 90
4.2.3 Cruise time performance relationship for hybrid propulsion systems 91
4.2.4 Cruise range performance relationship for hybrid propulsion systems 99
4.2.5 Payload mass performance relationship for hybrid propulsion systems 100
4.2.6 Hybrid propulsion system performance relationship discussion 102

4.3 Modular hybrid propulsion system performance relationships 103
4.3.1 Modular takeoff spread performance relationship 105
4.3.2 Modular cruise time spread performance relationship 106
4.3.3 Discussion of the modular performance relationships 108
4.3.4 Relationship between modularity and hybridization levels . . . 108
4.4 Assessment of performance relationship applicability 109
4.5 Summary 113

5 Hybrid propulsion system energy management and component matching 117

5.1 Introduction 117
5.2 Energy management policy determination through DP 119
5.2.1 DP implementation 121
5.2.2 DP results 124
5.3 MHPS component matching 126
5.3.1 Efficiency map matching 127
5.3.2 Dynamic characteristic component matching 134
5.3.3 Single-shaft configuration dynamics 135
5.3.4 Separate-shaft configuration dynamics 135
5.4 Design implications 136
5.5 Summary 137

6 Summary and conclusion 141

6.1 Summary 141
6.2 New findings and conclusion 146
6.2.1 System-level findings 146
6.2.2 Performance relationship design implications 148

7 Recommendations for future work 151

A Derivation of Hybrid Performance Relationships 153

A.1 Takeoff distance performance relationship derivation 153

A.2 Cruise time performance relationship derivation 155
A.3 Cruise range performance relationship derivation 157
A.4 Payload performance relationship derivation 158
A.5 Climb rate performance relationship derivation 160
A.6 Modular takeoff distance spread derivation 160
A.7 Modular cruise time spread derivation 161
A.8 Anergy scaling group derivation 162

B Flight segment performance modeling derivation 163
B.1 Takeoff performance modeling 163
B.2 Climb rate performance modeling 164
B.3 Cruise time and range performance modeling 165
B.4 Total efficiency derivation for a parallel hybrid propulsion system . . 167

C Hybrid configuration component tradeoff study for large UAV retrofit 169
C.1 Carbon-fuel engine selection 169
C.2 Electric motor selection 170
C.3 Battery selection 171

D Propulsion system dynamic performance relationship derivation 173

E Example of MHPS design 176
E.1 Large UAV design scenario 176
E.2 Component sizing 178
E.2.1 Determining propulsion system type 178
E.2.2 Sizing of fixed and baseline components 179
E.3 Sizing of modular components to meet operational requirements . . . 181
E.4 Choosing specific components 182
E.4.1 Component selection scenario 182

List of Figures

1-1 Hybrid propulsion systems combine desirable performance characteristics from carbon-fuel and electric propulsion systems. +, - and = signs are qualitative indicators for advantages, disadvantages, and neutral attributes of each propulsion system type. 28

1-2 Series hybrid configuration for the Fisker Karma automobile taken from [19]. The internal combustion engine for series configurations does not provide propulsive power and is only used to generate electricity through a electrical generator. 37

1-3 Mild parallel hybrid configuration for the Honda Civic automobile taken from [19]. The internal combustion engine for a parallel configuration combines with an electric motor to provide traction power to the main drive shaft. 40

1-4 Parallel power-split configuration of the Toyota Prius automobile taken from [19]. The internal combustion engine for a parallel power-split configuration is connected to an electric motor and the main drive shaft through an e-CVT. This allows the ICE to both power the wheels and generator; wheel power can be augmented by the EM connected to the e-CVT. 41

1-5 BMW ActiveHybrid5 parallel power-split configuration taken from [19]. The internal combustion engine drives the wheels and an electric motor depending on which clutches are engaged. Both the EM and ICE can power the wheels. 42

2-1 Relationship between total mass, fixed mass, free mass, propulsion system mass, and ESS mass definitions. 48
2-2 Notational aircraft performance variation with a MHPS. Total aircraft performance is the sum of the performance provided by fixed components and performance provided by the modular components. The configuration on the left is an empty airframe with only fixed components, which provides some amount of performance. The middle illustration is the modular component set to be installed, which has some performance level. The right illustration is the aircraft with modular components installed, with the total performance equal to the empty airframe and modular component set. 49
2-3 Modular hybrid propulsion system potential performance. For each instance, a component set can be used to emphasize a different performance metric. MHPS potential performance is the maximum of each performance metric that can be achieved with a particular component set. 52
2-4 Dynamic programming splits a decision making problem into several sub-problems to reduce computational cost. Constraints can be added to each block and the solution is found recursively. 54
2-5 Total efficiency map of a hybrid propulsion system is a linear combination of the EM and ICE efficiency maps, when the ICE and EM are attached to a single shaft with no gearing. 56

3-1 Reconnaissance flight profile used to evaluate aircraft performance. . 60
3-2 Power flow paths in a series hybrid configuration. Arrows indicate direction of allowable energy flow and color indicates whether power flow is mechanical or electrical. 60
3-3 Power flow paths in a parallel hybrid configuration. Arrows indicate direction of allowable energy flow and color indicates whether power flow is mechanical or electrical. 61

3-4 Free-body diagram of the aircraft during climb. Thrust force is parallel to the aircraft axis. Angle of attack is defined as the angle between the horizon and the aircraft axis. 65
3-5 A procedure for determining climb rate given available battery energy 67
3-6 Energy transfer chain between the generator and electric motor(s). . . 70
3-7 Illustration of a propeller operating curve and ICE operating map. The propeller operating curve does not match well with the ICE so the maximum power output of the ICE-propeller system is limited. 76
3-8 Illustration of a propeller operating curve modified by a transmission. The transmission shifts the shape of the propeller operating curve such that it intersects the maximum power point of the ICE, enabling the system to leverage its maximum power output. 77
3-9 Illustration of a propeller operating curve and EM operating map. EMs have a wide constant maximum power range, so it is more probable that a propeller-EM system can leverage its maximum power output without the use of a transmission. 78
3-10 Diagram of MHPS retro-fit configuration. A pusher-puller propeller configuration is considered, one of which is driven by an internal combustion engine and one of which is driven by an electric motor. A generator/battery connects the ICE and EM. 79
3-11 Off-the-shelf component form factors used in the retro-fit analysis. YASA P400 from [36], YASA motor controller from [37], Mercedes OM660 from [1] and Kokam battery pack from [21]. 80

4-1 Parametric curves of the takeoff performance relationship shown in 4.2 as a function of power hybridization factor H_P for various ratios of EM to CF engine specific power. Ratios of 1, 3, 9, and 13 are chosen as they are representative of current (2018) ratios between EMs and turbofans, small turbine generators, internal combustion engines and between future EMs and ICEs respectively. 88

4-2 Parametric curves for the scaling relationship shown in Equation 4.16. The cruise time scaling group as a function of battery mass ratio for various values of battery specific energy ratios are shown. The electric motor to CF engine energy flow efficiency ratio is kept constant with a value of 3. 95
4-3 Specific energy extraction ratio and corresponding ESS mass to fixed mass ratio required for the fuel-burn cruise energy reduction battery sizing condition to equal to zero. 97
4-4 Cruise time scaling group as a function of battery mass proportion r_m for various levels of battery technology. ESS mass fraction $\frac{m_{ESS}}{m_{total}}$ is set to 0.2 in this case. 98
4-5 Payload mass ratio as a function of power hybridization factor for various values of EM to CF engine specific power ratio. Structure, fuel and battery represent 70% of the total aircraft mass. Aircraft specific power is set to 20% of CF engine specific power. 101
4-6 Relationship between total mass, baseline mass, and free mass 103
4-7 Component configurations of the baseline, minimum takeoff distance and maximum cruise time configurations. 104
4-8 Modular takeoff distance spread as a function of modular free mass for various values of EM to CF engine specific powers. CF engines considered are ICEs, small turbines, and turbofans. The baseline CF engine represents 10% of the total aircraft mass. 106
4-9 Modular cruise time spread as a function of modular free mass for various values of baseline fuel mass ratios. Modular free mass is assumed to be filled with carbon fuel. 107
4-10 A schematic illustrating the relationship between modularity and hybridity assuming free mass is optimally utilized as outlined in this section. 108
4-11 Percentage difference in the estimated takeoff distance utilizing the takeoff distance performance relationship and values given in Table 4.1 110

4-12 Percentage difference in the estimated cruise range utilizing the cruise range performance relationship and values given in Table 4.1 111
4-13 Relative discrepancy between the calculated author-designed aircraft takeoff performance and takeoff performance from the performance relationships 112
4-14 Relative discrepancy between the calculated author-designed aircraft cruise range performance and cruise range performance from the performance relationships 113

5-1 Optimal solution to the DP problem considered. Fuel is used initially only, with the battery used exclusively to finish cruise. 120
5-2 DP results for the cruise energy control management problem. The top plot indicates the fuel mass and battery energy levels while the bottom plot indicates the proportion of cruise time resulting from fuel or battery usage. 125
5-3 Total efficiency map of a hybrid propulsion system is a linear combination of the EM and ICE efficiency maps, when the ICE and EM are attached to a single shaft with no gearing. 127
5-4 Illustration of the optimization opportunity for a parallel propulsion system. The torque split can be set to optimize the efficiency of the components and thus total system efficiency. 128
5-5 Efficiencies for the single shaft, parallel hybrid efficiency comparison. The efficiencies along a constant total torque line are considered. . . . 130
5-6 Efficiencies for the single shaft, constrained parallel hybrid efficiency comparison. The efficiencies along a constant total torque line are considered. Furthermore, the EM has a maximum power constraint that manifests as a torque constraint dependent on the rotational speed. 131

5-7 Efficiencies for the separate shaft, parallel hybrid efficiency comparison. Setting a power split value sets the CF engine/propeller operating point. The EM must provide the remaining power to meet the total power requirement; the power is derived from the generator, which adds an additional torque load to the CF engine. 139

5-8 Effect of dynamic constraints on the optimal operation path of a system. The blue points represents the optimal operating points, with the orange line indicating the unconstrained operation path and the red line indicating the dynamically constrained operation path. 140

6-1 A single airframe for a GA aircraft could potentially take on several diverse roles with a MHPS 147

List of Tables

1.1 Flown hybrid-electric aircraft (adapted from [7]) 34

1.2 Proposed hybrid-electric aircraft (adapted from [7]) 34

3.1 Four cases of flight mission profile requirements to evaluate the two hybrid configurations. 62

3.2 Aircraft masses for the series and parallel hybrid configurations for the flight profile cases shown in Table 3.1 72

3.3 Component efficiencies used for assessing hybrid configuration trade-offs 74

3.4 Hybrid configuration total system efficiencies for various ratios of EM to total power output. N/A indicates the value is not available. For a series configuration the output power is equal to the EM power only and cannot be some proportion of the total power. 74

3.5 List of primary propulsion system components for the MHPS retro-fit and traditional propulsion system. Form factors are shown in Figure 3-11 80

3.6 Propulsion system component performances and masses 81

3.7 Performance values and comparison of the MHPS and traditional propulsion system aircraft 81

3.8 Performance values and comparison of the MHPS with and without the additional EM 82

4.1 Hybrid aircraft from literature used for the assessment of performance relationship applicability 109

4.2 Author-designed hybrid aircraft used for the assessment of performance relationship applicability 115
4.3 Carbon-fuel engines used in the author-designed aircraft study. 116
4.4 Electric motors used in the author-designed aircraft study. 116

5.1 Primary hybrid propulsion system performance parameter values used in the DP framework example. 124
5.2 Primary hybrid propulsion system performance parameter values used in the DP framework example. 129

C.1 Carbon-fuel engines considered for the large UAV MHPS retrofit . . . 169
C.2 Electric motors considered for the large UAV MHPS retrofit 171

E.1 Battery mass ratio requirements for a pure-electric aircraft to meet . 179
E.2 Modular component mass ratios required to meet operational mission requirements 182
E.3 Modular component mass ratios required to meet operational mission requirements 183
E.4 Considered component sets for the MHPS component selection scenario 183

Nomenclature

Symbols

α	Aircraft angle of attack
$\Delta R_{takeoff}$	Takeoff distance
$\Delta t_{cruise,baseline}$	Cruise time achievable with the baseline configuration in a modular propulsion system
$\Delta t_{cruise,best}$	Best cruise time achievable with a modular propulsion system
Δt_{cruise}	Cruise time
$\dot{\omega}$	Rotational acceleration
$\dot{A}^*$	Propulsive anergy generation rate; power dissipated due to aerodynamic losses
η	Efficiency from input energy/power source to output energy/power
$\eta_{CF,compare}$	CF comparison efficiency, efficiency of the CF engine when it runs at the total system operating point
$\eta_{CF,flow}$	Flow efficiency for the carbon-fuel system, for the power chain between the carbon-fuel and CF engine propeller
$\eta_{convert}$	Propulsion system power output to kinetic energy increase conversion efficiency

$\eta_{EM,compare}$	EM comparison efficiency, efficiency of the EM when it runs at the total system operating point
$\eta_{EM,flow}$	Flow efficiency for the electric system, for the power chain between the battery pack and EM engine propeller
η_{flow}	Flow efficiency; overall efficiency from the energy source to propeller output power
$\eta_{total,system}$	Total propulsion system overall efficiency
η_{trans}	Electric transfer efficiency between battery and electric motor
$\frac{dh}{dt}$	Rate of climb
Γ	Modularity level or free mass ratio
λ	Ratio of CF engine propeller power to total propeller power
ω	Rotational speed
π	Specific power, power divided by mass
ρ	Air density
σ	Ratio of EM power to total power output
AR	Aircraft wing aspect ratio
$BSFC$	Brake specific fuel consumption, defined as fuel consumption per unit energy output
c_D	Coefficient of drag
c_D0	Zero lift coefficient of drag
c_L	Coefficient of lift
c_P	Propeller coefficient of power

CF	Carbon fuel
D	Drag
D_{prop}	Propeller diameter
DP	Dynamic programming
E	Energy
e	Battery pack specific energy
E_{source}	Energy of some energy storage source, either a battery pack or carbon-fuel tank
$E_{stored,total}$	Total stored energy, equal to sum of battery and fuel energy
EM	Electric motor
ESS	Energy storage system, totality of fuel and battery stores
$eVTOL$	Electric vertical takeoff and landing
F	Force
g	Acceleration due to gravity
h	Altitude
H_E	Hybrid propulsion system energy hybridization level
H_P	Hybrid propulsion system power hybridization level
I	Moment of inertia
KE	Kinetic energy
L	Lift
m	Mass

m_{fixed}	Fixed mass, total aircraft mass minus fuel and battery masses
m_{free}	Mass available for modular components
$m_{prop,base}$	Baseline propulsion system mass in a modular propulsion system
$m_{propSystem}$	Propulsion system mass
$MHPS$	Modular hybrid propulsion system
P	Power
$P_{propulsive}$	Propulsive power, equal to the thrust multiplied by aircraft velocity
Pay	Payload
PE	Potential energy
r_m	Ratio of battery mass to ESS mass
S	Wing area
T	Torque
t	Time
Th	Thrust
UAV	Unmanned Aerial Vehicle
v	Velocity
v_{stall}	Stall velocity
$VTOL$	Vertical takeoff and landing

Subscripts

$aircraft$	Aircraft
avg	Average

baseline	Reference to the baseline configuration for a modular propulsion system, abbreviated by *base*
batt	Battery
CF	Carbon-fuel engine
cruise	Cruise
drag	Aerodynamic drag
drive	Automobile driving
EM	Electric motor
ESS	Energy storage system mass, sum of battery and fuel
fuel	Carbon-fuel
generator	Electric generator, abbreviated by *gen*
ICE	Internal combustion engine
initial	Initial, for cruise
int	Integration
max	Maximum
mech	Mechanical transfer
min	Minimum
payload	Payload
propeller	Propeller
required	Required, abbreviated *req*
shaft	Shaft

thrust	Thrust
total	total, for the system

Chapter 1

Introduction

1.1 Background

1.1.1 Aircraft Propulsion Systems

The majority of powered aircraft throughout history have relied on carbon-fuel based propulsion systems. Examples include internal combustion engines (ICEs), turboprops, turbojets and turbofans, with airspeed and power level required dictating engine type [18]. Since these types of propulsion system have been in use, substantial advances have been made to improve their specific power (power per unit mass), efficiency and reliability. These advancements have enabled the aviation industry to achieve commercial success worldwide. However, carbon-fuel based propulsion systems have several disadvantages that include a relatively low rate of technological improvement, high mechanical complexity, and scale-dependent specific power.

Since 2010, electric propulsion systems have rapidly expanded into the aviation industry to mitigate the deficiencies of carbon-fuel propulsion systems. So far, electric systems have been limited to implementation on small unmanned aerial vehicles (UAVs), but numerous concepts utilizing electric propulsion on larger aircraft [20] have been proposed. Increased electrical complexity, certification challenges and lack of experience limit practical usage on larger aircraft. Electric propulsion systems have several advantages over carbon fuel systems, namely lower mechanical com-

plexity, a smaller acoustic signature, lack of harmful gas emissions [13], and relatively scale-independent specific power levels [14]. These advantages (particularly lower mechanical complexity) have enabled electrical propulsion systems to be utilized in novel aircraft designs such as swiveling engines for vertical takeoff and landing (VTOL) [1] and distributed propulsion schemes [34]. While these design-based benefits are not well quantified on a general basis, electrical propulsion systems are likely to enable greater flexibility in aircraft design and capabilities based on qualitative arguments. However, electric propulsion systems suffer from one major limitation - battery specific energy (the amount of energy per unit mass) is inferior to carbon fuel specific energies by a factor of approximately 60 [10]. This limitation restricts the flight time/range of pure-electric aircraft to a fraction of what is achievable with a carbon-fuel powered aircraft. Other limitations that must be taken into account for practical implementation include thermal management challenges and for larger aircraft, scaling of the power electronics and electric motors.

To utilize the advantages provided by electrical propulsion systems while maintaining the flight time/range of carbon fuel propulsion systems, electric-carbon fuel hybrid propulsion systems have increasingly come under investigation and assessment for use in aircraft. Hybrid propulsion systems of this type utilize carbon-fuel to provide the majority of energy while utilizing electric propulsion system components to provide power and design flexibility. While hybrid propulsion systems show promise in enabling step changes in aircraft performance enhancement, there are few flown hybrid aircraft and there is no existing set of unified design standards or practices.

1.1.2 Propulsion System Sizing and Design

The mechanical complexity and cost of a carbon-fuel based propulsion system (referred to as a traditional propulsion system in this thesis) requires it to be fixed for the lifetime of the aircraft it is installed on. Consequentially, traditional propulsion systems are designed for the highest thrust or power requirement scenario that an

[1] While swiveling propulsion has been implemented for aircraft such as the V-22 Osprey, carbon fuel propulsion system mechanical complexity has limited its implementation to a select few aircraft.

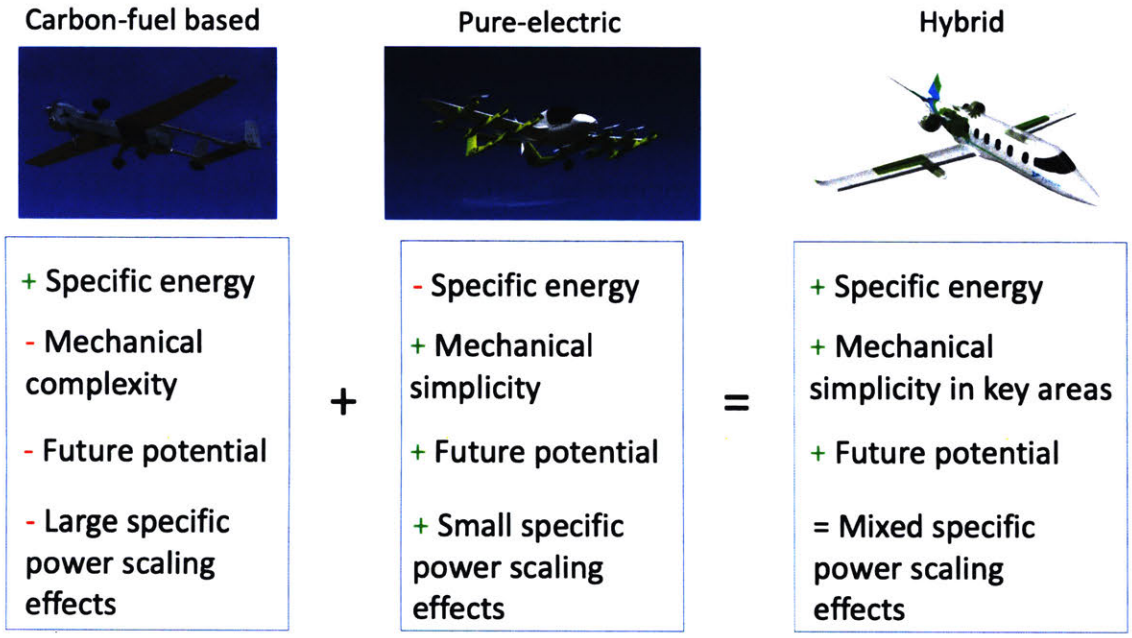


Figure 1-1: Hybrid propulsion systems combine desirable performance characteristics from carbon-fuel and electric propulsion systems. +, - and = signs are qualitative indicators for advantages, disadvantages, and neutral attributes of each propulsion system type.

aircraft may encounter on a mission throughout its lifetime. For commercial airliners, this could be takeoff at high altitudes (approx. 2000 m) on a hot day or meeting the top-of-climb rate-of-climb requirement [9].

The implication of this "worst-case scenario" design philosophy is that the resulting propulsion system will be oversized for missions other than the worst/design case. Since the propulsion system is a permanent fixture on an airplane, if it is oversized, it means that it is heavier than it needs to be for the aircraft to accomplish any off-design mission. Extra mass results in either reduced payload mass or greater fuel consumption than would be possible if the propulsion system were optimally sized for that mission. An example of this over-sizing effect can be shown by comparing the thrust required for takeoff at standard sea level (SSL) [9] and "hot and high" (H&H) (defined here as 3000 m altitude and 40° C) conditions. Air density at these conditions are 1.225 kg/m^3 and 0.78 kg/m^3 respectively - a ratio of 0.637 between the H&H and SSL conditions. With propulsion system thrust output proportional to air

density [9], a propulsion system designed for the H&H condition will be approximately 36% larger (and heavier) than if it were designed for the SSL condition.

1.2 Motivation

Among UAV manufacturers, particularly those who work with the military, there is a growing need for aircraft with diverse performance capabilities that are capable of accomplishing a wide-range of missions. An example would be a UAV that is required to fly large-payload, high endurance, and short-takeoff missions. Traditional propulsion systems are ill-prepared to meet these requirements due to their fixed, designed-for-"worst-case" nature. A new type of propulsion system is required that can enable performance flexibility while maintaining or improving aircraft performance.

A novel modular hybrid propulsion system (MHPS) is proposed in this thesis to meet the growing need for flexible aircraft propulsion systems. In this context, a carbon fuel - electric hybrid is considered while modularity refers to the ability to change propulsion system components, namely electrical components, to alter propulsion system performance. Modularity enables propulsion system performance to be tailored to each mission that the aircraft flies, enabling increased aircraft performance flexibility. Power hybridization (equation 1.1) and energy hybridization (equation 1.2) are utilized to quantify the degree of hybridization for each propulsion system configuration.

$$H_P = \frac{P_{EM,propulsive}}{P_{total,propulsive}} \tag{1.1}$$

$$H_E = \frac{E_{battery}}{E_{stored,total}} \tag{1.2}$$

1.3 Literature Review

1.3.1 Electrical propulsion systems for aircraft

The advancement of electric motor and battery technology coupled with increased public concern about the environment has sparked interest in electric propulsion concepts in recent years. This interest has resulted in numerous electric vertical takeoff and landing (eVTOL) concepts from companies such as Airbus, Cora Aero, and Uber. Meanwhile in academia, focus has been on three main areas: 1) specific electric propulsion concepts and analyses, 2) tools to analyze electric propulsion systems and 3) technologies enabled by electrified propulsion (large amounts of boundary layer ingestion, distributed propulsion).

Electric aircraft concepts and demonstrators

Currently (as of 2018), all flown electric aircraft concepts (such as the Airbus E-fan [15], Airbus Vahana [2], and other eVTOL concepts) have been of a general aviation (GA) class, with a gross takeoff mass of less than 1500 kg [7]. There are three main reasons for this. First, electric motor development in the automotive sector can be leveraged for GA-class aircraft as the power requirements are similar (50-200 kW). Second, there are significant technological barriers to implementation of higher power electric motors on aircraft, including thermal management, power transfer/control, and electric motor specific power scaling [20]. Third, battery technology limits the feasible range of all-electric aircraft. A NASA LEARN study concluded that even with optimistic estimates of battery technology, all-electric aircraft are infeasible for replicating the missions required of conventional commercial airliners [16].

Quantitative tools/models for electric propulsion systems

The use of electric propulsion systems has necessitated development of new tools to analyze their performance during various portions of the aircraft design process.

For the conceptual design process, various metrics have been proposed for characterizing system-level performance such as electric system drive efficiency, electric drive

system specific power and electric propulsion factor [10]. Performance estimation relations for aircraft using electrified propulsion such as the Breguet Range Equation have been derived by various authors, which is shown in Equation 1.3[7]. The first term is the cruise range due to carbon-fuel usage and the second term is the cruise range due to battery usage. Note that in Equation 1.3, it is implicitly assumed that battery is utilized solely before fuel, and fuel is only utilized once battery energy is depleted.

$$Range = \frac{L}{D}\eta_{CF}\eta_{prop}\eta_{int}\frac{e_{fuel}}{g}\ln\left(\frac{1}{1-m_{fuel}/m_{total}}\right) + \frac{L}{D}\eta_{EM}\eta_{prop}\eta_{int}\frac{e_{batt}}{g}\frac{m_{batt}}{m_{total}} \tag{1.3}$$

From Equation 1.3 it can be seen that the specific energy of fuel and battery are directly proportional to the carbon-fuel range and battery range respectively. The relationship between the specific energies and total range and/or cruise endurance is a major focus of this thesis and further examined in Section 4.2.

Technologies enabled by electrified propulsion

With the difference in power transfer methods between electric and carbon-fuel propulsion systems, there are numerous technologies that may be enabled by the use of electric propulsion systems. These concepts include distributed propulsion, large-scale boundary layer ingestion, solar panel usage, and swiveling propulsion [7]. These technologies have potential benefits in system performance or flexibility that are not easily achievable with traditional propulsion systems. Large amounts of boundary layer ingestion and distributed propulsion in particular have been shown to significantly reduce aircraft energy usage and are enablers for electrical propulsion systems in commercial airliners [16].

Battery technology

One of the major hindrances to wide-spread adoption of pure-electric propulsion systems is the current state of battery technology, primarily battery specific energy.

Currently (2018), commercially available battery packs have specific energies around 170 Wh/kg (612 kJ/kg) [24]. This value is approximately 1.5% that of commonly used hydrocarbon fuels. Therefore, with current technology, long-range pure-electric aircraft are impractical as too much battery mass would be required to meet performance requirements (mainly cruise range/time) [29].

Several conceptual aircraft design studies have determined that battery pack specific energies of 750 Wh/kg (440% of current) and greater than 1000 Wh/kg (588% of current) are required for practical implementation of large hybrid [6] and pure-electric aircraft [24] respectively. Current projections of battery specific energy growth range from 5% to 8% increases per year [24], which would result in battery pack specific energies reaching 750 Wh/kg and 1000 Wh/kg in 2036 and 2040 respectively [2].

Complicating matters further is that to maintain these battery specific energy growth rates, breakthroughs in battery chemistry are required. This is because each battery chemistry has theoretical limits on energetic potential; for example, the limiting theoretical specific energy of lithium-ion (state-of-the-art) batteries is 387 Wh/kg [8]. One promising battery chemistry that is the focus of major research is lithium-air (Li-O2) with a limiting theoretical specific energy of 3582 Wh/kg (roughly 30% of hydrocarbon fuels) [8]. However, Li-O2 batteries have many issues that must be resolved before they are commercially ready, with primary issues relating to stability, life, and cost[8]. While there are substantial research efforts devoted to overcoming these issues, there are no reliable projections as to when they will be commercially viable. It is likely that it will take 15+ years before Li-O2 batteries are ready for implementation onto aircraft [24].

Finally, for aircraft, battery pack specific energy rather than battery cell specific energy is the metric of interest as cells have to be packaged to be utilized in aircraft propulsion systems. This packaging effect can reduce cell specific energy levels by approximately 15% to 40% [16]. For future discussion in this thesis, battery pack specific energy is assumed and simply referred to as battery specific energy for brevity.

[2]based on a consistent growth rate of 8% per year from 2017

Electric motor technology

Electric motor (EM) technology, specifically specific power, has grown significantly in the last decade, with a focus on developing high specific power motors for automotive and aviation applications. Current (2018) state-of-the-art EMs have specific powers of approximately 5 kW/kg [32] [36] (machine only, without cooling) for both aviation and automotive applications. The specific power growth rate of EMs is approximately 3.5% per year [23].

Future projections of EM specific power range from 13 to 16 kW/kg for non superconducting machines and up to 20+ kW/kg for superconducting machines [20]. The specific power required for aviation viability depends on the class of aircraft and which type of carbon-fuel engine is typically used. The specific power requirement results because the specific power of carbon-fuel based propulsion systems tends to grow with power class, with the specific power of GA propulsion systems starting around 1 kW/kg [22] increasing up to 16 kW/kg for large turbofans such as the GE90 [24].

Anderson et al. [4] conducted a study comparing the system masses of different electric motor topologies. Permanent magnet synchronous machine, doubly-fed reluctance machine, and induction machine topologies were investigated. The study considered the total mass of the electrical sub-system associated with each electric motor topology, including the power electronics and control circuitry. The authors concluded that permanent magnet synchronous motors had the highest system specific power caused by the high specific power of the EM rotor and stator assembly itself.

1.3.2 Hybrid propulsion systems for aircraft and automobiles

With state-of-the-art batteries possessing inferior specific energies (when compared to hydrocarbon fuels), interest in carbon-fuel electric hybrid propulsion systems has rapidly increased. This is because hybrid propulsion systems can serve as a platform to utilize electric propulsion architecture benefits while maintaining the cruise

time/range of conventional propulsion systems [28]. Hybrid propulsion systems can utilize a central carbon-fuel system to provide the majority of energy required for flight while using the electric system to either supplement or fully-supply the power required to start and maintain flight.

With the relative novelty of hybrid propulsion system usage for aircraft propulsion, few practical implementations have flown. Table 1.1 summarizes flown aircraft with hybrid propulsion systems; data is adapted from [7]. In addition, there are several proposed hybrid aircraft in literature, which are summarized in Table 1.2 (data is again adapted from [7]). Tables 1.1 and 1.2 show that most flown aircraft have been sub-megawatt (MW) propulsion systems while the aircraft in-development have power levels above 1 MW. Issues with scaling electrical machines and power electronics [7] to higher power levels limits practical implementation of super-megawatt systems.

Name	Year	Hybrid configuration	Max power	Battery $e_{batt}\left(\frac{W-hr}{kg}\right)$
Siemens/Diamond E-Star	2011	Serial	70 kW	N/A
Embry-Riddle Eco-Eagle	2011	Parallel	105 kW	125
Siemens/Diamond E-Star 2	2013	Serial	80 kW	N/A
Cambridge SOUL	2014	Parallel	20 kW	144
Airbus E-Fan 1.2	2016	Serial	60 kW	N/A

Table 1.1: Flown hybrid-electric aircraft (adapted from [7])

Name	Year	Hybrid configuration	Max power	Battery $e_{batt}\left(\frac{W-hr}{kg}\right)$
Boeing SUGAR Volt	2035	Parallel	1 MW	750
Airbus/R-R E-Thrust	2050	Serial	9 MW	1000
XTI Tri-Fan 600	2024	Serial	1.5 MW	N/A
Zunum Aero	2020s	Serial	1 MW	N/A

Table 1.2: Proposed hybrid-electric aircraft (adapted from [7])

Beyond the practical implementation of hybrid aircraft, there have been several studies on computational design of hybrid-electric aircraft. Pornet et al. [28] investigated the performance of an existing commercial aircraft retro-fit with an hybrid-electric propulsion system and showed that for short distances fuel consumption could be reduced by up to 13% in certain situations. A further study on clean-sheet turbofan-electric transport aircraft design demonstrated that to meet cruise range requirements of over 1100 nautical miles, hybrid aircraft architectures are infeasible compared to conventional designs, in accordance to previous studies on battery technology requirement for aircraft. The authors concluded that completely integrated approaches between the electric propulsion system and fuselage should be investigated to fully realize the potential of hybrid propulsion architectures [29]. Sliwinski et al. came to a similar conclusion when considering hybrid-electric propulsion for unmanned aircraft, finding that internal combustion engine only aircraft had a superior cruise range compared to electric and hybrid-electric counterparts. The author noted that future technologies enabled by electrified propulsion such as energy harvesting or distributed propulsion could enable cruise ranges closer to those of conventional propulsion systems [33]. Panagiotou et al. conducted a study on a long-endurance hybrid-electric UAV which supports this assertion, finding that solar cell usage and increases in solar cell efficiency could lead to large increases in UAV endurance [26].

Ludowicy et al. designed a GA aircraft with a series hybrid-electric propulsion system with current and near-future technology. The author showed that a hybrid setup resulted in an aircraft mass increase of 20% and higher fuel consumption when compared to an aircraft with a conventional propulsion system [22]. A similar result was obtained by Voskuijl et al. for a hybrid-electric regional turboprop design; the resulting aircraft was 14% heavier even considering a futuristic battery specific energy of 1000 Wh/kg [35].

One issue arising from these computational design studies is that the introduction of an electric sub-system leads to additional design variables (hybridization values for energy and power). Traditional aircraft design methods and tools are not suitable to deal with these additional design variables [31]. Studies in the past few years

have focused on higher-fidelity design tools, incorporating a mix of first-principle and empirical electrical component performance and mass models [27][31]. Furthermore, these studies have proposed high-level performance metrics that could be used to evaluate hybrid-electric propulsion system performance and operational strategies [27]. Riboldi et al. also uses high-level performance metrics to present an optimal design approach for small hybrid-electric aircraft [31].

The design studies presented emphasize the importance of hybrid configuration on aircraft performance and the need to quantify the differences in hybrid configuration.

Hybrid configurations

Several different hybrid configurations have been conceived or implemented in aircraft [7] and automobiles [11], each with different performance properties but can broadly be split into three categories: serial hybrids, parallel hybrids and parallel power-split hybrids.

Most if not all hybrid configurations considered for aircraft have been adapted from the automotive industry as the automotive industry has pioneered their implementation. While automotive operational and certification requirements are different from aviation requirements, the difference primarily affects how the propulsion system is operated and the matching between the components. Power transfer and high-level component matching methods are independent of application, and automotive application experiences are readily transferred to aviation applications. Therefore the main architectural differences between the hybrid configurations and effect on performance hold between automotive and aviation applications.

Series hybrid configurations

For automotive applications, series architectures consist of a primary carbon-fuel burning power source (typically an internal combustion engine), generator, battery, power-controller, and electric motor connected sequentially (in series). In this configuration, the electric motor is the sole provider of power to the drive components and the carbon fuel engine is mechanically separated from the drive shaft. This separation

allows the carbon fuel engine to operate at its optimal efficiency point. Additionally, the separation of fuel-burning engine operation from load allows the engine to be sized smaller than it otherwise would be since it only needs to be large enough to support average power requirements. However, since the electric motor is the only source of shaft power, it must be sized large enough to meet peak power requirements. The resulting hybrid electric system (HES) typically is of larger mass than other hybrid architectures. In small UAVs, the difference is estimated to be roughly 8% of the gross UAV mass [17]. Series hybrid architectures are typically best suited for situations where the engine must be turned on and off repeatedly and for high torque, low speed applications. These are the situations where typical engine systems operate inefficiently. For general automotive applications, series architectures are not typically used, with the Fisker Karma (shown in Figure 1-2) being one of the only cars that has been developed using this architecture [11].

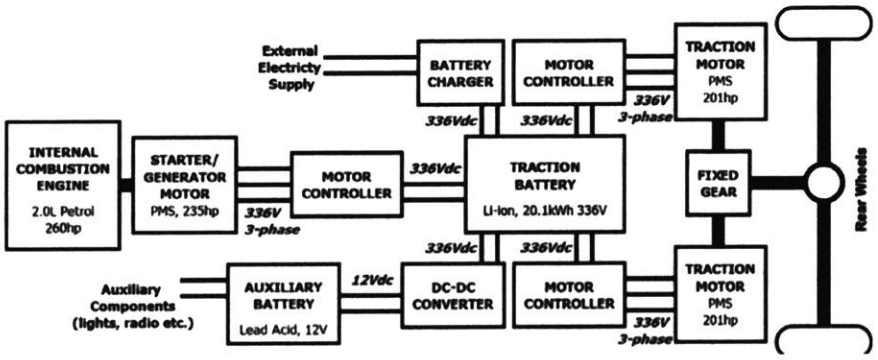


Figure 1-2: Series hybrid configuration for the Fisker Karma automobile taken from [19]. The internal combustion engine for series configurations does not provide propulsive power and is only used to generate electricity through a electrical generator.

The sizing of components in a series configuration is accomplished by adhering to the following principles [11]:

- The electric motor is sized to meet peak drive shaft power requirements

$$P_{EM,max} = P_{peak,required} \tag{1.4}$$

- The internal combustion engine is sized to meet average power requirements

or to meet cruise/long distance power requirements, whichever is greater. The power requirement is modified by the transmission efficiency η_{trans} from the ICE to the motor

$$\eta_{trans}\eta_{EM}P_{ICE} = max(P_{avg}, P_{cruise}) \tag{1.5}$$

- The battery is sized such that it can supply sufficient energy to cover the deficiency between EM and ICE power for the amount of time required to meet an acceleration or climbing requirement

$$E_{battery} = \int (P_{drive} - \eta_{trans}\eta_{EM}P_{ICE})dt \tag{1.6}$$

- Capacitors are added such that peak electric discharge requirements are met if needed

With the above principles, the primary components of a series hybrid architecture can be sized. Further details such as the system's torque-speed relationship require more detailed analysis and design, particularly of the gearing configuration. However, for automotive applications, the series architecture usually does not need to rely on sophisticated gearing configurations since EM characteristics are well matched for automotive load cycles [11].

Parallel hybrid configurations

Parallel architectures consist of the same components as the series architecture but differ in that the fuel-burning engine is also connected to the drive shaft, such that it always provides a portion of the torque. Connecting the fuel-burning engine to the drive shaft has two primary consequences:

- The operating point of the fuel-burning engine is dependent on the load carried by the drive shaft: its speed must match that of the drive shaft, modified by the gearing involved. This forces the fuel-burning engine to run outside its optimal efficiency range in certain driving situations as in traditional ICE-driven automobiles.

- The drive shaft receives power from both the electric motor and fuel-burning engine, such that the electric motor is smaller than in the series configuration.

Currently, parallel configurations are a significant portion of the total automobile market of roughly 3.3% [19]. A mild hybrid system (from a Honda Civic) is shown in Figure 1-3. In the context of automobiles, parallel architectures are unable to drive the automobile under purely electric power and are generally considered mild hybrids. This is in contrast to full hybrids which are generally of the power-split architecture to be discussed later. Sizing of the parallel hybrid electric system (P-HES) components is accomplished adhering to the following principles [11]:

- The sum of the electric motor and fuel-burning engine (considered an ICE in this case) powers must equal the drive shaft peak power requirement modified by separate transmission efficiencies

$$\eta_{mech} P_{ICE} + \eta_{trans} P_{EM} = P_{peak,required} \tag{1.7}$$

- The ICE is sized to meet cruise power requirements or average power requirements. This is the same as for the series configuration, except that the transmission efficiency is generally higher since the energy does not have to change forms before reaching the drive shaft

$$\eta_{mech} P_{ICE} = max(P_{avg,drive}, P_{cruise,drive}) \tag{1.8}$$

- The battery is sized to be large enough to allow the electric motor to run at peak power for enough time to meet acceleration or climb requirements

$$E_{battery} = \int \frac{(P_{peak,drive} - \eta_{mech} P_{ICE})}{\eta_{trans}} dt \tag{1.9}$$

- Capacitors are added to meet peak discharge requirements

As with the series architecture, the above principles allow sizing of the main P-HES components with sizing of additional components requiring application-specific

analysis. The main component that requires careful design in a P-HES system is the transmission. Since the ICE is mechanically connected to the drive train, it must be geared to be able to provide power through the entire speed range of the drive shaft.

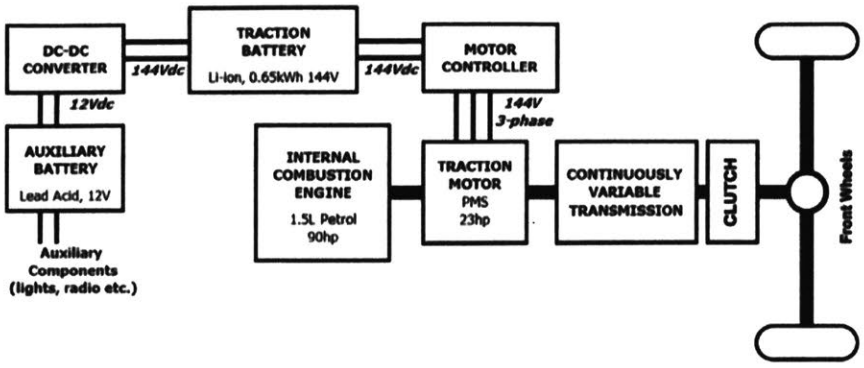


Figure 1-3: Mild parallel hybrid configuration for the Honda Civic automobile taken from [19]. The internal combustion engine for a parallel configuration combines with an electric motor to provide traction power to the main drive shaft.

Parallel power-split hybrid configurations

The final common electric hybrid architecture is power-split architecture which attempts to merge the series and parallel architectures to combine each of their benefits at the cost of mechanical complexity. In the power-split architecture, the system is setup similarly to the parallel system, with the drive train connected to the ICE. However, the ICE is also connected to a generator; with clutches or other torque/power split elements, the ICE can solely power the generator during travel or be used to provide power to the drive shaft. Most automotive hybrid vehicles in use are of the power-split type; the two most common configurations are the Hybrid Synergy Drive (HSD) used in the Toyota Prius (shown in Figure 1-4), and the in-line configuration which includes the BMW ActiveHybrid 5 (shown in Figure 1-5) [19]. The power-split architecture differs from the parallel and series architectures in the following:

- The EM has the ability to power the drive shaft fully without assistance from the ICE.

- The ICE can power the drive shaft and generator(s) simultaneously at varying proportions.

The above traits give the power-split architecture more flexibility in operating modes and an increased number of power management strategies available than the parallel or series architectures. Additionally, the power-split architecture benefits from the increased transmission efficiency of parallel architectures while allowing the ICE to operate near maximum efficiency as in the series architecture, further reducing fuel consumption of the system. However, these benefits require an increase in mechanical complexity with either complicated gearing (such as the epicyclic gear in the HSD, which is labeled e-CVT) or a number of clutches to control the power split of the ICE (such as in the in-line configuration) [11]. In most cases, sizing of the power-split architecture's main components is identical to the parallel configuration apart from the battery. The battery capacity is generally increased to allow for extended use of only the EM for propulsion per individual requirements.

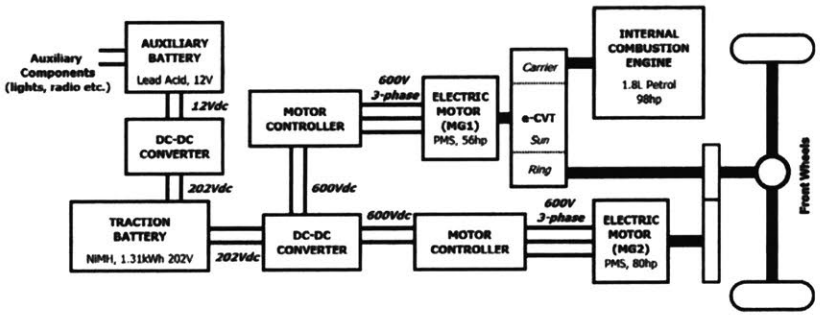


Figure 1-4: Parallel power-split configuration of the Toyota Prius automobile taken from [19]. The internal combustion engine for a parallel power-split configuration is connected to an electric motor and the main drive shaft through an e-CVT. This allows the ICE to both power the wheels and generator; wheel power can be augmented by the EM connected to the e-CVT.

Summary of hybrid configurations for automobiles

The primary differences in the hybrid configurations can be summarized as follows. First, for the same propulsive power output, the parallel configuration will have the

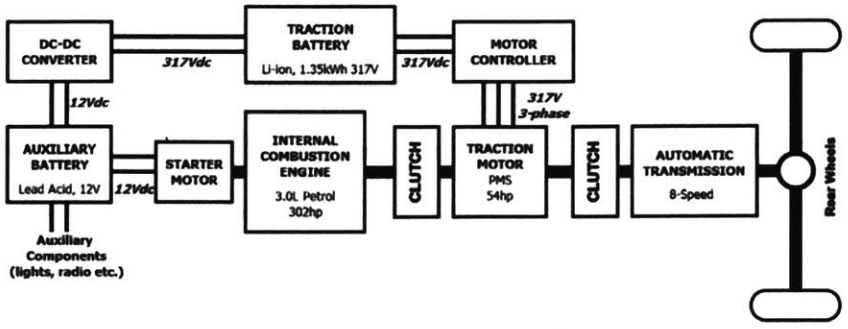


Figure 1-5: BMW ActiveHybrid5 parallel power-split configuration taken from [19]. The internal combustion engine drives the wheels and an electric motor depending on which clutches are engaged. Both the EM and ICE can power the wheels.

lowest mass because both the EM and CF engine can generate propulsive power and there is no generator. Next is the parallel power-split configuration as it is the same as the parallel configuration except it contains a generator. The series configuration mass is greatest as only the EM can generate propulsive power.

Second, the total thermal efficiency of the parallel and parallel power-split configurations is higher than the series configuration. This is because the CF engine can directly provide propulsive power in the parallel configurations, while fuel power has to be transformed multiple times in the series configuration before it becomes propulsive power.

Third, the series configuration will be have more integration flexibility than the parallel and power-split configuration because the CF engine does not need to be attached to the drive shaft in the series configuration.

Fourth, the mechanical complexity is highest with the parallel power-split configuration as it has the most components and operational functionality.

1.4 Technical Innovation: A Modular Hybrid Propulsion System

The key innovation presented in this thesis is the idea of a propulsion system for which the individual components can be interchanged as necessary to modify the propul-

sion system's performance characteristics. Interchangeability is enabled with the use of hybrid architecture due to the fact that electrical components are mechanically simpler than traditional systems, especially in the power-transfer method (electrical wiring vs. mechanical shafts). Mechanical simplicity increases the feasibility of interchangeability, as it is more probable that there are fewer integration constraints with a simpler mechanical system. Furthermore, electrical components are typically less cost-prohibitive than their carbon-fuel counterparts at similar power level. Interchangeability therefore is likely more cost feasible than it would be with carbon-fuel components, but this assertion is not tested further in this thesis.

For the reasons articulated, modularity of only the electrical components are considered, with fixed (for each aircraft) carbon-fuel power-transfer components, except the fuel-tank which is considered to be modular. Even with the restriction of modularity to electrical components and the fuel tank, it will be shown that the power, endurance (cruise time), and mass of the aircraft can be modified through interchanging of components.

1.5 Research Objectives

The overall research objective is to quantitatively determine the flexibility afforded by the modular hybrid propulsion system and the functional relationship of performance metrics with hybridization values and component technology. Specific focus is placed on aircraft performance during takeoff, climb, and cruise flight segments in terms of takeoff distance, climb rate, and cruise time respectively. A large UAV serves as a platform for an in-depth performance assessment of the MHPS concept with current technology. Research questions that must be addressed to accomplish the research objective are:

1. What level of performance and flexibility can be achieved with a MHPS with current technology relative to traditional propulsion systems?

2. How do power and energy hybridization levels affect MHPS performance and

flexibility?

3. How are hybridization performance trends affected by component technology levels?

4. What are the trade-offs between hybrid configurations for aircraft propulsion in terms of propulsion system performance, mass, and flexibility?

5. What is the functional dependence between MHPS performance and flexibility and design choices and aircraft size?

6. How should hybridization values be selected during MHPS design?

7. How should the operation strategy of a MHPS be determined?

8. How does the performance of the individual components of a MHPS affect the system's static and dynamic (time-varying) performance and flexibility?

9. Where should research efforts be focused to most improve the performance and flexibility characteristics of MHPSs?

The above research questions guided thesis research and are addressed in this thesis.

1.6 Original Contributions

Contributions of this thesis are:

1. **A novel idea of propulsion system modularity.** Modularity enables an adaptive design space that broadens mission capabilities for a given fixed flight vehicle. This is the first instance of propulsion system modularity being proposed to enable aircraft performance flexibility.

2. **A set of quantitative performance relationships for modular hybrid propulsion systems.** These performance relationships quantify the functional dependence of performance on hybridization level, component technology level,

and aircraft design choices. Furthermore, the performance relationships enable MHPS sizing and determination of MHPS constituent components.

3. **Quantitative criteria for selecting the extent of electrified propulsion contribution relative to carbon-fuel based propulsion contribution.** These criteria include the conditions under which to use carbon-fuel based or electrified systems based on the relationship between cruise time, energy hybridization level, and electric technology. Also included are quantitative guidelines for determining energy and power hybridization levels based on propulsion system technology relative to carbon-fuel technology. This is the first instance of a set of quantitative guidelines for selecting the extent of electrified propulsion in a hybrid propulsion system for aircraft.

1.7 Thesis Organization

This thesis is organized as follows. Chapter 2 outlines the technical approach taken to address the stated research questions. Chapter 3 details the framework used to model hybrid aircraft performance and usage to estimate the performance of a large UAV retro-fit with a MHPS. Chapter 4 walks through the MHPS performance relationship derivation and discusses the design implications. Chapter 5 details an optimal energy management approach for hybrid propulsion systems and operational matching characteristics of the MHPS. Chapter 6 provides a summary of the primary findings and implications for aircraft propulsion system usage and design. Chapter 7 outlines recommendations for future work.

Chapter 2

Technical Approach

2.1 Introduction

The Modular Hybrid Propulsion System (MHPS) introduces two major features to consider during the propulsion system design process: the use of an electrical sub-system (hybridization) to provide propulsion and the ability to swap the electrical sub-system components to tailor propulsion performance to each mission (modularity). Each of these features increases the complexity of the propulsion system design process by introducing new component sizing questions that a designer must address. These issues are encapsulated in the research questions outlined in Section 1.5. To address the research questions, a scale-agnostic approach is taken when possible to ensure the thesis findings are applicable to all scale of aircraft. Quantification of MHPS performance achievable with state-of-the-art current technology against traditional propulsion systems is accomplished by utilizing a large UAV platform. The large UAV platform also enables the assessment of the impact of hybridization and modularization on the propulsion system performance.

Hybridization enables the propulsion system to meet performance requirements with different sets of components, since hybrid propulsion systems typically have two (or more) components that can produce propulsive power (EM and/or carbon-fuel engine) and/or store energy (carbon-fuel and battery). By having multiple components that satisfy similar functions, various proportions of these components can be used

to meet the same overall performance requirement. Consequently, the designer must decide how to proportion components that have similar functions. The primary proportion values of interest are the power hybridization value and energy hybridization value, shown in equations 1.1 and 1.2 respectively.

Traditional propulsion systems typically only have one component that can satisfy a particular function and so the one component must be sized to meet a particular performance requirement. For example, only the engine can provide power/thrust and only carbon fuel can store energy. For these cases, no decision needs to be made regarding component sizing. However, to enable a designer to make informed decisions on how to proportion a hybrid propulsion system, it is necessary to establish quantitatively how propulsion system performance is affected by hybridization levels, technology level, and hybrid configuration (serial vs. parallel). These propulsion system performance relations can then be analyzed to establish the effect of technology level on performance trends. Therefore, one of the focuses of this thesis is to establish a quantitative link between propulsion system performance and hybridization and technology levels thath is applicable to all aircraft scales.

By enabling component changes for each mission, modularity enables the designer to modify the hybridization level and component mass ratios (see equation 2.1 and 2.2).

$$\frac{m_{propSystem}}{m_{aircraft,total}} = \frac{m_{carbon-fuelengine} + m_{EM}}{m_{aircraft,total}} \tag{2.1}$$

$$\frac{m_{ESS}}{m_{aircraft,total}} = \frac{m_{batt} + m_{fuel}}{m_{aircraft,total}} \tag{2.2}$$

The range of hybridization levels and component mass ratios that are accessible with a modular propulsion system are dependent on technology level and the amount of mass available on the aircraft available for use with modular propulsion components (denoted as m_{free}). Modularity is therefore quantifiable and referred to as the ratio of m_{free} to the total aircraft mass (see equation 2.3).

$$\Gamma = \frac{m_{free}}{m_{aircraft,total}} \tag{2.3}$$

The relationship between equations 2.1, 2.2, and 2.3 is shown in Figure 2-1.

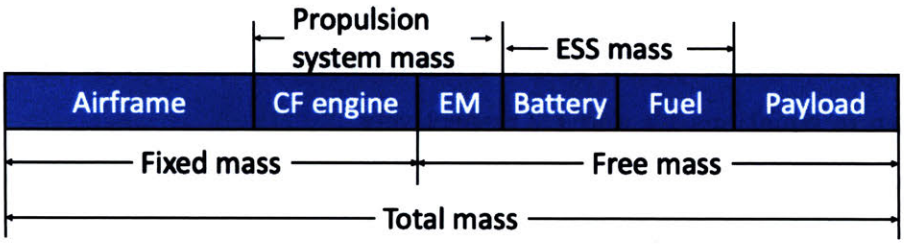


Figure 2-1: Relationship between total mass, fixed mass, free mass, propulsion system mass, and ESS mass definitions.

With modularity, a propulsion system designer now must determine how much mass should be budgeted for the fixed set of components and the modular set of components. The fixed set of components provides a fixed amount of performance for the aircraft for its lifetime, while the modular set of components provides a variable amount of performance for each mission. This idea is visualized in Figure 2-2. It is therefore necessary to quantify the effect of modularity level on achievable aircraft performances. With a quantifiable link between modularity and performance spread, a designer can choose the fixed-modular mass balance on a quantifiable basis.

While the MHPS introduces new design challenges, it also introduces additional operational challenges when compared to traditional propulsion systems due to the presence of the electrical sub-system. The first challenge is the determination of how to operate the propulsion system over the course of a mission. With at least two energy sources, there is a need to manage these energy sources to most effectively accomplish mission objectives. By choice of an appropriate energy management policy, the on-board energy stores can be utilized to minimize mission carbon-fuel usage (or meet some other optimization objective) while meeting mission operational requirements. The energy management policy referred to here determines the power output and operation point of each EM, generator and carbon-fuel engine. The chosen operating points in turn determine the power draw from the battery and carbon-fuel stores at each point of time during a mission. This thesis formulates and develops an effective framework for determining an optimal energy management policy to minimize mission carbon-fuel usage.

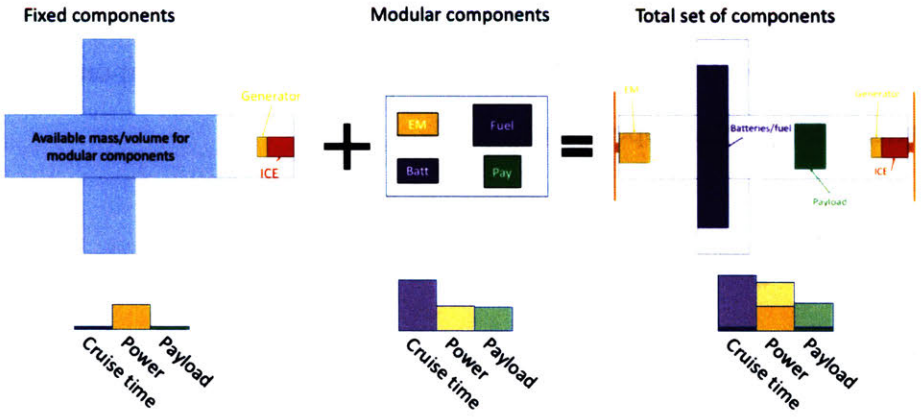


Figure 2-2: Notational aircraft performance variation with a MHPS. Total aircraft performance is the sum of the performance provided by fixed components and performance provided by the modular components. The configuration on the left is an empty airframe with only fixed components, which provides some amount of performance. The middle illustration is the modular component set to be installed, which has some performance level. The right illustration is the aircraft with modular components installed, with the total performance equal to the empty airframe and modular component set.

The second operational challenge is determining how secondary component performance characteristics affect operation of the MHPS. In this context, secondary performance characteristics refer to component dynamics (how quickly the component can change its performance, i.e. engine shaft acceleration) and how component performance changes with operating point (i.e. efficiency as a function of EM rotational speed and torque output, typically represented as an "efficiency map"). Component dynamics determine how responsive the propulsion system is to changes in operational requirements in-mission due to the energy management policy used. There is a need to quantify component dynamic effects to provide a framework for evaluating dynamic matching between components. Component efficiency maps on the other hand determine how the components may interact with each other during propulsion system operation. Again, since some components perform similar functions, the output of similar components can be set to various proportions while maintaining the same total output. One example of this is that to maintain total output power of 100 kW, the EM and carbon-fuel engine output can be set to either 30/70 kW or 70/30 kW. Since the efficiency of each component is affected by its output, these two

choices could result in vastly different component efficiency values depending on their efficiency maps. There is therefore a need to determine how component efficiency characteristics affect system operation.

2.2 Hybrid propulsion system performance

In this thesis, quantification of the functional relationship between hybridization levels, technology, and aircraft performance has the following requirements in order to address the research questions enumerated in Section 1.5:

1. Performance relations must be applicable for all aircraft scales and sizes.

2. Performance relations are direct functions of hybridization level and technology level metrics (such as specific power) when possible.

3. Performance relations are system-level and formulated in such a way to allow for applicability to serial and parallel hybrid configurations with minimal modifications.

To meet these requirements, a sequential approach is taken. First, a candidate hybrid propulsion system is sized and designed on a system-level, for a large unmanned aerial vehicle (here large is defined according to the U.S. Department of Defense Group IV standard - greater than 598 kg with a ceiling of less than 4000m [25]). Second, MHPS performance is generalized through a set of hybrid and modular performance relationships. The scaling performance are derived through a first-principles approach to ensure applicability to all scales. In this context a first-principles approach refers to utilizing well-established physical laws such as Newton's second law and conservation of energy to derive performance relations without the use of empirical relations.

For MHPS performance estimation, large UAVs are chosen because they are generally tasked with accomplishing a wide variety of missions, making them an ideal platform for assessing propulsion system flexibility. A candidate hybrid propulsion system design is undertaken to: 1) evaluate the effect of hybrid configuration choice

on system performance, 2) determine the components required for implementation of a hybrid propulsion system and 3) compare hybrid propulsion system performance against a traditional propulsion system with current technology levels, off-the-shelf components, and a similar air-frame. The large UAV platform provides the basis for performance generalization by highlighting the primary components that influence propulsion system performance and the effects of hybrid configuration on performance.

Following the candidate hybrid propulsion system design for the large UAV, a set of performance relationships are derived to generalize MHPS performance. With the first-principles approach, the derived performance relations are ensured to be applicable to all aircraft scales and technology levels. The performance relations are non-dimensionalized to reveal the functional dependence of performance on aircraft design parameters and component technology levels. Performance trends and their dependence on technology level determine the technology levels required for hybridization to improve aircraft performance.

2.2.1 Scope of research

The presented research is applicable to fixed-wing aircraft only and does not consider vertical takeoff and landing (VTOL) or hovering capability. Furthermore, throughout this thesis focuses on the performance tradeoffs between carbon fuel components and electric components in aircraft. If electrical components cannot replace their carbon fuel counterparts without radically modifying the aircraft, then the results presented here are not applicable. For example, for an aircraft that utilizes a ramjet propulsor, there is no readily available electric motor replacement. The performance relationships therefore cannot be applied to this type of aircraft.

Additionally the results presented focus on high-level performance parameters are at the vehicle system level. Lower level component performance values are not considered in most cases.

For the performance relationships presented in Chapter 4 and operational considerations in Chapter 5, several assumptions are made and the resulting functional

dependencies are only applicable given these assumptions.

2.3 Propulsion system modularity

To quantify aircraft performance spread as a function of free mass (equation 2.3), EM/CF engine specific powers, and battery/fuel specific energies, an approach similar to the hybrid performance relationship quantification assessment is taken. In this case, performance spread is defined as the best possible performance the aircraft can achieve with a modular component set subtracted by the baseline performance of the aircraft as a percentage of the baseline performance. For example the cruise time performance spread metric is formulated as $\frac{\Delta t_{cruise,best} - \Delta t_{cruise,baseline}}{\Delta t_{cruise,baseline}}$. Best possible performance is considered because the maximum possible spread of performance achievable with a modular hybrid propulsion system is of interest in order to capture the full potential of the MHPS for each performance metric. This idea is illustrated in Figure 2-3.

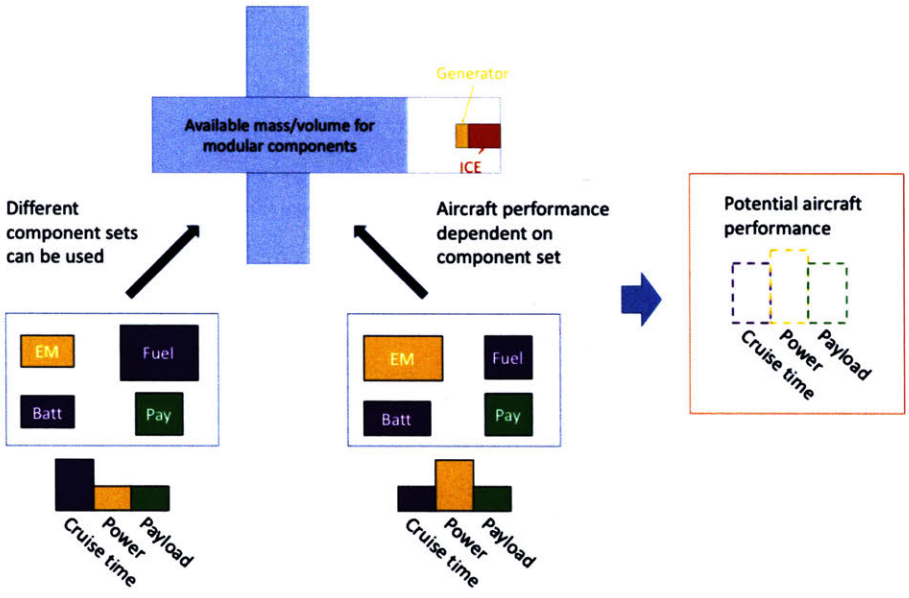


Figure 2-3: Modular hybrid propulsion system potential performance. For each instance, a component set can be used to emphasize a different performance metric. MHPS potential performance is the maximum of each performance metric that can be achieved with a particular component set.

2.4 Operational considerations

As noted above, the two primary operational considerations of a MHPS are the management of carbon-fuel and battery energy stores and the matching of components in terms of both static and dynamic performances. The goal of the energy management policy is to either minimize the fuel usage or maximize cruise time while meeting the operational requirements of any particular mission. Operational requirements are typically power/thrust requirements but can also include segments with only EM usage (to lower the acoustic signature) or payload power requirements (for high power payloads such as radar). Energy usage throughout the mission is time dependent and accounting for the time dependency is the main challenge associated with determining the optimal energy management policy.

An example of how the energy usage time-dependency is shown through the following situation: assume that a UAV starts a mission with some amount of battery and fuel energy on-board. Early in the mission, the UAV enters a situation where it can either use battery energy or fuel energy; if the UAV uses battery energy, it won't be available later in the mission and if it uses fuel energy, it may have less fuel remaining at the end of the mission. Later in the mission, the UAV needs to climb and requires battery energy to drive the EM; if the battery energy was used earlier, the UAV must spend extra time regenerating battery energy before initiating climb, spending extra fuel to do so. If it used fuel energy earlier, it can initiate climb immediately. From this situation, it can be seen that energy-usage choices early in a mission can affect operation later in a mission and that to determine the optimal energy management policy, the entire mission has to be taken into account.

To address the energy management time-coupling challenge, a Dynamic Programming (DP) framework is proposed. Dynamic programming is a branch of optimization that focuses on optimal sequential decision making by splitting up the optimization problem into several smaller sub-problems to reduce the computational cost. Further details on the mathematical formulation of DP can be found in [30] and [5]. DP is often used for time-coupled decision making problems and well suited to han-

dle constraints at any point in time. To cast energy management optimization as a DP problem, the mission profile is discretized into a pre-specified number of blocks, each spanning a period of time during the mission. Operational constraints are then added for each block depending on the mission. Finally, DP is invoked to determine the propulsion system's energy management policy to minimize fuel usage. DP considers how decisions for one block affect the optimal decision for the other blocks by finding the optimal operation strategy recursively. The DP idea and problem set-up are illustrated in Figure 2-4.

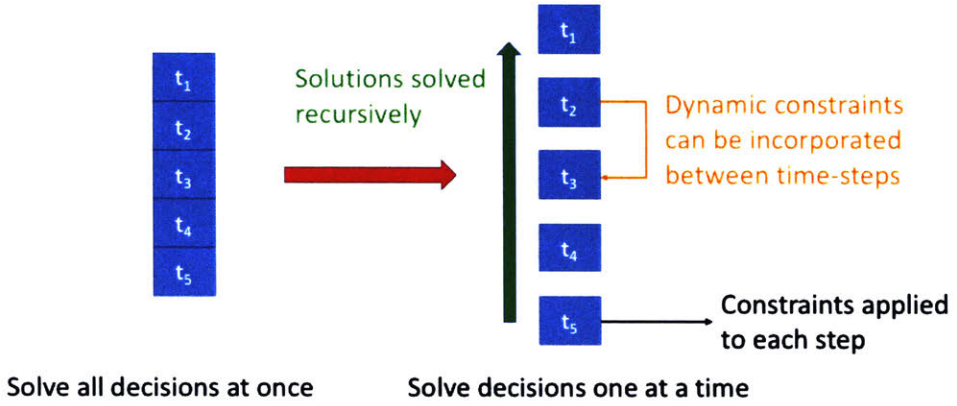


Figure 2-4: Dynamic programming splits a decision making problem into several subproblems to reduce computational cost. Constraints can be added to each block and the solution is found recursively.

The second operational consideration is component matching between the hybrid propulsion components from both a dynamic and static context. Dynamic performance is analyzed through a first-principles approached, focusing on performance analysis set by Newton's Second Law. First, the component performances are characterized. Second, system connections between components are then analyzed and finally system performance is derived as a function of the component performances. Once the system's dynamic performance is characterized, the effect on mission performance is determined. This approach ensures that the effect of component dynamic performance on mission performance can be traced, regardless of scale.

The static performance analysis focuses the effect of EM efficiency and carbon-fuel engine thermal efficiency on total system power source-to-output efficiency (referred

to as efficiency for brevity from now on), and specifically how the system's operation point-based efficiency is affected by the efficiency maps of the carbon-fuel engine and EM(s). Operating point refers to the rotational speed and torque output of a particular drive component (e.g. EM or ICE), with the output power equal to the product of rotational speed and torque. For any system-level operating point of a parallel hybrid configuration, the total hybrid system efficiency is a combination of the EM and carbon-fuel efficiency values. To illustrate how the EM and ICE efficiency maps can affect the performance of a hybrid system, consider the following situation. For a single-shaft propulsion system, with both a single ICE and EM attached, the total system efficiency is shown in equation 2.4 (derivation in Appendix B, assumption of battery energy derived from fuel):

$$\eta_{total} = \frac{\eta_{prop}\eta_{EM}\eta_{gen}\eta_{batt}\eta_{CF}}{\frac{P_{ICE}}{P_{total}}\eta_{EM}\eta_{gen}\eta_{batt} + \frac{P_{EM}}{P_{total}}} \tag{2.4}$$

Assuming that the generator and battery efficiencies are approximately 1 yields the following approximation for total system efficiency:

$$\eta_{total,system} \approx \frac{P_{ICE}}{P_{shaft,total}}\eta_{ICE} + \frac{P_{EM}}{P_{shaft,total}}\eta_{EM} \tag{2.5}$$

For this single shaft example, there are two constraints: 1) the sum of the EM and ICE power is equal to the total propulsive power requirement, and 2) the rotational speeds of the EM and ICE are identical (for this case, it is assumed there is no gearing involved). These constraints are shown below:

$$P_{shaft,total} = P_{EM} + P_{ICE}, \quad \omega_{shaft} = \omega_{EM} = \omega_{ICE} \tag{2.6}$$

With the constraints shown in equation 2.6, the efficiency values of the EM and ICE are functions of the shaft power-split only, defined in Equation 2.7.

$$\sigma_P = \frac{P_{EM}}{P_{shaft,total}} \tag{2.7}$$

Additionally, these constraints imply that the total efficiency at any operating

point is at minimum the efficiency of either the EM or ICE if they were solely responsible for driving the shaft. This is because either only the EM or only the ICE can be used to provide the total required power output, meaning that the total efficiency is equal to the EM/ICE efficiency, whichever is utilized. Therefore, the total efficiency map becomes a linear combination of the efficiency maps. This concept is shown in Figure 2-5. Note that the implicit assumption is that the EM or ICE have a capacity at least equal to the total required power output at any point in time.

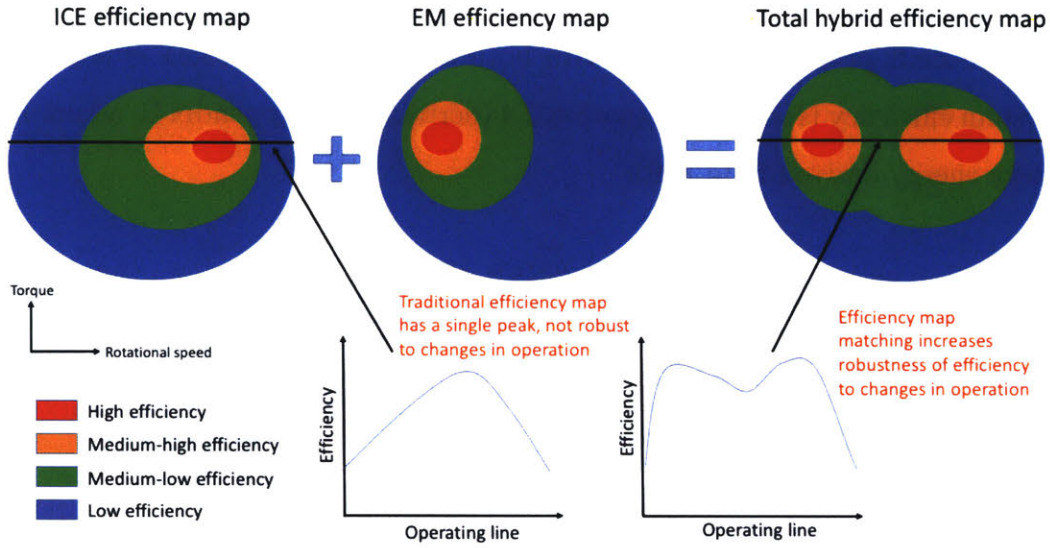


Figure 2-5: Total efficiency map of a hybrid propulsion system is a linear combination of the EM and ICE efficiency maps, when the ICE and EM are attached to a single shaft with no gearing.

From this example, it is clear that it may be beneficial for the EM and ICE efficiency maps to have dissimilar high-efficiency regions to generate a total efficiency map with relatively high efficiency throughout its entire operating range. The static matching analysis is focused on quantifying the effect shown in Figure 2-5, and uses sample EM and ICE efficiency maps to qualitatively investigate matching behavior. Furthermore, a single-shaft configuration (EM and CF engine on the same shaft) and separated shaft configuration (EM and CF engine on different shafts) were investigated.

2.5 Summary

The Modular Hybrid Propulsion System introduces two challenges to the design process that are not present for a traditional propulsion system and which provide an opportunity for flexibility: the addition of an electric sub-system that works in conjunction with the carbon-fuel sub-system (hybridization) and the ability to swap out components to tailor propulsion system performance to each mission (modularity). Hybridization changes how an aircraft propulsion system is designed and sized by requiring the designer to consider how the carbon-fuel and electric sub-systems influence overall system performance from both a static and dynamic standpoint. Modularity on the other hand, shifts the paradigm of single-point performance design to instead designing a propulsion system for a range of performances. The primary goal is on quantifying the performance relationships of a MHPS with respect to technology and hybridization/modularity levels and also on addressing the operational issues related to a MHPS.

The performance and design changes due to hybridization are quantified first. Hybridization is characterized in terms of the energy (Equation 1.2) and power hybridization (Equation 1.1) levels. The effect of hybridization levels on performance is dependent on hybrid configuration. Serial and parallel hybrid configurations are assessed to determine the performance and sizing differences between the two configurations. Following selection of a hybrid configuration, quantification of hybridization-performance trends is accomplished with a first-principles approach which ensures that the findings are applicable to all aircraft scales. A large UAV is used as the platform for assessing hybrid propulsion system performance with current technology and to illustrate the performance strengths and weaknesses of a hybrid system at present (2018).

Modularity enables a propulsion system to potentially have a wide-range of performance depending on which system components are used. It is necessary to quantify how the modularity level and technology level affect MHPS performance spreads to enable the designer to choose the modularity level of the aircraft during design.

Quantification of this relationship is accomplished using a first-principles approach to ensure that the resulting relationship is applicable toward all scale of aircraft.

There are two primary operational challenges related to the MHPS. First is the determination of the energy management policy for hybrid propulsion systems. The second is determination of how propulsion system components interact (matching) with each other to influence system-level performance in both a static and dynamic context. A dynamic programming (DP) framework is proposed to determine the hybrid energy management policy due to its ability to account for mission operational constraints throughout each mission and ability to couple energy usage decisions through time. To quantify component matching effects, the interactions between components are first characterized, followed by a first-principles approach to quantify dynamic and static interactions.

Chapter 3

Modular Hybrid Propulsion System Modeling and Large UAV Retro-fit

3.1 Introduction

Development of the performance relationships for a hybrid propulsion system depends implicitly on the hybrid configuration considered. The hybrid configuration determines how propulsion system components interact, as the hybrid configuration sets how system components are connected. A large UAV platform is utilized as a platform for evaluating hybrid configuration options on the basis of system performance. There are two focuses for this chapter: 1) formulating a quantitative framework for characterizing the performance of multiple hybrid propulsion configurations for aircraft, and 2) providing the rationale for utilizing a parallel configuration moving forward. Furthermore, performance model and configuration assumptions are detailed and justified.

Aircraft performances in terms of takeoff distance, rate of climb, cruise time, and static payload are evaluated. These performance metrics are chosen because they encompass the metrics that are most commonly used in practice to determine propulsion system requirements and performance goals. The reconnaissance flight profile shown in Figure 3-1 is used as the basis for performance evaluation.

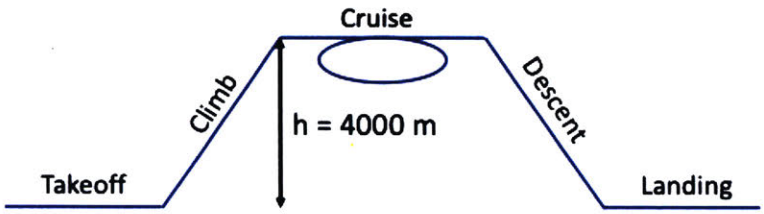


Figure 3-1: Reconnaissance flight profile used to evaluate aircraft performance.

3.2 Aircraft hybrid configurations

Several performance metrics are utilized to determine the performance and flexibility trade-offs between series and parallel hybrid configurations for use in aircraft. For cases where aircraft performance estimation is required, the performance estimation framework described in section 3.3 is utilized. A large UAV serves as the platform for assessment.

The hybrid configurations considered are the series configuration and parallel power-split configuration (referred to here as the parallel configuration). As detailed in section 1.3.2, these two configurations differ in the energy paths available, with the primary difference in which components directly provide propulsive power.

The series configuration considered and energy pathways available are shown in Figure 3-2. In the considered configuration, the carbon-fuel engine is only connected to an electric generator and propulsive power provided by the EM(s) only.

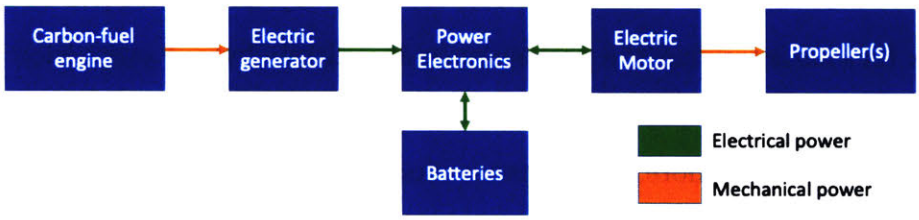


Figure 3-2: Power flow paths in a series hybrid configuration. Arrows indicate direction of allowable energy flow and color indicates whether power flow is mechanical or electrical.

The parallel configuration considered and energy pathways available are shown in Figure 3-3. The primary difference between the series and parallel configurations is that the carbon-fuel engine in the parallel configuration is also connected to its own

propeller. With this additional connection, propulsive power can be provided by both the EM(s) and carbon-fuel engine in the parallel configuration.

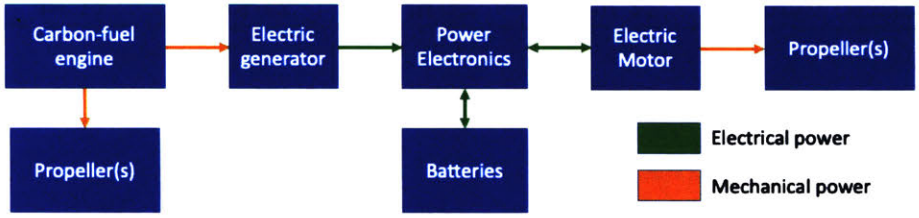


Figure 3-3: Power flow paths in a parallel hybrid configuration. Arrows indicate direction of allowable energy flow and color indicates whether power flow is mechanical or electrical.

Each of the two configurations are assessed and contrasted with the following metrics:

1. Propulsion system mass with equivalent performance. The large UAV platform is utilized to generate quantitative values and a reconnaissance flight profile is used to set the performance requirements. The profile illustrated in Figure 3-1 with various performance requirements (shown in Table 3.1) are used. These profiles are chosen as they are representative of large UAV requirements with variations on climb and takeoff requirements. With the large UAV platform, it is assumed that an internal combustion engine (ICE) is used as the carbon-fuel engine.

2. Thermal efficiency/fuel consumption. The power flow paths in Figures 3-2 and 3-3 are considered for efficiency calculations.

3. Integration flexibility. This is a qualitative measure which represents the ease of propulsion system integration into the airframe.

4. Mechanical transmission requirements. These requirements indicate if a transmission is required for hybrid configuration operation. Transmissions may be required to match the rotational speed of components if they operate on the same shaft.

Segment	Case 1	Case 2	Case 3	Case 4
Takeoff distance	100 m	100 m	40 m	30 m
Climb rate	200 m/min	300 m/min	200 m/min	200 m/min
Cruise time	21 hr	21 hr	21 hr	21 hr

Table 3.1: Four cases of flight mission profile requirements to evaluate the two hybrid configurations.

3.3 Propulsion system performance modeling

Either Newton's Second Law or the First Law of Thermodynamics (conservation of energy) are invoked to formulate the propulsion system performance models. Usage of physical laws avoids usage of empirical relations and ensures applicability across all aircraft scales and scenarios.

3.3.1 A model for takeoff performance estimation

The assumptions of the takeoff performance model and justification for each are enumerated below:

1. Component efficiency values are constant. Examples include carbon-fuel engine thermal efficiency, propeller efficiency and electric motor thermal efficiency. This constant efficiency assumption is taken to simplify the model and removes the need for additional performance models for each component. Variations in component efficiency would require reformulation of the takeoff performance model described in Appendix B.

2. Aircraft aerodynamic properties (coefficients of lift and drag) are constant during the takeoff run. This assumption is taken to avoid the need to model the functional dependence of aerodynamic coefficients on Reynolds Number, which varies depending on each specific aircraft design.

3. For the takeoff run, engines (carbon-fuel and electric) are operated at maximum power/thrust. This is taken because minimum takeoff distance is the performance parameter of interest, which corresponds to maximum power/thrust out-

put of the engines. Furthermore, this output thrust/power is constant during takeoff.

4. Aircraft mass is constant during takeoff, or equivalently, fuel mass burned during takeoff is minimal. Although engines are assumed to be operated at maximum power during takeoff, the takeoff time is typically short enough that the mass of fuel burned is negligible compared to the total mass of the aircraft. Fuel consumption can be taken into account through adding the consumption rate during the takeoff run integration.

5. Takeoff occurs once aircraft velocity reaches 120% of the stall velocity, with stall velocity derived in equation 3.1. The usage of 120% of stall velocity as the takeoff velocity is standard in aerospace engineering.

$$v_{stall} = \sqrt{\frac{2m_{aircraft}}{\rho S c_{Ltakeoff}}} \tag{3.1}$$

   In Equation 3.1, ρ is the air density, S is the wing area, and $c_{Ltakeoff}$ is the takeoff lift coefficient.

6. The only force in the opposite direction of movement is the force due to aerodynamic drag. Friction and resistance from the tires rolling on the ground are assumed to be negligible. Drag force is determined through the conventional definition of drag coefficient (shown in Equation 3.2).

$$D = \frac{1}{2}\rho S c_D v^2 \tag{3.2}$$

Due to the assumptions taken, estimated takeoff distance values from the takeoff performance model are likely optimistic. This is primarily because friction can be a significant force during takeoff and thrust is generally not constant during the takeoff run.

For takeoff modeling, the goal is to determine the distance required for the aircraft to reach its takeoff velocity from a stand-still. Acceleration during takeoff is modeled

through Newton's Second Law, with the assumptions outlined previously:

$$m_{aircraft,total}\frac{dv_{aircraft}}{dt} = \sum_i F_i = Th - D \tag{3.3}$$

Here the takeoff distance and velocity are linked by the differential change in distance per differential change in time:

$$dR_{takeoff} = v_{aircraft}dt \tag{3.4}$$

Equations 3.3 and 3.4 are integrated with respect to time to quantify the velocity-distance relationship during takeoff, with the drag D updated as the velocity changes according to Equation 3.2. Per assumption 5 from above, takeoff distance is considered to be equal to the distance for the aircraft to reach 120% of stall velocity.

3.3.2 A model for climb performance estimation

The assumptions of the climb performance estimation model and justification for each assumption are enumerated below:

1. Component thermal efficiency values are constant during climb. Reasoning is similar to that given for takeoff, though efficiency values may differ between the two flight segments.

2. Constant aerodynamic properties during climb. Again, reasoning is similar to that given for takeoff, with values differing between the two flight segments.

3. For climb, the rate of climb is assumed constant. This assumption enables calculation of climb performance with a simple climb profile.

4. Thrust force is assumed to be aligned with the axial axis of the aircraft. This simplifies the analysis and removes the need for specification of the thrust angle of attack. The free-body diagram of the aircraft during climb is shown in Figure 3-4.

5. If the required thrust power is greater than the power of the carbon-fuel engine, it is assumed that the carbon-fuel engine is operated at maximum power output, and the EM(s) provide the remaining power to meet the required thrust power. In this situation, the EM draws energy from the batteries only, with the generator detached via clutch from the ICE.

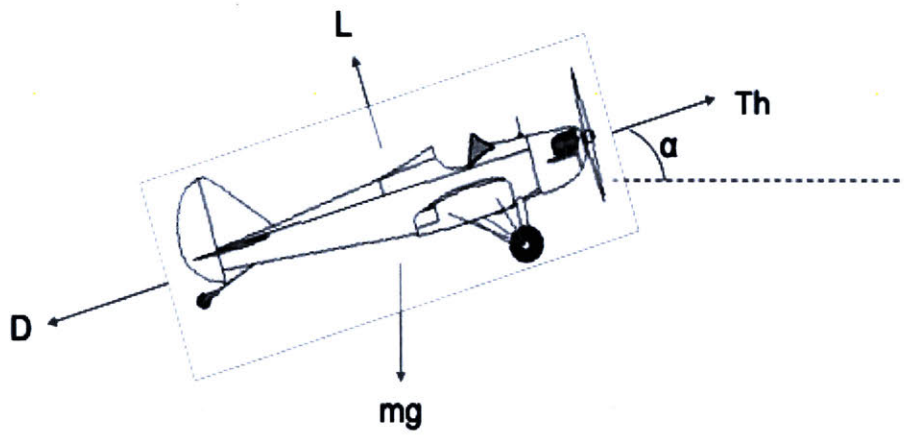


Figure 3-4: Free-body diagram of the aircraft during climb. Thrust force is parallel to the aircraft axis. Angle of attack is defined as the angle between the horizon and the aircraft axis.

The goal of the climb performance model is to determine the rate of climb that the aircraft can sustain from the end of takeoff to cruise altitude. Climb performance is based upon conservation of energy while maintaining static force balance on the aircraft during climb. For a given rate of climb, the rate of change in potential energy (PE) is:

$$\frac{d(PE)}{dt} = m_{aircraft} g \frac{dh}{dt} \tag{3.5}$$

The power dissipated by aerodynamic drag is the drag force multiplied by the flight velocity:

$$P_{drag} = \frac{1}{2} \rho S c_D v^3 \tag{3.6}$$

The total output thrust power of the aircraft is therefore the sum of the rate of potential energy change and power dissipated due to drag. This relationship is shown

in equation 3.7.

$$P_{thrust} = (Th)v = \frac{d(PE)}{dt} + P_{drag} \tag{3.7}$$

Required climb thrust and velocity are determined through solving the force-balance equations for the FBD in Figure 3-4. The set of force-balance equations at any point during climb are:

$$\sum F_x = (Th)\cos\alpha - D\cos\alpha - L\sin\alpha = 0 \tag{3.8}$$

$$\sum F_y = (Th)\sin\alpha + L\cos\alpha - D\sin\alpha - m_{aircraft}g = 0 \tag{3.9}$$

In equations 3.8 and 3.9, g is the gravitational constant (9.81 m/s^2), L is the lift force, defined according to the lift coefficient definition (equation 3.10), D is the drag force defined according to equation 3.2, and α is the angle of attack, defined as shown in Figure 3-4. For climb performance estimation, the drag coefficient is modeled as the sum of the zero-lift drag and induced drag, shown in equation 3.11. Furthermore, the rate of climb and forward velocity are linked through kinematics, shown in equation 3.12.

$$L = \frac{1}{2}c_L\rho S v_{aircraft}^2 \tag{3.10}$$

$$c_D = c_{D0} + \frac{c_L^2}{\pi AR} \tag{3.11}$$

$$\sin\alpha = \frac{dh/dt}{v} \tag{3.12}$$

The required climb thrust power profile is determined by discretizing the climb into sub-segments and solving Equations 3.5 through 3.12 to find the required angle of attack, velocity, and thrust power for each sub-segment. Once the climb thrust power profile is found, the total battery energy required to maintain the specified climb rate is calculated by integrating the difference between the required thrust power and

carbon-fuel thrust power (as previously mentioned, a parallel hybrid configuration is assumed) over the climb sub-segments (shown in 3.13).

$$E_{batt,req} = \int_0^{t_{climb}} (P_{climb} - P_{CF})dt \tag{3.13}$$

For climb performance estimation, the required battery energy is assessed against the battery energy available on the aircraft. If the required battery energy is larger than the available battery energy, the rate of climb is reduced; this process is iteratively repeated until the required and available battery energies are equal. The procedure to estimate the climb rate is illustrated in Figure 3-5.

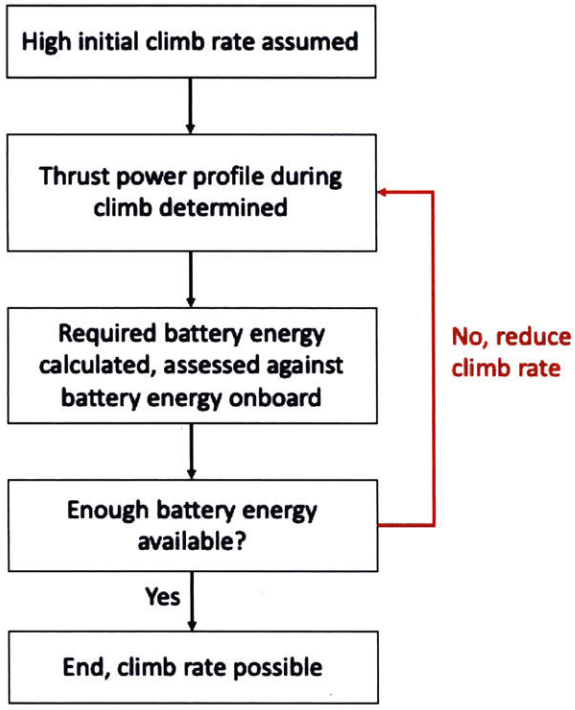


Figure 3-5: A procedure for determining climb rate given available battery energy

3.3.3 A model for cruise time estimation

Assumptions of the cruise performance model and justification for each are enumerated below:

1. Constant aerodynamic properties for the duration of cruise. Similar reasoning as

for takeoff and climb. Furthermore, the aircraft is designed to have its maximum lift-to-drag ratio during cruise.

2. For maximal cruise time determination, the velocity is determined through the coefficient of lift definition (equation 3.14); when the aircraft mass decreases due to carbon-fuel burn, velocity therefore decreases to maintain steady, level flight.

$$v_{aircraft} = \sqrt{\frac{2\ m_{aircraft}\ g}{c_L S \rho}} \tag{3.14}$$

3. For maximal cruise range determination, the velocity is assumed constant and the altitude (air density) varies to maintain a constant forward velocity. The required air density is determined through the coefficient of lift definition (equation 3.15).

$$\rho = \frac{2 m_{aircraft} g}{c_L S v_{aircraft}^2} \tag{3.15}$$

Operationally, the altitude is varied in-flight to meet this air density requirement.

4. Constant system component efficiency levels during cruise. Similar reasoning as for takeoff and climb. Furthermore, the operating point during cruise is assumed to be steady such that total source-to-propeller efficiency is constant.

5. Cruise power delivery is split between the EM(s) and carbon-fuel engine at a constant proportion; defined in equation 3.16. When there is insufficient battery energy to drive the EM, power is drawn from the carbon-fuel engine through the generator, if possible. The constant proportion is chosen according to the propeller area ratios attached to the EM(s) and carbon-fuel engine as this ensures maximum propulsive efficiency. This is because this power-split ensures that the theoretical (actuator disk) efficiency is equivalent between the two propellers. For example, the power proportion is set to 0.66 (2 to 1 power split) if the area ratio between the CF and EM propellers is 2.

$$\lambda = \frac{P_{propeller,CF}}{P_{propeller,total}} \tag{3.16}$$

For cruise performance estimation, the goal is to determine the time that an aircraft can maintain flight or the range that an aircraft can fly, depending on the goal of the mission. The aircraft is considered to have a static force balance during cruise, with zero net force in each direction. For steady flight, the magnitudes of thrust and drag and the magnitudes of lift and weight are approximately equal (dependent on the angle of attack). With a small angle of attack, the thrust power ($P_{thrust} = v_{aircraft}(Th)$) is approximately equal to the momentum power dissipated by drag (equation 3.6). To determine cruise time or range, it is necessary to link the cruise thrust power required to fuel consumption and battery energy usage.

Furthermore for cruise, the thrust power generated is the mechanical power on the shaft that drives the propeller, modified by the propeller efficiency, shown in equation 3.17.

$$\eta_{propeller} = \frac{P_{thrust}}{P_{driveshaft}} \tag{3.17}$$

For a parallel hybrid configuration, the drive shaft power is provided by either the carbon-fuel engine or EM and equal to the component output powers modified by the mechanical transfer efficiency ($\eta_{transfer}$). The rate of fuel consumption required to operate the carbon-fuel engine is the fuel power P_{fuel} consumed divided by the specific energy of the fuel e_{fuel} (shown in equation 3.18). Fuel power consumption P_{fuel} is equal to the power generated by the carbon-fuel engine $P_{carbon-fuel}$ divided by the thermal efficiency of the carbon-fuel engine ($\eta_{carbon-fuel}$).

$$\dot{m}_{fuel} = \frac{P_{fuel}}{e_{fuel}} = \frac{P_{carbon-fuel}}{\eta_{carbon-fuel}\ e_{fuel}} \tag{3.18}$$

In a parallel hybrid configuration, two loads are attached to the carbon-fuel engine, 1) the generator, and 2) the propeller. As a result, the carbon-fuel engine output power is the sum of the powers of these two components. The generator power consumption is dependent on the operation of the electric motor. If battery energy is used to provide power to the EM(s) P_{EM}, the generator power consumption $P_{generator}$ is zero; if there is insufficient battery energy available, the generator power $P_{generator}$

is set to provide sufficient power to make up the deficiency. This is encapsulated in equation 3.19, where η_{gen} is the generator efficiency, and η_{batt} is the battery efficiency. The energy transfer chain between the generator and EM(s) is shown in Figure 3-6.

$$P_{generator} = \frac{P_{EM} - P_{batt}}{\eta_{batt}\eta_{generator}} \tag{3.19}$$

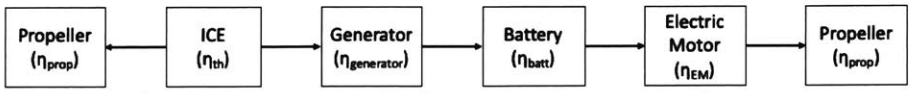


Figure 3-6: Energy transfer chain between the generator and electric motor(s).

With the steady thrust power requirement, the total power balance on the aircraft is:

$$P_{drag} = P_{thrust} = P_{propeller,CF} + P_{propeller,EM} \tag{3.20}$$

Substitution of equations 3.17, 3.19, and 3.20 into equation 3.18 yields the following:

$$\dot{m}_{fuel} = \frac{\frac{P_{thrust}\lambda}{\eta_{prop,CF}} + \frac{\frac{P_{thrust}(1-\lambda)}{\eta_{prop,EM}} - P_{batt}\eta_{EM}}{\eta_{generator}\eta_{batt}\eta_{EM}}}{\eta_{CF}e_{fuel}} \tag{3.21}$$

The corresponding battery energy usage is determined from Equation 3.22:

$$\frac{dE_{batt}}{dt} = \frac{P_{batt}}{\eta_{batt}} \tag{3.22}$$

Fuel consumption at any point during cruise can be determined through equation 3.21 with the assumptions outlined. To determine the cruise time or range achievable with a given amount of fuel and battery energy, an iterative approach is used along with equations 3.21 and 3.22.

Cruise time is determined by incrementally increasing time by a constant amount dt until the available fuel and battery energy reaches zero. With the assumptions taken, this generally results in battery energy depletion before fuel depletion (in-flight energy hybridization value reaches goes to zero during flight). For each increment, the

aircraft mass is reduced by the fuel mass burned in the preceding increment and the required cruise velocity and power are recalculated before equation 3.21 is updated. For the cruise range calculation, an identical process is implemented, except the cruise altitude is recalculated instead of velocity; the incremental range for each update is the product of dt and flight velocity.

3.4 Assessment of hybrid configurations

3.4.1 Hybrid configuration mass comparison

For mass comparison, component efficiency values are held constant between configurations along with payload and airframe masses to ensure consistency. Propulsion system components are sized such that the flight profile performance requirements are met. The EM and ICE specific powers are considered constant. For both configurations the ICE is sized such that it can meet the cruise power requirement independent of the EM. The reason is that carbon-fuel must be the sole cruise energy source due to low relative battery specific energy. Both the fuel and battery specific energies are considered constant.

Operation of the parallel configuration is as follows:

- To meet the takeoff distance requirement for takeoff, the ICE is operated up to its maximum power before the EM is utilized. If the required power output is higher than what the ICE can provide, the EM is operated to augment the ICE to meet the required power output. In these cases, the energy utilized by the EM is supplied by the batteries.

- For climb the ICE is again operated up to maximum power first in order to meet the required climb rate. Past this point, the EM is operated to meet the required rate. For these cases, the energy for the EM is supplied by the batteries.

- For cruise, the ICE drives the propeller it is attached to and the electric genera-

tor, which in turn sends power to the EM. The power split proportion between the ICE propeller and generator is set according to the propeller area ratios.

Operation of the series configuration is as follows:

- For all flight segments, the EM is operated such that the profile requirements are met. Power is supplied first via the ICE/generator; once the EM demand is greater than the capacity of the ICE/generator, energy is provided by the batteries.

The key difference between sizing of the two configurations is that the power that the parallel configuration can transfer to the environment is the sum of the EM and ICE power values while only the EM can transfer power to the environment in the series configuration. Therefore, for the parallel configuration, the EM can be sized to have a lower power output than the peak total power requirement, while for the series configuration the EM must be sized to meet the peak total power requirement.

The aircraft mass breakdown for the two configurations is shown in Table 3.2.

Configuration	Case 1	Case 2	Case 3	Case 4
Series	945.6 kg	974.9 kg	963.4 kg	1000.6 kg
Parallel	882.6 kg	911.9 kg	886.7 kg	917.0 kg
Difference	-6.7 %	-6.5 %	-8.0 %	-8.4 %

Table 3.2: Aircraft masses for the series and parallel hybrid configurations for the flight profile cases shown in Table 3.1

For all cases, the mass of the parallel hybrid configuration is lower than the series configuration with differences ranging from -6.5% to -8.4%. This reduction is primarily due to two reasons. First, since the ICE contributes directly to propulsive power output in the parallel configuration, the EM is smaller than it is in the series configuration. Second, the total thermal efficiency of the parallel configuration is higher than the total thermal efficiency of the series configuration, enabling a lower required fuel mass. The efficiency difference is elaborated in the next section.

3.4.2 Hybrid configuration fuel consumption evaluation

To evaluate the fuel consumption characteristics of each hybrid configuration, the power flow paths shown in Figures 3-2 and 3-3 are evaluated. In both cases a generic carbon-fuel engine is considered, denoted with the subscript CF. This is to emphasize that the results of this section are applicable to carbon fuel engines other than an ICE. For the series configuration, power has only one possible flow path from the fuel storage to the environment, so the total efficiency is the product of the efficiency of the components in the power flow chain:

$$\eta_{total} = \eta_{CF}\eta_{gen}\eta_{batt}\eta_{EM}\eta_{prop,EM} \tag{3.23}$$

The parallel hybrid configuration is similar to the series configuration in that there is an energy flow path from the carbon fuel stores and EM, but for a parallel configuration there is also a path directly from the CF engine to a propeller. With this additional energy flow path, the total efficiency is estimated from Equation 3.24. Note that it is assumed that EM and CF propeller efficiencies are equal in this case. Derivation of the total efficiency equation can be found in Appendix B. It can be seen that the total efficiency is set by the efficiencies of the two energy flow paths and power output of the CF engine and EM(s) relative to the total system power output.

$$\eta_{total} = \frac{\eta_{prop}\eta_{EM}\eta_{gen}\eta_{batt}\eta_{CF}}{\frac{P_{CF}}{P_{total}}\eta_{EM}\eta_{gen}\eta_{batt} + \frac{P_{EM}}{P_{total}}} \tag{3.24}$$

With the component efficiency values shown in Table 3.3, the series and parallel system efficiencies are calculated and compared in Table 3.4 for several different EM power proportions. Note that while efficiencies are considered constant here for all power-split cases, in general they are dependent on operating point.

From Table 3.4, it is seen that the parallel hybrid configuration has a superior total efficiency compared to the series configuration for all EM power proportions, with the difference decreasing for increasing EM power proportion. Note that the analysis assumes the propeller/fan propulsive efficiency remains constant with EM or CF engine power output. The difference in efficiencies is due to the energy flow

Component	Efficiency value
Electric motor	93 %
Electric generator	93 %
Battery	98 %
Carbon-fuel engine	30 %
Propeller	70 %

Table 3.3: Component efficiencies used for assessing hybrid configuration trade-offs

Configuration	$\frac{P_{EM}}{P_{total}} = 0$	$\frac{P_{EM}}{P_{total}} = 0.25$	$\frac{P_{EM}}{P_{total}} = 0.5$	$\frac{P_{EM}}{P_{total}} = 0.75$	$\frac{P_{EM}}{P_{total}} = 1.0$
Series	N/A	N/A	N/A	N/A	0.178
Parallel	0.210	0.201	0.193	0.185	0.178

Table 3.4: Hybrid configuration total system efficiencies for various ratios of EM to total power output. N/A indicates the value is not available. For a series configuration the output power is equal to the EM power only and cannot be some proportion of the total power.

path directly from the CF engine to the environment; with the assumed component efficiencies, the parallel flow path has a maximum higher relative efficiency of 18% compared to the series path.

3.4.3 Configuration integration flexibility

Integration flexibility refers to the ease of installing a propulsion system onto an airframe, given mass and volume constraints. There are several factors which affect integration flexibility:

- Whether or not components are restricted in their placement within the airframe.
- What type of connections each component has and how restrictive these connections are.

The primary mechanical difference between the parallel and series configurations is that the CF engine must be connected to the main drive shaft in the parallel configuration. Otherwise, the components are the same between the configurations.

Because of the drive shaft restriction in the parallel configuration, the CF engine must be in close proximity to the drive shaft and be connected mechanically through some mechanism. This is in contrast to the series configuration, where the CF engine can be placed anywhere along the fuselage as long as it is near the generator. Generator placement requirements are less restrictive than drive shaft location requirements as power from the generator can be sent to the batteries through wires/cables rather than a mechanical connection. Therefore in a traditional setup, the series configuration offers greater integration flexibility than the parallel configuration.

3.4.4 Transmission requirements

In some cases, gearing is necessary to enable an engine to drive a propeller/fan by allowing the engine and propeller torque and speed characteristics to match more closely. The need for gearing is evaluated qualitatively for series and parallel configurations.

The need for a transmission between a CF engine and propeller/fan is well-documented, with transmission requirements typically dependent on propulsion system scale. However, in most cases a transmission is necessary or beneficial for increasing efficiency or power transfer to the environment. This need is illustrated in Figure 3-7 by superimposing the operating curve of a propeller onto the operation map of an internal combustion engine (ICE). Both the operating curve and operation map are functions of output torque and rotational velocity. The system can operate at any point along the propeller operating line while it is within the ICE operating map. Due to the maximum operating envelope of the ICE, the maximum power output is achieved at a single point and therefore the propeller operating curve must pass through this point for the system to leverage the maximum power output of the ICE.

In most cases, the propeller operating curve will not match the CF engine and a transmission is used to shift the operating curve such that the operating curve goes through the maximum power point of the CF. The transmission effect is shown Figure 3-8.

In contrast to CF engines, most electric motors are able to leverage their maximum

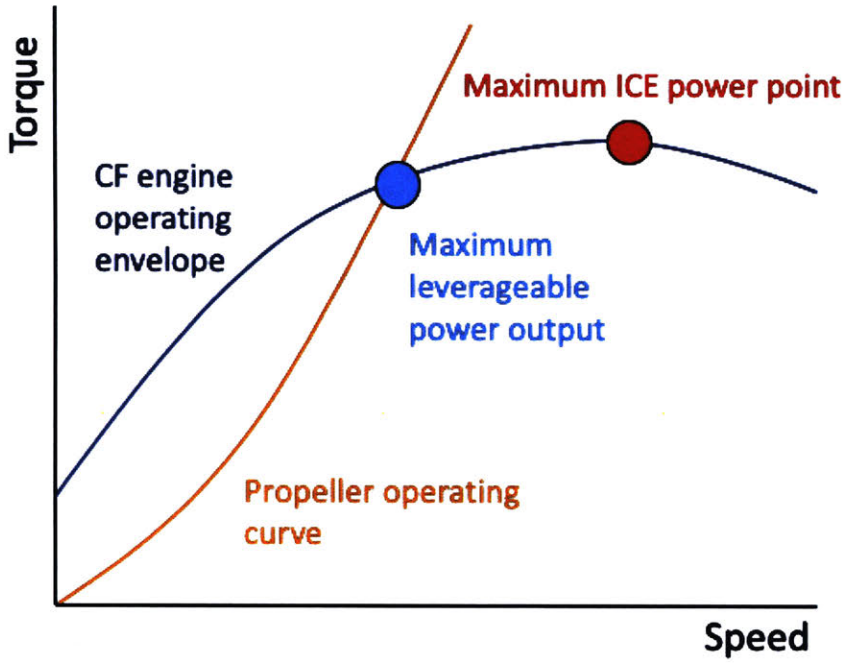


Figure 3-7: Illustration of a propeller operating curve and ICE operating map. The propeller operating curve does not match well with the ICE so the maximum power output of the ICE-propeller system is limited.

power output across a wide range of rotational speeds, with torque decreasing as rotational speed increases. With a relatively large constant power region, the EM is more likely that a propeller's operating curve will pass through this region without modification. This advantage of electric motors is illustrated in Figure 3-9.

Out of the two hybrid configurations, the parallel configuration has one additional mechanical connection compared to the series configuration: the propeller connection to the CF; all other mechanical connections are similar. From the propeller matching phenomenon illustrated in Figures 3-7 to 3-9, it can be reasoned that the potential need for a transmission in the parallel configuration is higher, mainly between the CF engine and its propeller. The size and choice of the transmission in this case follows similar reasoning as to traditional propulsion systems.

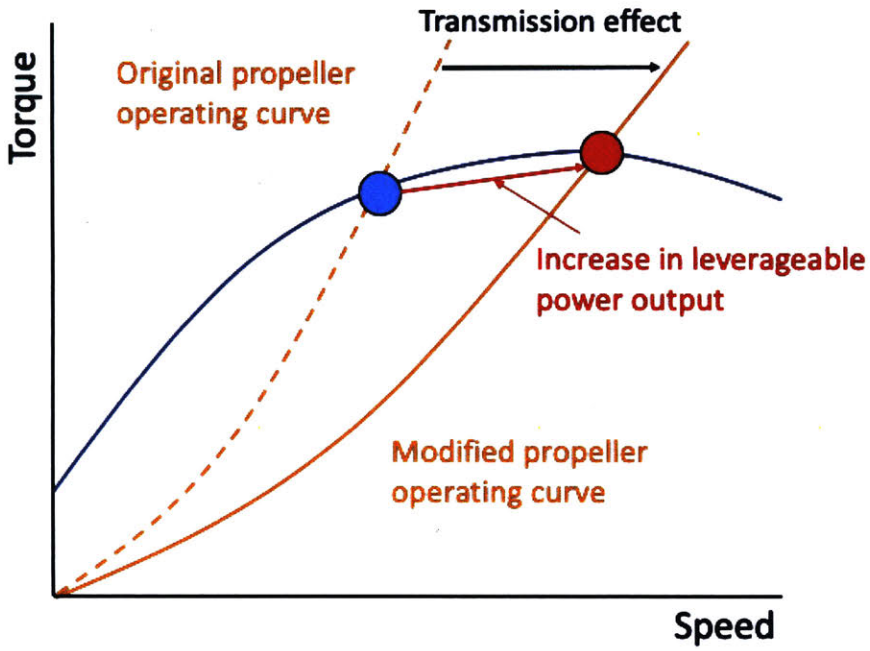


Figure 3-8: Illustration of a propeller operating curve modified by a transmission. The transmission shifts the shape of the propeller operating curve such that it intersects the maximum power point of the ICE, enabling the system to leverage its maximum power output.

3.4.5 Hybrid configuration performance evaluation

Based upon the evaluation criteria and comparisons detailed in the previous sections, a parallel hybrid configuration was chosen to be the focus of thesis research for the following reasons:

- Parallel hybrid propulsion system mass is lower than series propulsion system mass by enabling the CF engine to provide propulsive power in addition to generating electrical energy. Mass reductions of 5-8 % are possible.

- Parallel hybrid configuration total system efficiency is higher than the series configuration, with the difference dependent the proportion of total power sent directly to the propeller from the CF engine. The relative difference in efficiencies is dependent on the efficiency of the electrical components between the CF and EM propeller. With representative values of generator, battery and electric motor efficiencies, the relative difference is up to 18%.

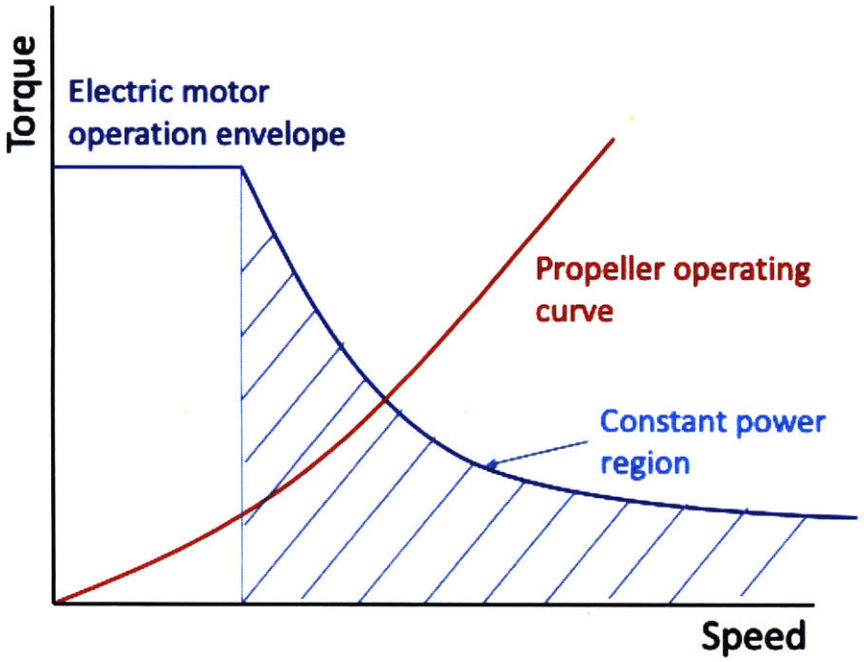


Figure 3-9: Illustration of a propeller operating curve and EM operating map. EMs have a wide constant maximum power range, so it is more probable that a propeller-EM system can leverage its maximum power output without the use of a transmission.

- Although the series hybrid configuration has greater integration flexibility and lower potential transmission requirements, the parallel hybrid configuration can mitigate deficiencies in these areas with appropriate design and component choice/matching respectively.

3.5 Large UAV retro-fit comparison analysis

A large UAV platform is utilized to evaluate MHPS performance against traditional propulsion system performance, as these aircraft typically have high performance flexibility requirements. For a consistent comparison between traditional and modular hybrid propulsion systems, a retro-fit case is considered; here the performances of a traditional propulsion system and MHPS are compared against each other when they are integrated onto the same airframe, with the same payload. The airframe and payload masses considered are 350 kg and 150 kg respectively. Fuel mass is

held constant for the two configurations at 70 kg. For both propulsion systems a pusher-puller propeller configuration is considered. A diagram of the MHPS retro-fit component layout can be seen in Figure 3-10, in which one propeller is driven by an internal combustion engine and the other is driven by an electric motor. The ICE and EM are mechanically separated as this allows each propeller to be matched with ICE and EM independently and avoids the matching issues between the ICE and EM that would arise if they were on the same mechanical shaft. The propellers are therefore assumed to have a constant efficiency during each flight segment and constant between each other. In practice this would be unlikely due to the large power discrepancy and operational aspects of the ICE and EM. An electrical connection exists between the EM and ICE through a generator, battery, and power electronics (denoted by PE in this case). A generator is considered to ensure that the electrical generation capacity is sufficient; it is further assumed that the capacity of the alternator that is typically a part of the ICE is negligible.

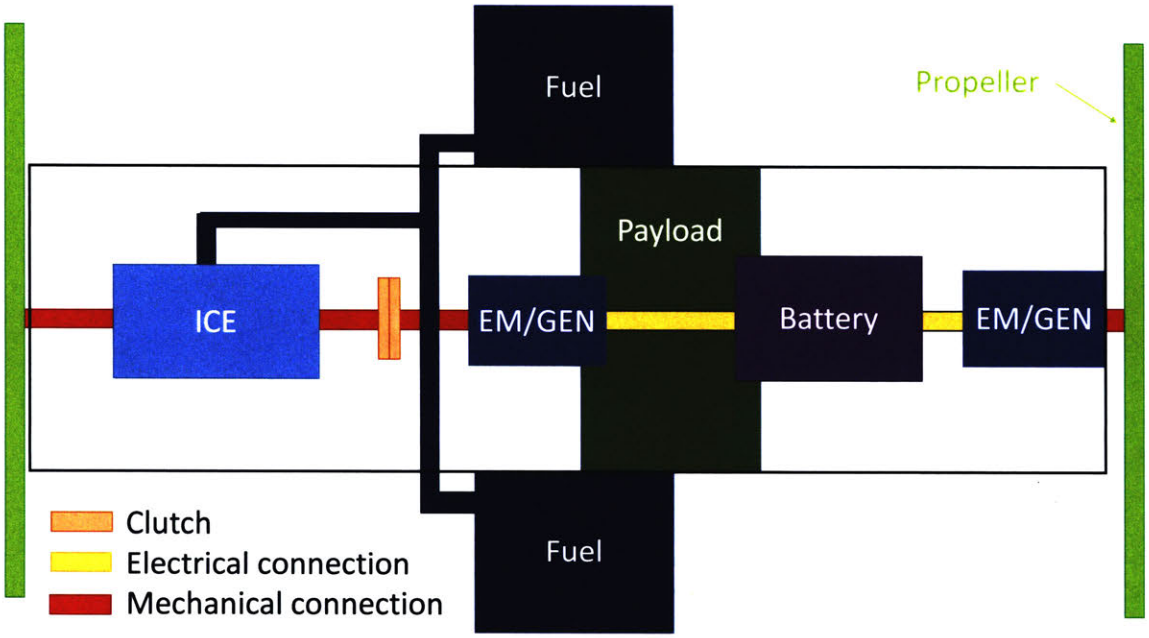


Figure 3-10: Diagram of MHPS retro-fit configuration. A pusher-puller propeller configuration is considered, one of which is driven by an internal combustion engine and one of which is driven by an electric motor. A generator/battery connects the ICE and EM.

Off-the-shelf components are considered for use in both the traditional and mod-

ular hybrid propulsion systems. Rationale for component choices are detailed in Appendix C. Chosen components are shown in Table 3.5. Component masses and performances are tabulated in Table 3.6. In this case, the main difference in components is that an ICE in the traditional system is replaced by a battery pack, EM, generator, and motor controllers in the MHPS.

Component type	MHPS	Traditional
ICE(s)	1x Mercedes OM660	2x Mercedes OM660
EM(s)	1x YASA P400	N/A
Battery	Kokam Ultra-high energy pack	N/A
Generator	1x YASA P400	N/A
Controller(s)	2x YASA controllers	N/A

Table 3.5: List of primary propulsion system components for the MHPS retro-fit and traditional propulsion system. Form factors are shown in Figure 3-11

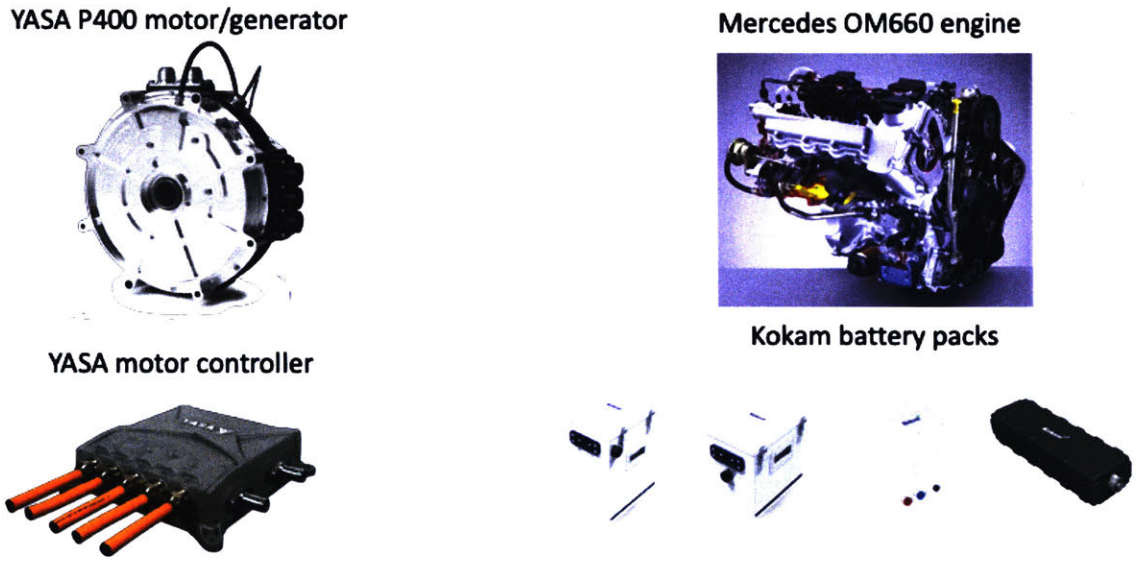


Figure 3-11: Off-the-shelf component form factors used in the retro-fit analysis. YASA P400 from [36], YASA motor controller from [37], Mercedes OM660 from [1] and Kokam battery pack from [21].

The aircraft with the MHPS and the traditional propulsion system are assessed against each other on three metrics:

- Maximum cruise time achievable at 4000 m altitude

Component name	Mass	Performance
Mercedes OM660	65 kg	40 kW
YASA P400	24 kg	160 kW peak, 100 kW continuous
Kokam Ultra-high energy pack	36.8 kg	186 Wh/kg
YASA Controller	5 kg	N/A

Table 3.6: Propulsion system component performances and masses

- Minimum takeoff distance at sea level. For the MHPS, EM peak power output is used.
- Maximum average rate of climb from sea level to 4000 m altitude.

3.5.1 Large UAV retro-fit performance evaluation

The performances of the MHPS and traditional propulsion system aircraft and relative differences are tabulated in Table 3.7.

Performance metric	MHPS	Traditional	Difference
Total aircraft mass	722.3 kg	713.7 kg	+1.2 %
Takeoff distance	75.2 m	219.3 m	-65.8 %
Average climb rate	1.13 m/s	3.72 m/s	-69.6 %
Cruise time	14.9 hrs	15.9 hrs	-6.8%

Table 3.7: Performance values and comparison of the MHPS and traditional propulsion system aircraft

Comparison of the aircraft performance metrics shows that the use of a MHPS with the specified components has the following performance impacts:

- Total aircraft mass increases slightly by 1.2 % due to the difference in mass between the electrical components and the single ICE that they replace.
- Takeoff distance decreases significantly by 65.8 % due to the increased peak power output of the MHPS compared to the traditional propulsion system.
- Climb rate decreases significantly by 69.6 % due to limited battery capacity, which limits average EM power output during climb.

- Cruise time decreases slightly by 6.8 % for two reasons. First, the MHPS aircraft mass is higher and second, the total efficiency is lower for the MHPS due to the use of the energy flow path from the ICE to the EM driven propeller.

From the performance comparison, it can be seen that the use of a hybrid propulsion system with the technology considered in large UAVs results in vastly superior takeoff performance at the cost of reduced climb rate, a slight increase in aircraft mass, and slight reduction in cruise time. The hybrid performance deficiencies can be mitigated through improvements in electrical component technology. For example, battery specific energy improvements can either directly improve climb rate performance (if battery mass is held constant) or decrease aircraft mass (if battery energy is held constant).

To determine the potential for further takeoff performance improvements achievable with modularity, the MHPS was modified by trading 24 kg of fuel mass for an additional electric motor. The total aircraft mass is thus held constant through this exchange. The modified MHPS aircraft performance compared against the original MHPS aircraft performance is shown in Table 3.8.

Performance metric	MHPS original	MHPS modified	Difference
Total aircraft mass	722.3 kg	722.3 kg	0.0 %
Takeoff distance	75.2 m	39.8 m	-47.1 %
Average climb rate	1.13 m/s	1.13 m/s	-0.0 %
Cruise time	14.9 hrs	10.1 hrs	-32.3 %

Table 3.8: Performance values and comparison of the MHPS with and without the additional EM

Trading fuel mass for an additional EM results in a further 47.1 % reduction in takeoff distance at a cost of 32.3 % in cruise time. This example illustrates the potential benefits of a modular propulsion system - with the ability to interchange components with a mass of 3.3 % (24 kg) of aircraft mass, aircraft performance can be modified significantly.

3.6 Summary

Aircraft performance evaluation is based on four metrics: takeoff distance, climb rate, cruise time, and aircraft mass. Modeling of aircraft performance has been formulated using physical relations such as Newton's Second Law and energy conservation to ensure applicability for all scale of aircraft.

Tradeoffs between the series and parallel hybrid configurations were examined in four areas: total aircraft mass for equivalent performance, total efficiency/fuel consumption, airframe integration requirements, and transmission/gearing requirements. The parallel configuration was found to be superior in the areas of aircraft mass and efficiency, while a series configuration was found to be slightly superior in the areas of integration and transmission/gearing. A parallel configuration was chosen to be the focus of the large UAV performance evaluation moving forward due to the mass and efficiency benefits. Nevertheless, the framework is applicable equally to other aircraft, configurations, and scales.

The large UAV platform used to evaluate MHPS performance has a pusher-puller propeller configuration, with one propeller driven by an ICE and the other driven by an EM. MHPS performance was assessed against a traditional propulsion system utilizing two ICEs in the same airframe and propeller configuration. Two MHPS component sets were examined, one with a single EM and the other with two EMs, with a reduction in fuel mass equal to the additional EM mass. Comparison of aircraft performances revealed that hybridization with current (2018) technology results in increased takeoff performance at the cost of reduced climb rate and slightly reduced cruise time performance. By interchanging one EM for fuel mass in the MHPS, takeoff distance can be further reduced at the cost of cruise time. This tradeoff is accomplished by altering a relatively small (3.3 %) amount of total aircraft mass, showing the potential of the MHPS.

The MHPS performance evaluation results are confined to the single large UAV platform. To generalize MHPS performance to other aircraft scales, a set of performance relationships that are applicable to all scales are required. These are developed

and elaborated in the chapter that follows.

Chapter 4

Functional dependence of MHPS performance on hybridization and modularity levels

4.1 Introduction

The MHPS performance results presented in Section 3.5.1 are limited to a single large UAV configuration. To generalize the large UAV performance results to other aircraft scales, a first principles approach for evaluating aircraft performance is required. Quantitative relationships between aircraft performance and propulsion system design choices and component technology levels are established in this manner. In this chapter, performance relationships are first developed for a hybrid propulsion system, followed by incorporating modularity to extend the relationships to a MHPS.

4.2 Hybrid propulsion system performance relationships

Hybrid performance relationships are developed for takeoff, climb, and cruise flight segments. Payload capacity is additionally considered. Focus is placed upon estab-

lishing the functional dependence of hybrid component technological parameters and design choices on aircraft performance. The primary technological parameters that affect hybrid propulsion system performance are:

- Electric motor specific power, $\pi_{EM} = \frac{P_{EM}}{m_{EM}}$
- Carbon fuel engine specific power $\pi_{CF} = \frac{P_{CF}}{m_{CF}}$
- Electric motor efficiency, η_{EM}
- Carbon fuel engine efficiency η_{CF}
- Battery specific energy e_{EM}
- Carbon fuel specific energy e_{fuel}

Propulsion system design choices utilized are:

- Total aircraft mass proportion of the hybrid engine, $\frac{m_{EM}+m_{CF}}{m_{total}}$
- Total aircraft mass proportion of the energy storage system, $\frac{m_{battery}+m_{fuel}}{m_{total}}$
- Electric energy hybridization factor $H_E = \frac{E_{battery}}{E_{battery}+E_{fuel}}$
- Electric power hybridization factor $H_P = \frac{P_{EM}}{P_{EM}+P_{CF}}$

4.2.1 Takeoff performance relationship for hybrid propulsion systems

The assumptions taken for formulating the takeoff performance relationship are as follows:

1. Takeoff occurs once the aircraft has reached stall velocity with the takeoff lift coefficient value. $v_{stall} = v_{TO} = \sqrt{\frac{2\ m_{total}\ g}{\rho_{TO} S c_{LTO}}}$
2. Aircraft mass remains constant through the takeoff run.

3. The aircraft propulsion power conversion efficiency, defined as $\eta_{convert} = \frac{\frac{d(KE_{aircraft})}{dt}}{P_{total}}$, where KE refers to the kinetic energy of the aircraft, is constant through takeoff. Power conversion efficiency is used to allow for integrated propulsion system-airframe architectures, for which the delineation between thrust and drag is indistinguishable. Use of power conversion efficiency avoids the need to delineate between thrust and drag.

The above assumptions allow conservation of energy for the aircraft to be written as:

$$\frac{d(KE_{aircraft})}{dt} = m_{total} v \frac{dv}{dt} = P_{total} \eta_{convert} \tag{4.1}$$

Upon rearranging, substitution, and integration, the resulting takeoff performance relationship is found and shown in Equation 4.2. Full derivation of the takeoff performance relationship can be found in Appendix A.

$$\frac{\Delta R \left(\frac{m_{propSystem}}{m_{total}}\right)}{\left(\frac{m_{total}}{S}\right)^{\frac{3}{2}} \left(\frac{2g}{\rho}\right)^{\frac{3}{2}}} = \frac{1}{3} \frac{1}{{c_{LTO}}^{\frac{3}{2}}} \frac{1}{\eta_{convert}} \left(\frac{(1 - H_P)}{\pi_{CF}} + \frac{H_P}{\pi_{EM}}\right) \tag{4.2}$$

The left hand side (LHS) of the takeoff performance relationship (referred to as the takeoff distance scaling group) shows the following takeoff distance (ΔR) scaling effects:

- The propulsion system mass ratio $\frac{m_{propSystem}}{m_{total}}$ has a inverse relationship on takeoff distance.

- The wing loading $\frac{m_{total}}{S}$ has a superlinear proportional scaling effect on the takeoff distance. Superlinear refers to the fact that an increase in wing loading will have a greater than one-to-one increase on the takeoff distance.

- The takeoff lift coefficient c_{LTO} has a superlinear inverse scaling effect on the takeoff distance.

- The propulsion power conversion efficiency has an inverse relationship with takeoff distance.

The above scaling effects are clear from the formulation of Equation 4.2. Furthermore, these effects are not limited to hybrid propulsion systems, holding for traditional propulsion systems and thus well-known. However, the effects of CF engine and EM specific power (π_{CF} and π_{EM} respectively) and power hybridization factor H_P on takeoff distance are less clear. To illustrate the functional dependence of the takeoff distance scaling group on these parameters, several parametric curves for various values of EM to CF engine specific power ratio and power hybridization are shown in Figure 4-1. All parameters on the right hand side (RHS) of equation 4.2 are held constant with the exception of EM and CF engine specific powers (π_{EM} and π_{CF}) and power hybridization factor H_P.

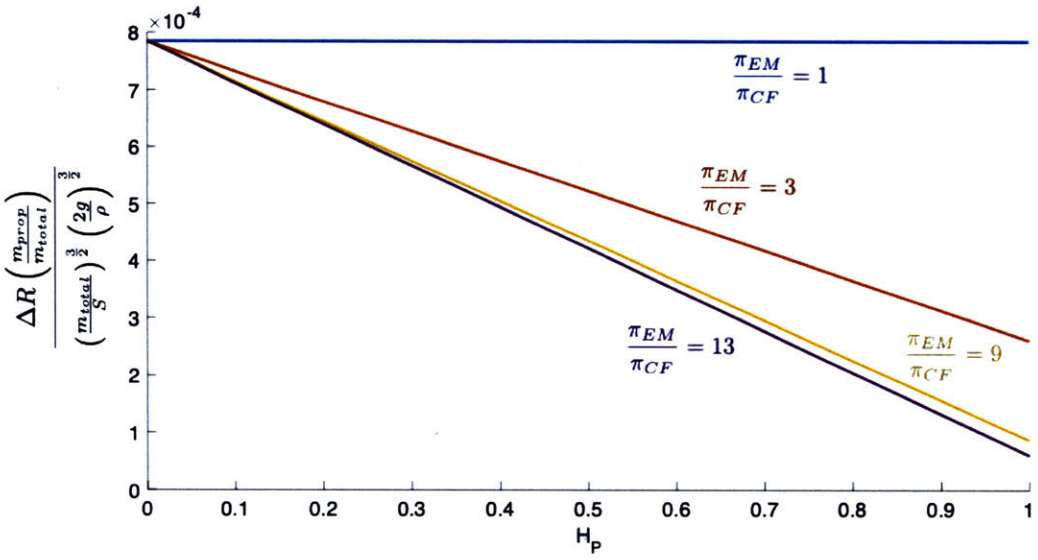


Figure 4-1: Parametric curves of the takeoff performance relationship shown in 4.2 as a function of power hybridization factor H_P for various ratios of EM to CF engine specific power. Ratios of 1, 3, 9, and 13 are chosen as they are representative of current (2018) ratios between EMs and turbofans, small turbine generators, internal combustion engines and between future EMs and ICEs respectively.

The takeoff distance scaling group is dependent on the relative level of EM technology compared to CF engine technology as shown in Figure 4-1. With higher EM specific power π_{EM} (relative to CF engine specific power π_{CF}), increases in H_P results in decreases in the the takeoff distance scaling group (LHS of equation 4.2). This is because increases in H_P will result in increases in total aircraft specific power, $\frac{P_{total}}{m_{total}}$

when EM specific power is greater than CF engine specific power $\pi_{EM} > \pi_{CF}$. When the CF engine specific power is greater than EM specific power ($\pi_{CF} > \pi_{EM}$), the trend is reversed, with increases in H_P resulting in increases in the takeoff distance scaling group. When specific powers are equal ($\pi_{EM} = \pi_{CF}$), the takeoff distance scaling group is independent of H_P. The second dependency that is apparent is that the rate of takeoff distance scaling group reduction with H_P is dependent on the value of specific power ratio $\frac{\pi_{EM}}{\pi_{CF}}$. Furthermore, from one parametric curve to another, the relative change is dependent on the relative increase in specific power ratio $\frac{\pi_{EM}}{\pi_{CF}}$. For example, from Figure 4-1 for a H_P value of 0.5, increasing the specific power ratio from 1 to 3 (200 % increase) reduces the takeoff distance scaling group by 35%. Further increasing the specific power ratio from 3 to 9 (200% increase) only reduces the takeoff distance scaling group by another 20%. This implies that to marginally reduce the value of the takeoff scaling distance group, the required marginal increase in specific power ratio is larger when the current specific power ratio is larger.

Effect of battery specific power

For a hybrid or an electrified aircraft propulsion system, the peak power output of the EM is typically utilized during takeoff. The battery pack is required to output the same power as the EM to enable the EM to operate in this condition. With a given battery size, this translates to a requirement on the battery pack specific power. From equation 4.2, a battery specific power requirement in terms of takeoff distance and design parameters can be derived:

$$\pi_{batt} = \frac{1}{3}\left(\frac{m_{total}}{m_{batt}}\frac{1}{\eta_{convert}}\right)\frac{1}{\Delta R_{takeoff}}\left(\frac{m_{total}}{S}\right)^{3/2}\left(\frac{2g}{\rho}\right)^{3/2}\frac{1}{c_L^{3/2}} - \frac{P_{CF}}{m_{batt}} \tag{4.3}$$

Equation 4.3 specifies the required battery specific power for a given takeoff distance requirement and battery mass. If this requirement is larger than the actual battery specific power capability, the battery mass needs to be increased until the requirement is met. Otherwise, the takeoff distance requirement needs to be relaxed.

To account for the value of battery specific power when utilizing equation 4.2, an "effective EM specific power" can be utilized in the analysis, defined in equation 4.4.

$$\pi_{EM,effective} = \frac{\pi_{EM}\pi_{batt}}{\pi_{EM} + \pi_{batt}} \tag{4.4}$$

4.2.2 Climb rate performance relationship for hybrid propulsion systems

The assumptions for the climb rate scaling relationship are the following:

1. Climb is steady-state, with a constant climb velocity, v_{climb}.
2. The carbon-fuel engine's power output is sufficient to overcome aerodynamic drag during steady-state climb.

$$P_{CF}\eta_{CF,flow} \geq P_{drag} = \frac{1}{2}\rho S c_{D,climb} {v_{climb}}^3 \tag{4.5}$$

3. Aircraft mass is constant during climb.

The climb rate performance relationship is determined from conservation of energy of the aircraft during climb. For climb, there is a balance between the propulsive power provided by the propulsion system, the rate of kinetic energy dissipated by drag, and increase in aircraft potential energy. This relationship is shown in Equation 4.6.

$$\frac{d(PE)_{aircraft}}{dt} = (m_{aircraft})g\frac{dh}{dt} = P_{propulsive} - P_{drag} \tag{4.6}$$

The propulsive power is the sum of powers derived from the carbon-fuel and battery stores on the aircraft for both series and parallel hybrid configurations, with the difference being the power flow path(s). Therefore:

$$P_{propulsive} = P_{fuel}\eta_{CF,flow} + P_{batt}\eta_{EM,flow} \tag{4.7}$$

Battery energy required for climb can be found by combining equations 4.6 and 4.7, and integrating over the climb time. The resulting battery energy requirement

relationship is shown in Equation 4.8. The key assumption is that the CF engine provides just enough power to overcome drag power dissipation. Full details of the derivation can be found in Appendix A.

$$E_{batt} = \frac{m_{aircraft} g \Delta h}{\eta_{EM} \eta_{batt} \eta_{EM,prop}} \tag{4.8}$$

From the climb performance relationship, it can be seen that under the assumptions taken, the battery energy required for climb is independent of the climb rate. This is because an increased climb rate has two effects: first, the required power increases and second, the time for climb decreases for a constant climb altitude change. These two effects counteract, resulting in battery energy becoming independent of climb rate. It is also apparent that the required battery energy is only dependent on aircraft mass and change in climb altitude. This is because with the assumption that CF engine power is greater or equal to drag power dissipated, the EM sub-system is responsible for generating the potential energy of the aircraft. Therefore the EM sub-system essentially converts battery chemical energy into aircraft potential energy during climb.

Equation 4.8 can be modified to generate a battery specific energy requirement by dividing through by the battery mass:

$$e_{batt} = \frac{\frac{m_{aircraft}}{m_{batt}} \, g \, \Delta h_{climb}}{\eta_{EM} \eta_{batt} \eta_{EM,prop}} \tag{4.9}$$

Equation 4.9 specifies the minimum battery specific energy required to complete climb with a pre-specified battery mass ratio. If battery specific energy is below this value, battery size must be increased until the requirement is met.

4.2.3 Cruise time performance relationship for hybrid propulsion systems

The assumptions taken for the cruise performance relationship formulation are the following:

1. Cruise power is derived from the carbon-fuel stores and battery pack separately. Cruise time or range is the sum of the times or ranges that are derived from these energy stores.

2. Aircraft aerodynamic characteristics are constant during cruise, namely the lift and drag coefficients.

3. For the cruise time performance relationship, it is assumed that the aircraft travels at stall velocity at all time where $v_{cruise} = \sqrt{\frac{2(m_{aircraft})g}{\rho S c_L}}$. Cruise altitude is held constant.

4. For the cruise range performance relationship, the cruise velocity is held constant and cruise altitude changes to maintain steady cruise. In this case, $\rho = \frac{2m_{aircraft}g}{Sc_L v^2}$.

Cruise range and time performance are considered here but only the derivation of the cruise time performance relationship is outlined for brevity. Cruise range scaling follows a similar thought process and the full derivation can be found in Appendix A.

In accordance with assumption 1, the cruise time relationship with fuel mass and battery energy are derived independently, and then summed together to recover the total cruise time. For both the fuel mass and battery energy contributions, conservation of energy and mass are invoked to derive the resulting scaling relationships. Conservation of energy dictates the fuel/battery energy depletion rate required to maintain cruise at any point in time:

$$\frac{dE_{source}}{dt} = \frac{P_{propulsive}}{\eta_{flow}} \tag{4.10}$$

Note that in Equation 4.10 η_{flow} refers to either $\eta_{CF,flow}$ or $\eta_{EM,flow}$ depending on the energy source. The propulsive power required $P_{propulsive}$ is equal to the momentum power dissipated due to aerodynamic losses, which is referred to as the propulsive anergy generation rate and denoted as $\dot{A}^*$. In traditional formulations, this value is equal to the drag power $P_{drag} = 1/2\rho S c_D v^3$.

For the fuel mass contribution, energy usage is directly tied to changes in mass:

$$\frac{dm_{fuel}}{dt} = -\frac{\frac{dE_{fuel}}{dt}}{e_{fuel}} \tag{4.11}$$

Combination of Equations 4.10 and 4.11 and integration over the available fuel mass yields the following contribution to cruise time from the fuel stores (full derivation details are found in Appendix A):

$$\Delta t = 2\eta_{CF,flow} e_{fuel} \frac{\sqrt{\rho S}}{g^{3/2}} \frac{L^{3/2}}{\dot{A}^* \sqrt{\rho S}} \left(\frac{1}{\sqrt{m_{fixed}}} - \frac{1}{\sqrt{m_{fixed} + m_{fuel}}} \right) \tag{4.12}$$

Note that the fixed mass refers to all of the mass on the aircraft that is fixed during flight, $m_{fixed} = m_{total} - m_{fuel}$. Furthermore the subscript "flow" denotes that total efficiency from source to thrust power. For example, $\eta_{CF,flow}$ denotes the product of CF engine and CF propeller efficiencies ($\eta_{CF}\eta_{prop,CF}$) while $\eta_{EM,flow}$ denotes the product of EM, EM propeller, battery, generator, and CF engine efficiencies ($\eta_{CF}\eta_{gen}\eta_{batt}\eta_{EM}\eta_{prop,EM}$) if energy is derived from CF. On the other hand if energy is derived from the batteries, $\eta_{EM,flow}$ refers to the product of EM, EM propeller, and battery ($\eta_{batt}\eta_{EM}\eta_{prop,EM}$).

For the cruise time contribution due to battery energy, aircraft mass remains constant, which yields the following cruise time contribution:

$$\Delta t = \frac{E_{batt}\eta_{EM,flow}}{\frac{\dot{A}^*}{L^{3/2}}(mg)^{3/2}} \tag{4.13}$$

In Equation 4.13, the aircraft mass m, is considered constant and must be specified. In this thesis, $m = m_{fixed}$ because usage of m_{fixed} is the lowest possible value of aircraft mass during cruise (after all the carbon fuel has been used). This maximizes the cruise time in Equation 4.13, which is an upper bound (optimistic) estimate for the cruise time contribution from battery energy. The implicit assumption is that fuel is used only until depleted, followed by battery usage only until depleted. Operation of a hybrid propulsion system is generally impossible because it would require the EM provide propulsive power by itself, which is only possible for certain hybrid

configurations. The implicit assumption is taken to show the ideal potential of a hybrid propulsion system and limited to this chapter. For situations where a reserve of fuel mass is required at the end of cruise, the fixed mass could be augmented by the required reserve fuel mass ($m_{fixed,new} = m_{fixed} + m_{fuel,reserve}$).

Combining Equations 4.12 and 4.13, and rearranging yields the final cruise time performance relationship:

$$\frac{\Delta t_{cruise} g^{3/2} \sqrt{\frac{m_{total}}{S}}}{\frac{L^{3/2}}{\dot{A}^* \sqrt{\rho S}} e_{fuel} \eta_{CF,flow} \sqrt{\rho}} = 2\left(\sqrt{\frac{1}{1-\frac{m_{fuel}}{m_{total}}}} - 1\right) + \frac{\eta_{EM,flow}}{\eta_{CF,flow}} \frac{e_{batt}}{e_{fuel}} \sqrt{\frac{1}{1-\frac{m_{fuel}}{m_{total}}}} \left(\frac{\frac{m_{batt}}{m_{total}}}{1-\frac{m_{fuel}}{m_{total}}}\right) \tag{4.14}$$

Note that the term $\frac{L^{3/2}}{\dot{A}^* \sqrt{\rho S}}$ (referred to as the "lift-anergy scaling group") is utilized because it allows power dissipation to be defined independent of thrust/drag accounting. In the traditional formulation of $\dot{A}^* = P_{drag}$, $\frac{L^{3/2}}{\dot{A}^* \sqrt{\rho S}} = \frac{{c_L}^{3/2}}{c_D \sqrt{2}}$, which is non-dimensional (derivation can be found in Appendix A). Defining the ratio of battery mass to total energy storage system mass as in Equation 4.15, Equation 4.14 can be rewritten as Equation 4.16.

$$r_m = \frac{m_{batt}}{m_{batt} + m_{fuel}} = \frac{m_{batt}}{m_{ESS}} \tag{4.15}$$

$$\frac{\Delta t_{cruise} g^{3/2} \sqrt{\frac{m_{total}}{S}}}{\frac{L^{3/2}}{\dot{A}^* \sqrt{\rho S}} e_{fuel} \eta_{CF,flow} \sqrt{\rho}} = 2\left(\sqrt{\frac{1}{1-(1-r_m)\frac{m_{ESS}}{m_{total}}}} - 1\right) + \frac{\eta_{EM,flow}}{\eta_{CF,flow}} \frac{e_{batt}}{e_{fuel}} \frac{r_m \frac{m_{ESS}}{m_{total}}}{\left[1-(1-r_m)\frac{m_{ESS}}{m_{total}}\right]^{3/2}} \tag{4.16}$$

From Equation 4.16, several direct scaling functionalities are apparent for the cruise time scaling group (LHS of Equation 4.16). First, the lift-anergy scaling group, fuel specific energy e_{fuel}, and CF flow efficiency $\eta_{CF,flow}$ have a direct proportional scaling effect on cruise time, so a 10 % increase in any of these values will result in a 10 % increase in cruise time (assuming the RHS of Equation 4.16 is held constant). Second, the wing loading $\frac{m_{total}}{S}$ and air density ρ have opposite sub-linear (less than a one to one change) scaling effects on the cruise time. To investigate the effects

of fuel mass ratio $\frac{m_{fuel}}{m_{total}}$, battery mass ratio $\frac{m_{batt}}{m_{total}}$, and the non-dimensional group $\frac{\eta_{EM,flow}}{\eta_{CF,flow}} \frac{e_{batt}}{e_{fuel}}$ (referred to as the specific energy extraction ratio), parametric curves of the cruise time scaling group against battery mass ratio are plotted in Figure 4-2 for various values of the specific energy extraction ratio. The proportion of battery mass is varied while the ESS mass (sum of the battery and fuel masses) is held constant.

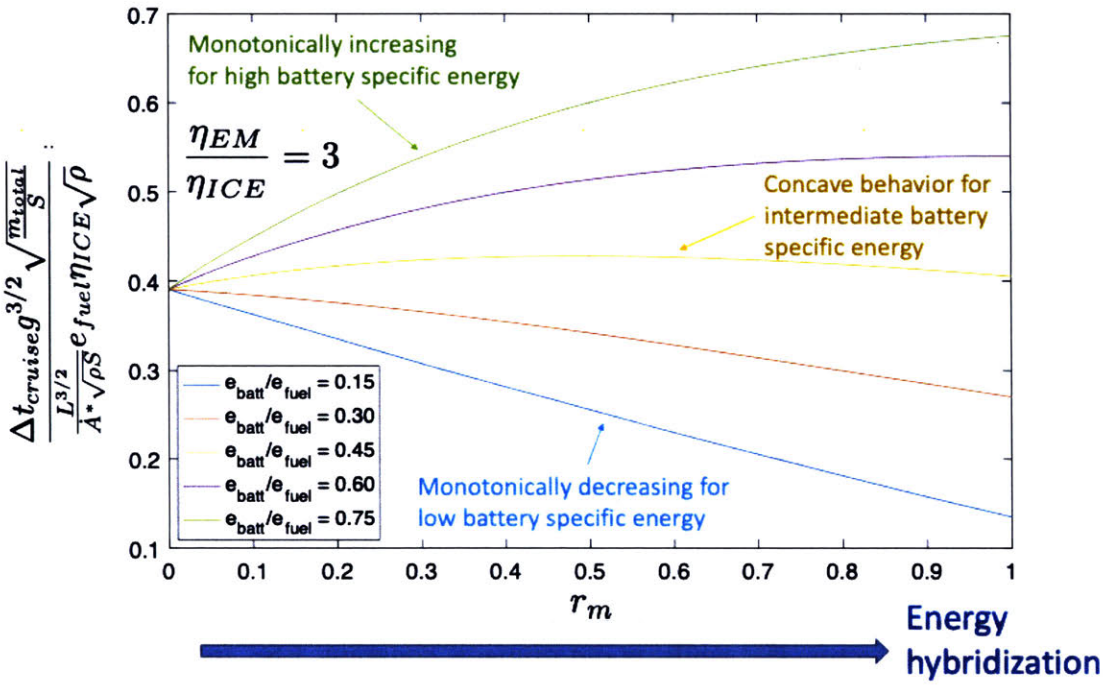


Figure 4-2: Parametric curves for the scaling relationship shown in Equation 4.16. The cruise time scaling group as a function of battery mass ratio for various values of battery specific energy ratios are shown. The electric motor to CF engine energy flow efficiency ratio is kept constant with a value of 3.

The change in the cruise time scaling group value with changes in battery mass proportion r_m is shown to be dependent on the battery to CF specific energy ratio $\frac{e_{batt}}{e_{fuel}}$ and by extension the specific energy extraction ratio $\frac{\eta_{EM,flow}}{\eta_{CF,flow}} \frac{e_{batt}}{e_{fuel}}$ (the specific energy ratio is grouped with the EM to CF engine flow efficiency ratio in Equation 4.16). For relatively low battery to CF specific energy ratios $\frac{e_{batt}}{e_{fuel}}$, the value of the cruise time scaling group decreases monotonically with increases in battery mass proportion r_m. On the other hand, relatively high battery to CF specific energy ratios $\frac{e_{batt}}{e_{fuel}}$ result in monotonically increasing values of the cruise time scaling group for increasing values

of battery mass proportion r_m. For relatively intermediate values of battery to CF specific energy ratios $\frac{e_{batt}}{e_{fuel}}$, the trend is concave, with the cruise time scaling group attaining a maximum value for a battery mass proportion r_m between 0 and 1. The parameter values that are required for the cruise time performance relationship trend to change are quantified by analyzing the derivative of Equation 4.16 with respect to battery mass proportion r_m, with the constraint that r_m is in the interval [0,1]. Here, the necessary condition for an optimum r_m is that the derivative must equal zero. In cases where the derivative is strictly positive or negative for r_m in the interval [0,1], no optimum r_m exists. Central to the cruise scaling relationship trend shape is the specific energy extraction ratio $\frac{e_{batt}\eta_{EM,flow}}{e_{fuel}\eta_{CF,flow}}$. The numerator indicates the amount of energy per unit mass that can be converted to propulsive energy from the battery, while the denominator indicates the same for the CF stores.

The parameter values that correspond to the three distinct trends described are as follows.

- Regime 1, $\frac{e_{batt}\eta_{EM,flow}}{e_{fuel}\eta_{CF,flow}} \leq 1$: In this case, the amount of useful energy extract-able per unit mass is lower for the battery than for carbon-fuel. Increases in energy hybridization factor H_E while maintaining a constant ESS mass proportion $\frac{m_{ESS}}{m_{total}}$ result in a monotonic decrease in cruise time. Therefore, to maximize cruise time in this case, a minimum battery mass should be employed.

- Regime 2, $\frac{e_{batt}\eta_{EM,flow}}{e_{fuel}\eta_{CF,flow}} > 1$ and $\frac{e_{batt}\eta_{EM,flow}}{e_{fuel}\eta_{CF,flow}}\left(\frac{2m_{fixed}}{m_{ESS}} - 1\right) - \frac{2m_{fixed}}{m_{ESS}} - 2 \leq 0$: The first condition in this case indicates that the amount of useful energy extract-able per unit mass is higher for the battery than for carbon-fuel. The second condition indicates that although the energy extracted per mass from the battery is greater than from fuel, it is not large enough to overcome the energy saved over cruise due to the fuel mass burn. Since fuel usage results in mass reduction during cruise, the aircraft velocity can be reduced. This reduction in aircraft velocity results in reduced dissipated power and overall lower energy usage during cruise. This effect is referred to as the "fuel-burn cruise energy reduction"; the total energy savings are larger when the fuel mass is larger rel-

ative to the total aircraft mass. When these two conditions are met, there is a optimum battery mass proportion r_m^*, where $r_m^* = \frac{2m_{fixed}\left(\frac{e_{batt}\eta_{EM,flow}}{e_{fuel}\eta_{CF,flow}}-1\right)}{m_{ESS}\left(\frac{e_{batt}\eta_{EM,flow}}{e_{fuel}\eta_{CF,flow}}+2\right)}$.

- Regime 3, $\frac{e_{batt}\eta_{EM,flow}}{e_{fuel}\eta_{CF,flow}} > 1$ and $\frac{e_{batt}\eta_{EM,flow}}{e_{fuel}\eta_{CF,flow}}\left(\frac{2m_{fixed}}{m_{ESS}}-1\right)-\frac{2m_{fixed}}{m_{ESS}}-2>0$ In this case, the extract-able energy per unit mass from the battery is large enough to overcome the fuel-burn cruise energy reduction effect. Battery mass proportion should be maximized to maximize cruise time.

As seen from above, there are two main conditions dictating the battery sizing rule for optimal cruise time. The first condition is the value of the specific energy extraction ratio, which simply indicates whether battery or fuel mass is more effective at storing useful energy. The second condition is less intuitive; its dependence on relative ESS mass and the specific energy extraction ratio is illustrated in Figure 4-3.

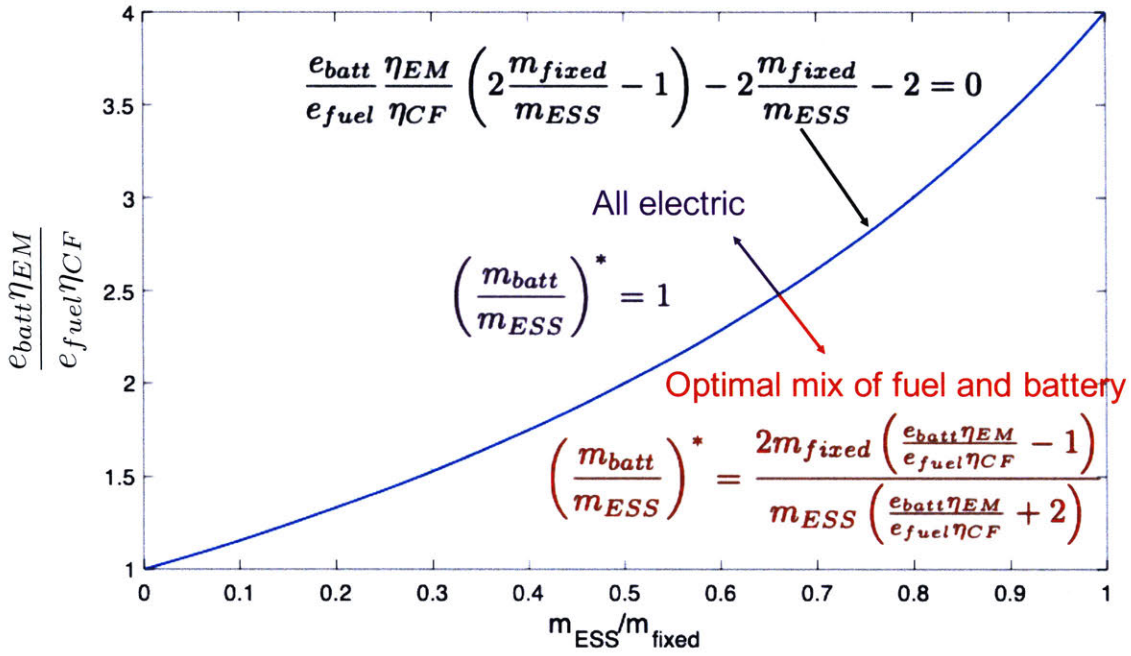


Figure 4-3: Specific energy extraction ratio and corresponding ESS mass to fixed mass ratio required for the fuel-burn cruise energy reduction battery sizing condition to equal to zero.

For the same value of battery to fuel energy extract-able per unit of mass ratio (if above 1), the optimum battery sizing rule will either be a mixture of fuel and battery or maximum battery size. The delineation is set by the ratio of ESS to fixed mass

$\frac{m_{ESS}}{m_{fixed}}$. As described previously, ESS mass sets this delineation because with a larger ESS mass (and therefore fuel mass), the relative aircraft mass reduction potential is greater, and vice versa. Note that the quantitative delineation is dependent on the implicit assumption of fuel-first usage taken during the derivation of equation 4.14. If fuel/battery usage differs from this assumption, then the delineation must be re-derived.

To anchor the cruise time scaling results with respect to current and future battery technology levels, the cruise time scaling group as a function of battery mass proportion r_m for various battery technology levels is plotted in Figure 4-4.

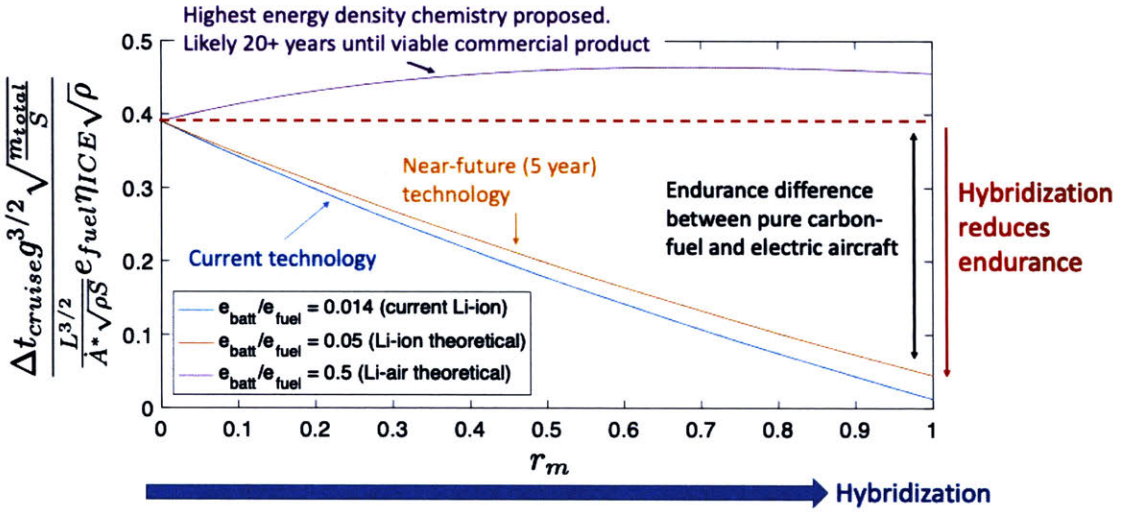


Figure 4-4: Cruise time scaling group as a function of battery mass proportion r_m for various levels of battery technology. ESS mass fraction $\frac{m_{ESS}}{m_{total}}$ is set to 0.2 in this case.

From Figure 4-4, it can be seen that for all batteries based on the lithium ion chemistry, increasing the battery fraction results in lower cruise times, indicating that the battery sizing rule is in regime 1. Even for the lithium-air chemistry which is regarded as possessing one of the highest potential specific energies, the optimum battery sizing rule is in regime 2 (ESS mass ratio of 0.2), with an optimum mix of fuel and battery. Based on these results, it is probable that the optimal battery sizing rule will be in regime 1 for the foreseeable future, indicating that fuel usage will still be responsible for the majority of cruise endurance for many years in the future.

4.2.4 Cruise range performance relationship for hybrid propulsion systems

The cruise time performance relationship can be modified to derive the cruise range performance relationship. The primary difference is that instead of assuming that cruise velocity changes to maintain lift-weight balance for a constant altitude, it is assumed that the cruise velocity remains constant and the altitude (and therefore air density) changes to maintain the lift-weight balance. All other assumptions remain.

With the change in assumptions and focusing on cruise range, the following cruise range performance relationship is derived (full derivation in Appendix A):

$$\frac{R_{cruise} g \sqrt{\frac{c_L}{2}}}{\left(\frac{L^{3/2}}{A^* \sqrt{\rho S}}\right) e_{fuel} \eta_{CF,flow}} = \ln\left(1 + \frac{m_{fuel}}{m_{fixed}}\right) + \frac{m_{batt}}{m_{fixed}} \frac{e_{batt} \eta_{EM,flow}}{e_{fuel} \eta_{CF,flow}} \tag{4.17}$$

From equation 4.17, a similar optimal battery sizing rule can be derived and summarized by the following:

1. Regime 1, $\frac{e_{batt}\eta_{EM,flow}}{e_{fuel}\eta_{CF,flow}} < 1$: In this case the battery mass proportion should be minimized to maximize cruise range.

2. Regime 3, $\frac{e_{batt}\eta_{EM,flow}}{e_{fuel}\eta_{CF,flow}} \geq \frac{m_{ESS}}{m_{fixed}} + 1$: In this case the battery mass should be maximized to maximize cruise range.

3. Regime 2, if the above requirements are not met, then there is an optimal battery mass proportion for maximum cruise range, $r_m^* = \frac{m_{fixed}}{m_{ESS}} \left(\frac{e_{batt}\eta_{EM,flow}}{e_{fuel}\eta_{CF,flow}} - 1\right)$.

From the above requirements, it can be seen that the relative battery and electrical component technologies required for maximal battery mass to be optimal for cruise range are less stringent compared to those for cruise time. This is because of the change from a constant altitude assumption (for cruise time) to a constant velocity assumption (for cruise range). Changes in air density result in a linear change in drag power (as for range), whereas changes in air velocity result in a cubic change in drag power (as for time).

4.2.5 Payload mass performance relationship for hybrid propulsion systems

To derive the payload mass performance relationship, it is assumed that aircraft mass consists of payload mass, structural mass, fuel mass, battery mass, EM mass, electrical generator mass, and CF engine mass. Furthermore, the generator's power capacity is assumed to be equal to that of the power output of the CF engine. Conservation of mass is invoked to generate the following payload performance relationship (full derivation found in Appendix A):

$$\frac{m_{payload}}{m_{total}} = 1 - \frac{m_{structure}}{m_{total}} - \frac{m_{fuel}}{m_{total}} - \frac{m_{batt}}{m_{total}} - \frac{P_{total}}{m_{total}} \left[(1 - H_P) \left(\frac{1}{\pi_{CF}} + \frac{1}{\pi_{gen}} \right) + H_P \frac{1}{\pi_{EM}} \right] \tag{4.18}$$

Equation 4.18 is essentially a statement of mass conservation, with the payload mass ratio available dependent on power hybridization, energy hybridization (indirectly through battery and CF mass), and aircraft power level. Note that the payload mass ratio available is not explicitly constrained to be greater than zero in equation 4.18; any payload mass ratio less than zero indicates that the aircraft design choices are not possible.

From equation 4.18, the relationship between payload mass ratio $\frac{m_{payload}}{m_{total}}$, structure mass ratio $\frac{m_{structure}}{m_{total}}$, fuel mass ratio $\frac{m_{fuel}}{m_{total}}$, and battery mass ratio $\frac{m_{batt}}{m_{total}}$ is straightforward. For a constant engine mass, as each of these values increases or decreases, the payload mass ratio decreases or increases respectively. The effects of power hybridization level and specific powers of the EM, generator, and CF engine, are illustrated in Figure 4-5. Parametric curves of the payload mass ratio as a function of power hybridization are plotted for various values of EM to CF engine specific power. Generator specific power π_{gen} is assumed to be equal to EM specific power $\pi_{gen} = \pi_{EM}$, other values in equation 4.18 are held constant. With constant fuel and battery mass ratio values, the cruise performance remains constant. This is because payload, EM, generator, and CF engine are fixed on the aircraft.

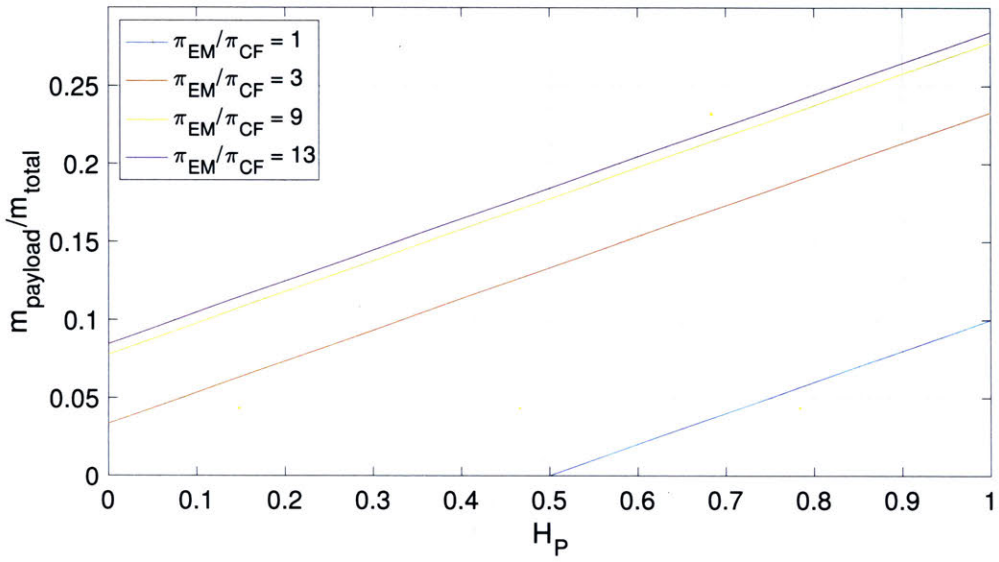


Figure 4-5: Payload mass ratio as a function of power hybridization factor for various values of EM to CF engine specific power ratio. Structure, fuel and battery represent 70% of the total aircraft mass. Aircraft specific power is set to 20% of CF engine specific power.

Several trends stand out in Figure 4-5. First, since the EM specific power is larger than the CF engine specific power in this case, increasing the power hybridization factor increases the available payload mass ratio. This is because with a constant required aircraft specific power, increasing the power hybridization factor results in a smaller engine. The mass savings with the smaller engine directly increases potential payload capacity. This trend holds even when the EM and CF engine specific power are equal ($\frac{\pi_{EM}}{\pi_{CF}} = 1$), which is because the generator is paired with the CF engine, so a smaller CF engine also results in a smaller generator. Second, a minimum power hybridization factor exists in certain situations, when the CF engine cannot provide adequate power by itself for a given available mass and required aircraft specific power. The minimum power hybridization value is indicated by the intersection of each parametric curve with the abscissa. Third, available payload mass ratio is larger for larger values of the EM to CF engine specific power ratio for all values of power hybridization factor.

4.2.6 Hybrid propulsion system performance relationship discussion

The effect of power and energy hybridization values on aircraft performance derived from the performance relationships can be summarized as follows:

1. For takeoff, increasing power hybridization decreases takeoff distance when the EM to CF engine specific power ratio is greater than 1. The magnitude of the takeoff distance reduction is dependent on the magnitude of the specific power ratio.

2. For climb, the required battery energy is independent of climb rate and only dependent on the change in altitude during climb. This is because of the assumptions taken and because climb rate and time required for climb are inversely related and counteract to make battery energy required independent of climb rate.

3. For cruise time, the optimal battery size for maximum cruise time is primarily dependent on the EM and CF flow efficiencies ($\eta_{EM,flow}$ and $\eta_{CF,flow}$ respectively), and battery and fuel specific energies (e_{batt} and e_{fuel} respectively). With current and near/medium future technology, the battery mass should be minimized to maximize cruise time due to the inferior battery specific energy e_{batt} relative to carbon-fuel specific energy e_{fuel}.

4. The payload capacity is dependent on the power and energy hybridization values along with the fuel and battery specific energies and EM and CF engine specific powers. It is assumed that aircraft takeoff, climb, and cruise performance requirements are held constant for changes in the hybridization values.

From the above effects, there are several hybrid propulsion system design implications:

1. For maximum cruise time, the battery size should be minimized. This rule should be maintained until the specific energy of batteries improves by more

than a factor of 15 (to roughly 1/3 of the CF specific energy). The minimum battery size is set by other operational performance requirements, such as those set by takeoff (specific power requirement) or climb (specific energy requirement).

2. The primary benefit of a hybrid propulsion system over a traditional CF propulsion system is the higher EM specific power relative to the CF engine. In cases where the CF engine specific power is equal or greater than the EM, there is limited benefit to utilizing a hybrid propulsion system from a performance standpoint.

4.3 Modular hybrid propulsion system performance relationships

Section 4.2 presents the performance relationships for a fixed hybrid propulsion system. In this section, the performance relationships for a modular hybrid propulsion system are presented. In particular, this section focuses on quantifying the takeoff, and cruise performance spread (defined as the proportional increase or decrease in cruise time or takeoff distance respectively, in reference to a baseline component configuration) as a function of available modular mass, referred to as the "free mass" m_{free}. Here the split between what is considered free mass and baseline mass is shown in Figure 4-6.

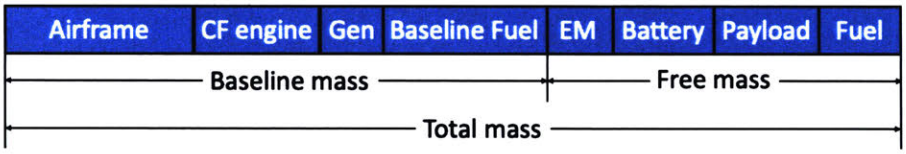


Figure 4-6: Relationship between total mass, baseline mass, and free mass

Focus is on the maximum performance spread in this section to capture the full potential of the MHPS. Payload performance is not considered because it is straightforward - free mass correlates directly with potential payload capacity on a one-to-one

basis.

For this section, the baseline component set is assumed to be the CF engine, and a baseline amount of fuel storage, with takeoff and the baseline cruise performance derived from these component performances.

With a modular propulsion system, any of the performance categories can be emphasized through selection of an appropriate modular component set. For example, takeoff distance reduction can be emphasized by using the free mass to increase EM size. Maximum/best performance is achieved by using all of the available free mass to emphasize that performance category. The results of section 4.2 are utilized to determine which components are used to fill the free mass to achieve the best performance in each category. The relationship between the baseline, minimum takeoff distance and maximum cruise time configurations is illustrated in Figure 4-7.

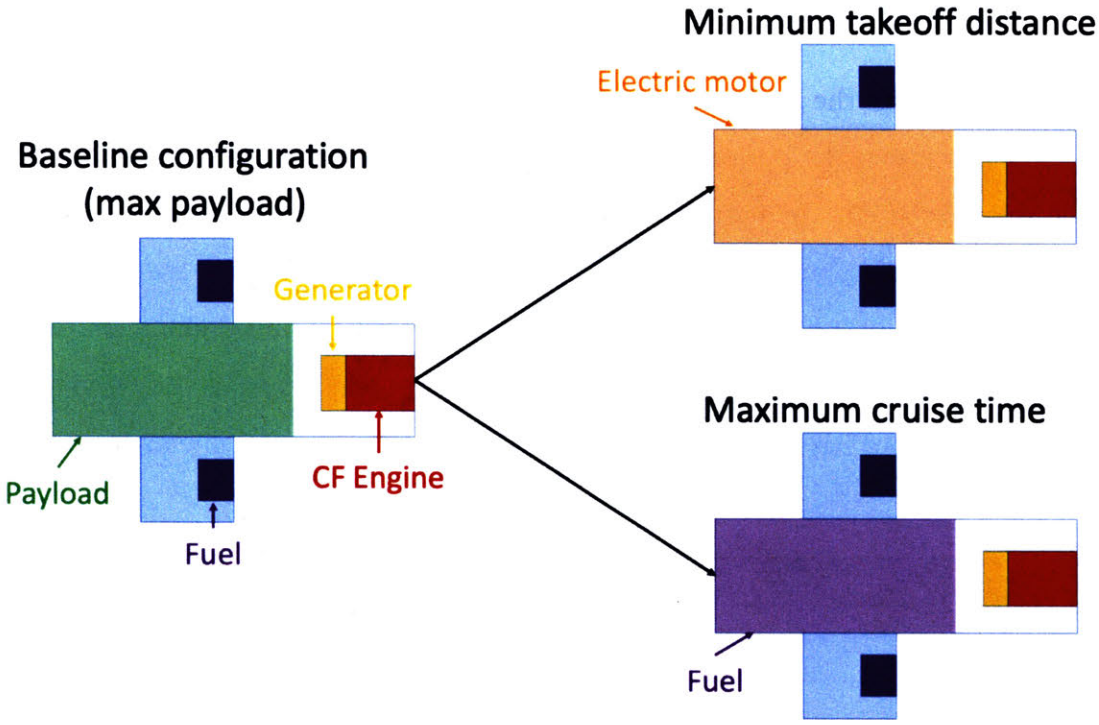


Figure 4-7: Component configurations of the baseline, minimum takeoff distance and maximum cruise time configurations.

4.3.1 Modular takeoff spread performance relationship

From the previous section, it was seen that the minimum takeoff distance is achieved when the component with the highest specific power contributes a greater proportion of the propulsive power. In most cases and class of aircraft, the EM will have a higher specific power and therefore it is assumed that the free mass modular mass is taken up by EM when takeoff distance reduction is emphasized.

The modular takeoff distance spread relationship is derived by utilizing equation 4.2 for the baseline aircraft configuration (free mass filled with payload) and the configuration for which the free mass is filled with EM. The EM-filled configuration represents an upper bound on the possible takeoff distance spread because there is no other useful payload and battery. Some amount of battery will be required in practice to drive the EM. The resulting relationship is shown below (full derivation in Appendix A):

$$\frac{\Delta R_{min} - \Delta R_{base}}{\Delta R_{base}} = \frac{\frac{m_{free}}{m_{total}}\pi_{EM}}{\left(\frac{m_{prop,base}}{m_{total}}\pi_{prop,base} + \frac{m_{free}}{m_{total}}\pi_{EM}\right)} \tag{4.19}$$

From equation 4.19, it can be seen that the relative modular takeoff distance spread is dependent only on the specific power of the baseline engine $\pi_{prop,base}$, specific power of the EM π_{EM}, mass proportion of the baseline engine $\frac{m_{prop,base}}{m_{total}}$ and amount of free mass relative to the total aircraft mass $\frac{m_{free}}{m_{total}}$. To illustrate the effect of the EM to baseline engine specific power ratio, the modular takeoff distance spread as a function free mass proportion is plotted in Figure 4-8. Here the baseline CF engine (propulsion system) mass ratio is taken to be 0.1.

From Figure 4-8, it can be seen that the magnitude of the takeoff distance spread $\frac{\Delta R_{min} - \Delta R_{base}}{\Delta R_{base}}$ is larger as the relative free mass increases. Additionally, there are diminishing returns in the magnitude of the takeoff distance spread as free mass increases. For example, for a specific power ratio of 3, increasing the free mass ratio from 0 to 0.1 increases the magnitude of the takeoff distance spread from 0 to 0.75. Further increasing the free mass ratio from 0.1 to 0.2 only increases the magnitude from 0.75 to 0.85. The slope of the magnitude of $\frac{\Delta R_{min} - \Delta R_{base}}{\Delta R_{base}}$ increase is dependent

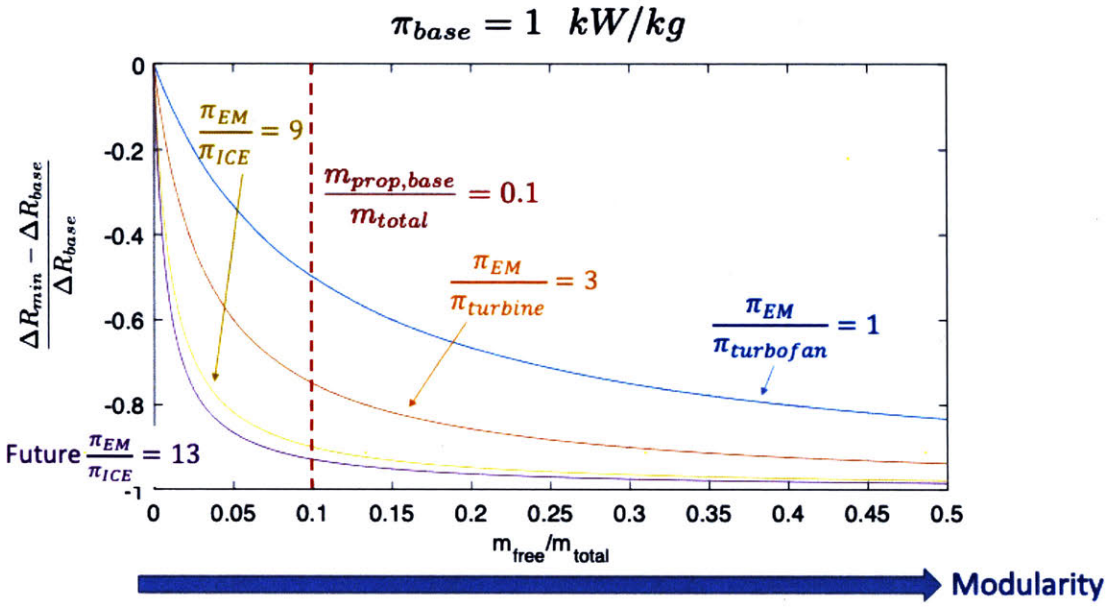


Figure 4-8: Modular takeoff distance spread as a function of modular free mass for various values of EM to CF engine specific powers. CF engines considered are ICEs, small turbines, and turbofans. The baseline CF engine represents 10% of the total aircraft mass.

on the ratio of EM to CF engine specific power $\frac{\pi_{EM}}{\pi_{CF}}$. Furthermore, it can be seen that even when the specific powers are equal ($\pi_{EM} = \pi_{CF}$), a significant reduction in takeoff distance spread $\Delta R_{min} - \Delta R_{base}$ can be achieved (50% change from the baseline) for a relatively small ($< 10\%$) amount of free mass relative to the total aircraft mass.

4.3.2 Modular cruise time spread performance relationship

For maximum cruise time spread $\Delta t_{cruise,best} - \Delta t_{cruise,baseline}$, it is assumed that the modular free mass m_{free} is utilized for additional carbon-fuel mass over battery mass. This assumption is taken because it was shown that battery specific energy e_{batt} must improve by a factor of approximately 15 before increasing battery mass has a greater benefit to cruise time than carbon fuel. With this assumption, equation 4.16 is utilized to derive the modular cruise time spread relationship (full derivation in Appendix A):

$$\frac{\Delta t_{cruise,best} - \Delta t_{cruise,baseline}}{\Delta t_{cruise,baseline}} = \frac{\sqrt{\frac{m_{fixed}+m_{fuel,base}}{m_{fixed}}} - 1}{1 - \sqrt{\frac{m_{fixed}+m_{fuel,base}}{m_{fixed}+m_{fuel,base}+m_{free}}}} \tag{4.20}$$

From equation 4.20 it can be seen that the relative cruise time spread is only dependent on baseline fuel mass $m_{fuel,base}$, fixed mass m_{fixed}, and free mass m_{free}. These relationships are illustrated in Figure 4-9.

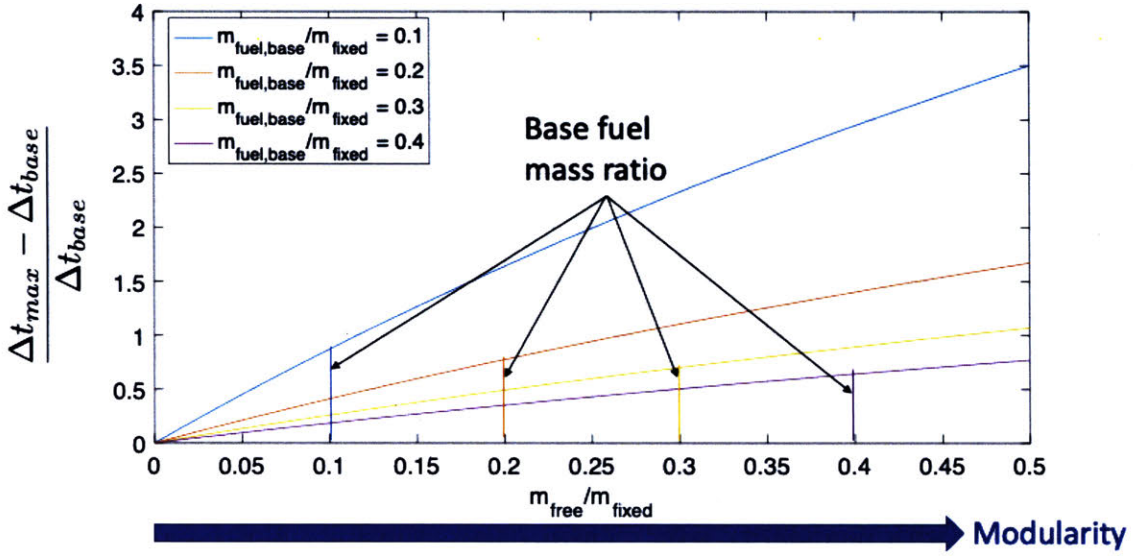


Figure 4-9: Modular cruise time spread as a function of modular free mass for various values of baseline fuel mass ratios. Modular free mass is assumed to be filled with carbon fuel.

Figure 4-9 shows that the relative cruise time spread $\frac{\Delta t_{max} - \Delta t_{base}}{\Delta t_{base}}$ increases with relative free mass $\frac{m_{free}}{m_{fixed}}$. The rate of relative cruise time spread increase is dependent on the baseline fuel mass ratio $\frac{m_{fuel,base}}{m_{fixed}}$. For example, for a baseline fuel mass ratio of 0.1, increasing the free mass ratio $\frac{m_{free}}{m_{fixed}}$ from 0 to 0.1 increases the relative cruise time spread from 0 to approximately 0.8. This is in contrast to the case where the baseline fuel mass ratio is equal to 0.2, where an increase in the free mass ratio from 0 to 0.1 only increases the relative cruise time spread from 0 to 0.45. This behavior is expected because a greater baseline fuel mass results in a greater baseline cruise time and larger increases in fuel mass (through the free mass) are required for the same relative increase in cruise time.

4.3.3 Discussion of the modular performance relationships

From the modular aircraft performance relationships, it can be seen that there is potentially a large amount of performance flexibility that may be attained through the use of a modular hybrid propulsion system. Under the conditions and assumptions taken, with 10% relative free mass, the endurance and takeoff distance can be modified by up to 100% and 50% respectively. Furthermore, these results hold for all scale of aircraft.

4.3.4 Relationship between modularity and hybridization levels

With the free mass usage assumptions, the relationship between modularity and hybridization levels can be illustrated. For takeoff performance enhancement, by utilizing the free mass to increase the EM size results in the power hybridization level increasing with modularity level. On the other hand, for cruise time enhancement, the free mass is utilized to increase the carbon-fuel mass, the energy hybridziation value decreases with modularity level. These relationships are illustrated in Figure 4-10.

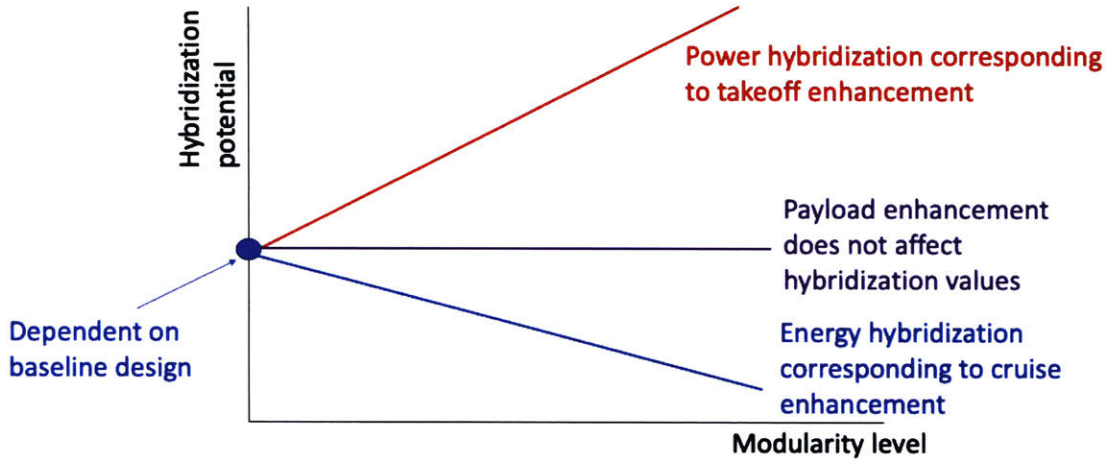


Figure 4-10: A schematic illustrating the relationship between modularity and hybridity assuming free mass is optimally utilized as outlined in this section.

4.4 Assessment of performance relationship applicability

To ensure that the performance relationships presented are applicable to all scale of aircraft, performance comparisons are conducted for a variety of 1) hybrid aircraft presented in literature, and 2) a set of "author-designed" aircraft. Here "author-designed" refers to the fact that the aircraft do not exist in literature or in reality and instead are aircraft sized by the author consisting of existing propulsion system components. For the aircraft in literature, the aircraft specifications are used in the performance relationships to determine aircraft performance and then compared to the specified aircraft performance presented in literature.

For the author-designed aircraft, the performance relationship results are compared against performance values attained with the performance modeling framework described in Section 3.3. The primary assumptions taken in the framework are 1) constant thrust output, 2) constant aerodynamic characteristics, and 3) the takeoff velocity is pre-specified. This was done to ensure that the performance calculation method is different from the performance relationships, because if they were similar, the performance comparison would become trivial.

The hybrid aircraft from literature used are tabulated in Table 4.1.

Source	Total mass (kg)	Hybrid configuration	Battery $e_{batt}\left(\frac{W-hr}{kg}\right)$	EM π_{EM} (kW/kg)
Pornet 2018 [27]	78990	Parallel	1500	20
Boeing SUGAR Volt [6]	63407	Parallel	750	5
Zunum Aero [3]	5216	Serial	170	7.5
Finger 2018 [12]	806	Parallel	250	5

Table 4.1: Hybrid aircraft from literature used for the assessment of performance relationship applicability

To utilize the developed performance relationships, several aircraft performance parameters must be estimated. For takeoff, the primary estimated parameter is the conversion efficiency $\eta_{convert}$. Using the estimated values for the conversion efficiency,

the takeoff distance differences between the values given in Table 4.1 and the values estimated with the takeoff distance performance relationship are shown in Figure 4-11. Error bars for a 10% uncertainty in the estimated value for $\eta_{convert}$ are also shown.

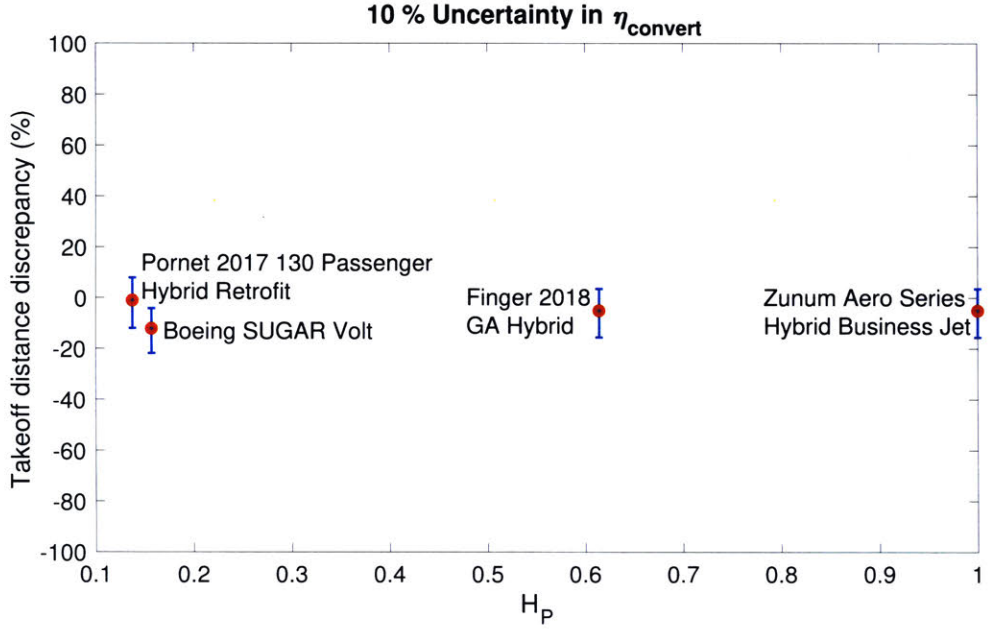


Figure 4-11: Percentage difference in the estimated takeoff distance utilizing the takeoff distance performance relationship and values given in Table 4.1

From Figure 4-11 it can be seen that the magnitude of takeoff distance estimate discrepancy ranges from approximately 0% to 12%, with the discrepancy independent of aircraft type or scale. Scale-independent discrepancy suggests that the takeoff distance performance relationship is applicable to all aircraft scales. Furthermore, the magnitude of the discrepancy suggests that the takeoff distance performance relationship provides a relatively good estimate for takeoff distance as a function of aircraft characteristics. Finally, the magnitude of the error bars show that the value of conversion efficiency has a significant effect on the value of the takeoff distance (and associated scaling group).

A similar comparison is made between the cruise range performance relationship and values shown in Table 4.1. Cruise range is shown instead of cruise time as aircraft cruise performance is specified in terms of cruise range in literature. For

the cruise range performance relationship, the aircraft propulsive efficiencies need to be estimated in a manner similar to the estimation of the conversion efficiency in the takeoff distance performance relationship. Error bars are shown for a 10% uncertainty in the estimated value for propulsion system propulsive efficiency. The resulting comparison is shown in Figure 4-12.

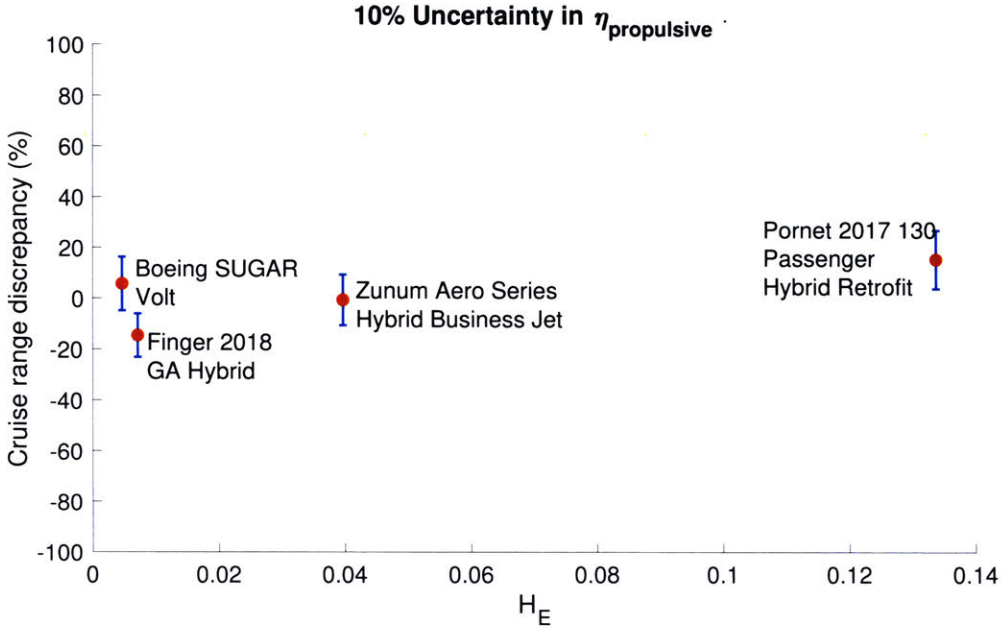


Figure 4-12: Percentage difference in the estimated cruise range utilizing the cruise range performance relationship and values given in Table 4.1

Figure 4-12 shows that similar to the takeoff distance performance relationship comparison, the cruise range performance relationship discrepancy is independent of aircraft scale, with discrepancy magnitudes ranging from 0% to approximately 15%. The cruise comparison similarly suggests that the cruise performance relationship is applicable toward all types of aircraft and scales.

As previously mentioned, to further support the applicability of the performance relationships to all aircraft scales, a set of author-designed aircraft are utilized. The author-designed aircraft used are tabulated in Table 4.2. CF engine and EM performance characteristics are shown in Tables 4.3 and 4.4 respectively.

Similar to the literature hybrid aircraft comparison, the conversion efficiency must be estimated in the takeoff distance performance relationship as it is not directly

specified in the author-designed aircraft design. However, in contrast, the propulsive efficiency for the cruise range performance relationship is specified directly in the author-designed aircraft design so it does not need to be estimated in the cruise range performance relationship. The takeoff comparison for the author-designed aircraft are shown in Figure 4-13, while the cruise range performance relationship is shown in Figure 4-14.

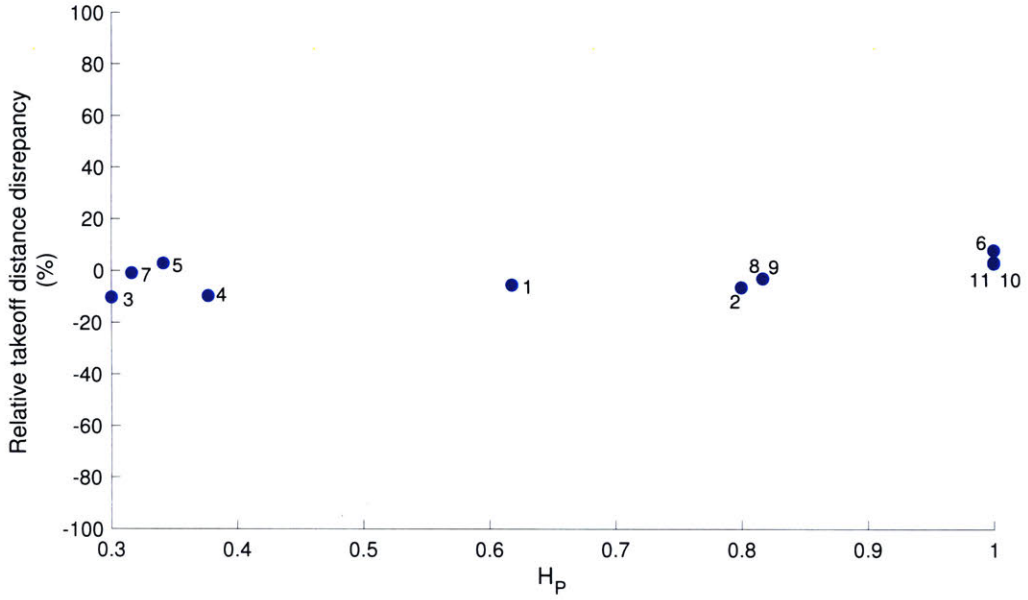


Figure 4-13: Relative discrepancy between the calculated author-designed aircraft takeoff performance and takeoff performance from the performance relationships

From Figures 4-13 and 4-14, it can be seen that the relative discrepancy magnitudes are similar for the author-designed aircraft as for the aircraft from literature. Furthermore, the discrepancy magnitudes are similar regardless of aircraft scale and hybridization values. Combined with the results from the comparison of aircraft in the literature, it can be inferred that the developed hybrid performance relationships can be applied to all aircraft scales.

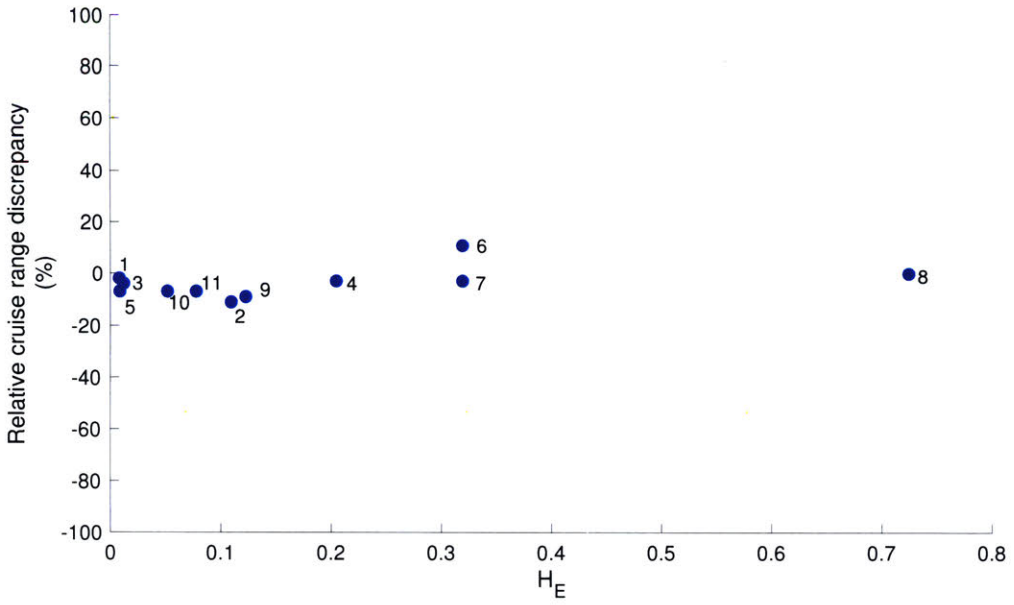


Figure 4-14: Relative discrepancy between the calculated author-designed aircraft cruise range performance and cruise range performance from the performance relationships

4.5 Summary

This chapter presents takeoff, climb, payload, and cruise performance relationships as a function of hybridization and modularity levels. Takeoff and payload performance (ΔR and $m_{payload}$ respectively) trends with power hybridization level are found to be dependent on the ratio of EM to CF engine specific powers $\frac{\pi_{EM}}{\pi_{CF}}$. When $\frac{\pi_{EM}}{\pi_{CF}} \geq 1$, takeoff and payload performance increase with increases in H_P while if $\frac{\pi_{EM}}{\pi_{CF}} < 1$, takeoff and payload performance decrease with increases in H_P.

Cruise time and range performance are found to be primarily dependent on energy hybridization level, with the relationship trend dependent on the specific energy extraction ratio $\frac{e_{batt}\eta_{EM}}{e_{fuel}\eta_{CF}}$. The numerator and denominator in this ratio represent the useful output energy per unit mass from the battery and carbon-fuel stores respectively. When $\frac{e_{batt}\eta_{EM}}{e_{fuel}\eta_{CF}} < 1$, cruise time decreases with increases in energy hybridization value, under the assumption that the sum of battery and fuel mass are held constant. When $\frac{e_{batt}\eta_{EM}}{e_{fuel}\eta_{CF}} \geq 1$, the performance trend can have one of two behaviors, dependent on the ESS mass ratio $\frac{m_{ESS}}{m_{total}}$. When the ESS mass ratio is relatively

high compared to $\frac{e_{batt}\eta_{EM}}{e_{fuel}\eta_{CF}}$, there is an optimum energy hybridization value for maximum cruise time. On the other hand, when the ESS mass ratio is relatively low compared to $\frac{e_{batt}\eta_{EM}}{e_{fuel}\eta_{CF}}$, increases in energy hybridization result in increases in cruise time. The delineation between the two trend behaviors is quantified by the value of $\frac{e_{batt}\eta_{EM,flow}}{e_{fuel}\eta_{CF,flow}}\left(\frac{2m_{fixed}}{m_{ESS}}-1\right)-\frac{2m_{fixed}}{m_{ESS}}-2$, which quantifies how electric technology compares to the benefit in cruise time gained from burning carbon fuel.

The modular performance relationships quantify the performance spread achievable as a function of modular free mass m_{free}. When the free mass ratio $\frac{m_{free}}{m_{total}}$ is of equal magnitude to the baseline fuel mass ratio $\frac{m_{fuel,base}}{m_{total}}$ and carbon-fuel engine mass ratio $\frac{m_{CF}}{m_{total}}$, cruise time may be increased by approximately 90% and takeoff distance reduced by approximately 50%.

An assessment was carried out to assess the applicability of the derived performance relationships. Performance estimates from the performance relationships were compared against 1) a set of hybrid aircraft reported in literature and 2) a set of author-designed aircraft (aircraft designed for the sole purpose of assessing the performance scaling relationships). For the set of hybrid aircraft from literature, performance estimates were compared against published aircraft performance. On the other hand, for the set of author-designed aircraft, performance estimates were compared against the performance derived from the framework described in Section 3. From the comparisons, the magnitude of the differences were relatively constant regardless of scale, suggesting the performance relationships are applicable to all aircraft scales.

To illustrate the usage of the scaling relationships presented in this chapter, the clean-sheet sizing of a MHPS for a large UAV design scenario is detailed in Appendix E.

Number	Total mass (kg)	Hybrid configuration	Battery $e_{batt}\left(\frac{W-hr}{kg}\right)$	Carbon-fuel engine	Electric motor(s)	H_E	H_P
1	846.6	Parallel	195	Mercedes OM660 Diesel x1	YASA P400 x1	0.0081	0.612
2	765	Parallel	195	Mercedes OM660 Diesel x1	YASA P400 x1	0.101	0.8
3	1978	Parallel	195	GE YT706-GE-700 Turboshaft x1	Magnax x5	0.0122	0.3
4	2525	Parallel	555	GE YT706-GE-700 Turboshaft x1	Magnax x7	0.205	0.377
5	26277	Parallel	555	CFM56 turbofan x1	Magnix250 x15	0.0087	0.341
6	83270	Series	2222	GE90-113 turbofan x1	Magnix250 x70	0.3195	1.00
7	83720	Parallel	2222	GE90-113 turbofan x 1	Magnix250 x70	0.3195	0.3162
8	3941	Parallel	4167	Deltahawk DH180A4 diesel x1	YASA 750 x3	0.725	0.817
9	3941	Parallel	222	Deltahawk DH180A4 diesel x1	YASA 750 x3	0.123	0.817
10	4147	Series	277	GE T901 turboshaft x1	Magnix250 x16	0.052	1.0
11	7409	Series	416	GE T901 turboshaft x2	Magnax x60	0.078	1.0

Table 4.2: Author-designed hybrid aircraft used for the assessment of performance relationship applicability

Engine Name	Type	Total mass (kg)	Total power or Thrust
Mercedes OM660	Diesel ICE	65	40 kW
Deltahawk DH180A4	Diesel ICE	154	134.2 kW
GE YT706-GE-700	Turboshaft	266.9	1967 kW
GE T901	Turboshaft	327.8	2950 kW
CFM56	Turbofan	2370	121 kN
GE90-113	Turbofan	8762	505 kN

Table 4.3: Carbon-fuel engines used in the author-designed aircraft study.

Engine Name	Total mass (kg)	Total power	Peak efficiency
YASA P400	24	160 kW	96%
YASA 750	37	200 kW	95%
Magnax	14	170 kW	95%
Magnix250	60	280 kW	93.8%

Table 4.4: Electric motors used in the author-designed aircraft study.

Chapter 5

Hybrid propulsion system energy management and component matching

5.1 Introduction

Operation of a hybrid propulsion system differs from operation of a traditional propulsion system in two significant areas. First, with a hybrid propulsion system, propulsive power can be derived from either the carbon-fuel stores or batteries at each point in time. This is in contrast to traditional propulsion systems where the carbon-fuel stores provide all of the propulsive energy to meet the propulsive power requirement is at any given time. Due to the additional energy source in a hybrid system, there is a need for an energy management control policy that determines which energy source is utilized at each point in time during flight. Here the term "energy management control policy" refers to the policy that chooses which energy source is utilized at each point in time during the flight profile. The policy is determined through a framework or method before flight. Second, the matching between propulsion components differs between hybrid and traditional propulsion systems due to the presence (or lack thereof) of electrical components. Here, matching refers to the effect of individual

component performance characteristics on the overall static and dynamic performance of the propulsion system. Examples include how the torque output of the EM(s) affects the system's ability to change its thrust output and how the total efficiency map is affected by the CF engine's efficiency map in relation to the EM efficiency map(s).

The primary requirements for the energy management control policy are:

1. Energy must be managed in such a way that ensures that all operational flight requirements are met. These requirements include completion of flight segments and operations such as payload energy usage.

2. Energy must be managed in a way that ensures components do not exceed their operational specifications. Examples include ensuring the EM does not exceed its power limit or ensuring that the battery charge level does not dip below a certain value.

To ensure that requirement 1 is met, the energy management policy must take into account how actions/decisions at one point in time affect the aircraft state at future points in time. This is because without this capability, mission operational requirement satisfaction is not guaranteed. For example, without knowledge of a battery usage requirement near the end of cruise, the policy may make the decision to use all the battery energy on-board at some point before the required time; in this case the operational requirement is not met.

To meet requirement 2, the energy management policy must be able to accept constraints on the propulsion system operational parameters at each point in time. These constraints are used to encode component operational limits and ensure that physical constraints are satisfied. Physical constraints control how the component states are related in time; for example, if fuel is used at some point in time, the fuel stores at the next point in time must be the value at the previous point in time minus the amount used.

As indicated in Chapter 2, Dynamic programming (DP) provides the framework for energy management control policy determination because of its capability to satisfy the stated requirements. Additionally, since DP is an optimization framework, an

objective function can be specified to encode the stakeholder's values/goals, ensuring that the resulting energy management control policy is optimal for those values/goals.

To determine propulsion system matching characteristics, the propulsion system configuration because component connections are determined by the configuration. Knowledge of component connections is essential for determining the system matching characteristics because the connections determine which components can directly interact with each other. In this chapter, the static and dynamic matching characteristics for several common hybrid system configurations are considered.

The objective of this chapter is to illustrate how operation of a hybrid propulsion system differs from that of a traditional propulsion system. The beneficial aspects of a DP framework for determining the energy management control policy are illustrated that provides the groundwork for future efforts in this area. Hybrid dynamic and static matching characteristics are outlined, and several component design/sizing implications are identified.

5.2 Energy management policy determination through DP

To illustrate the usage of DP for determining the optimal energy management control policy, a cruise scenario is used. In the scenario considered, an aircraft with a parallel hybrid propulsion system must complete a cruise that lasts for a pre-specified amount of time. At each point in time, propulsive power is provided by some combination of the CF engine and EM powered propellers. The aircraft begins cruise with some amount of fuel mass and battery energy. The objective is to end the cruise with the greatest amount of fuel mass remaining as possible. This objective is chosen as minimal fuel consumption is a common goal for missions to minimize costs. Additionally, the minimal fuel-consumption objective is similar to a maximal cruise time objective. Maximal cruise time would be accomplished by increasing the cruise time while maintaining the minimum fuel consumption objective until all fuel is consumed

by the end of cruise.

The amount of fuel mass and/or battery energy required to fly for some amount of time is modeled with the modified Breguet range equation (sum of equation 4.12 and 4.13). A cruise scenario modeled by the modified Breguet range equation is considered because the optimal solution is known apriori and the optimal solution requires knowledge of total cruise time required. In this case, the optimal use of the energy storage system is to utilize fuel stores exclusively, until the batteries can be used exclusively to complete cruise, with battery energy equal to zero at the end of cruise. The fuel and battery usage in the optimal case is illustrated in Figure 5-1.

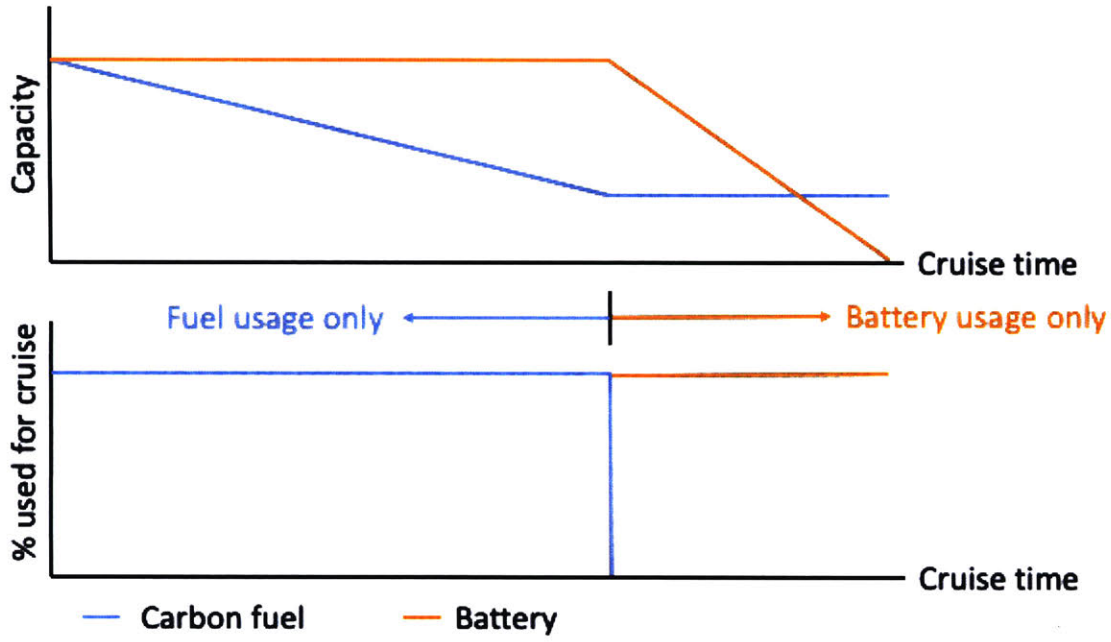


Figure 5-1: Optimal solution to the DP problem considered. Fuel is used initially only, with the battery used exclusively to finish cruise.

The solution illustrated in Figure 5-1 is optimal because carbon fuel usage results in a decrease in aircraft mass, while battery usage does not. With a lower mass, the aircraft velocity decreases to maintain steady-level cruise, which results in a reduction in drag power dissipated as seen in equation 3.6. Therefore the total amount of energy required for cruise is lower for a lower mass. Battery usage is therefore reserved for the end of cruise because this is when aircraft mass is at its lowest and battery usage does not change the aircraft mass.

5.2.1 DP implementation

A DP framework requires that the optimization problem is discretized into discrete time-steps, for which the system has a state $\boldsymbol{s}$ and action choice $\boldsymbol{a}$. For the energy management control problem, the flight profile of interest is discretized with the state and action vectors specified as follows:

- The state vector consists of the fuel mass and battery energy contained within the aircraft at each point in time. Formally the state vector is specified as:

$$\boldsymbol{s} = [m_{fuel}, E_{batt}] \tag{5.1}$$

- The action vector consists of the amount of fuel mass burnt and battery energy used at each point in time. Formally the action vector is specified as:

$$\boldsymbol{a} = [\Delta m_{fuel}, \Delta E_{batt}] \tag{5.2}$$

  The change in fuel mass Δm_{fuel} is set by the following:

$$\Delta m_{fuel} = \frac{P_{CF}}{\eta_{CF,flow} e_{fuel}} \tag{5.3}$$

  While the change in battery energy is:

$$\Delta E_{batt} = \frac{P_{EM}}{\eta_{EM,flow}} \tag{5.4}$$

Additionally, there are several parts of the DP framework that must be specified:

1. A cost function, which quantifies the objective to be optimized. In this case the end-of-mission fuel level is chosen to be the optimization parameter. The cost function can be set to other parameters according to stakeholder goals as necessary.

2. A transition constraint or function that specifies how the system state changes from one time to the next as a result of the action chosen.

3. Constraints that may exist each point in time. In this case, for every time step of cruise, the total power output of the aircraft has to be equal to the power dissipated due to aerodynamic drag.

DP cost function

The objective of the energy management control policy is chosen to be maximization of the fuel mass at the end of cruise. There are two ways to achieve this objective:

1. Maximize the fuel mass remaining at the last time step of the cruise.
2. Minimize the total fuel usage, which is the sum of fuel usage through all the cruise time steps.

For the case chosen, the methods are equivalent and the first is chosen as it directly encapsulates the objective of the DP framework. Formally, the cost function is then:

$$Cost = m_{fuel,N} \tag{5.5}$$

Here the N subscript indicates that the parameter is the value at the final time-step (time step N out of N total time steps).

DP transition function and initial values

The transition function ensures that physical continuity of quantities is respected in-between time-steps in the DP framework. In this case, the quantities that change each time-step and must be continuous are the fuel mass and battery energy levels. The transition function in this case is then shown in Equation 5.6, where i indicates the time step number in the discretization:

$$\boldsymbol{s}_{i+1} = \boldsymbol{s}_i - \boldsymbol{a}_i \tag{5.6}$$

The initial values of state vector are then the fuel mass and battery energy at the start of cruise:

$$\boldsymbol{s_0} = [m_{fuel,initial}, E_{batt,initial}] \tag{5.7}$$

DP constraints

DP constraints can broadly be split into two categories:

1. Constraints that are applicable and constant for all time-steps. These typically encode component operation limits and system dynamics.
2. Constraints that may change from time-step to time-step. This type of constraint typically refers to the system or component performances required to meet the flight profile requirements.

In this thesis, the action vector only contains the change in fuel mass and battery energy, so there are only limitations on these two parameters. For the fuel mass change, it is bounded between zero and the change in fuel mass that would result from operation of the CF engine at its maximum power. The bound is shown in Equation 5.8.

$$0 \leq \Delta m_{fuel} \leq \frac{P_{CF,max}}{\eta_{CF,flow} e_{fuel}} \Delta t \tag{5.8}$$

The change in battery energy bounds are similar:

$$0 \leq \Delta E_{batt} \leq \frac{P_{EM,max}}{\eta_{EM,flow}} \Delta t \tag{5.9}$$

In addition to the physical bounds on the fuel mass and battery energy changes, conservation of energy between the CF and electric sub-systems must be encoded. This is done through Equations 5.10 and 5.11, which are conservation of energy statements on the CF engine shaft and battery.

$$P_{shaft,CF} = P_{propeller,CF} + P_{generator} \tag{5.10}$$

$$P_{batt} = -P_{EM} + P_{generator} \tag{5.11}$$

The flight performance constraint is that the total propulsive power output at each point in time is equal to the power dissipated due to drag. For the parallel propulsion system considered, this constraint is shown in Equation 5.12.

$$P_{propulsive} = P_{prop,EM} + P_{prop,CF} = P_{drag} \tag{5.12}$$

For steady-level cruise, the aircraft is assumed to fly at a velocity to maintain force balance on the aircraft (equation 5.13), with the cruise lift coefficient set apriori; power dissipated by drag is then calculated using the stall velocity according to equation 3.6.

$$v_{cruise} = \sqrt{\frac{m_{aircraft}g}{c_{Lcruise}\rho S}} \tag{5.13}$$

Total aircraft mass at any point in time is the sum of the fixed mass and fuel mass.

5.2.2 DP results

The cruise scenario described is discretized into 7 time-steps, with the value of 7 chosen due to computational cost restrictions on the author's computer. Additionally, the feasible state and action choices are discretized into 2% increments (between 0 and 100%, where 0 corresponds to empty and 100% corresponds to full fuel tank or battery energy), again chosen due to computational cost restrictions. Primary parameter values used are shown in Table 5.1.

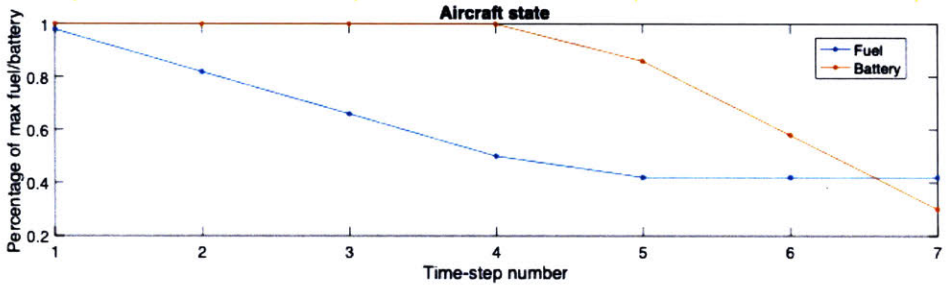
Battery specific energy	15 MJ/kg
Fuel specific energy	42.6 MJ/kg
Energy hybridization value	0.48
η_{EM}	0.9
η_{CF}	0.3

Table 5.1: Primary hybrid propulsion system performance parameter values used in the DP framework example.

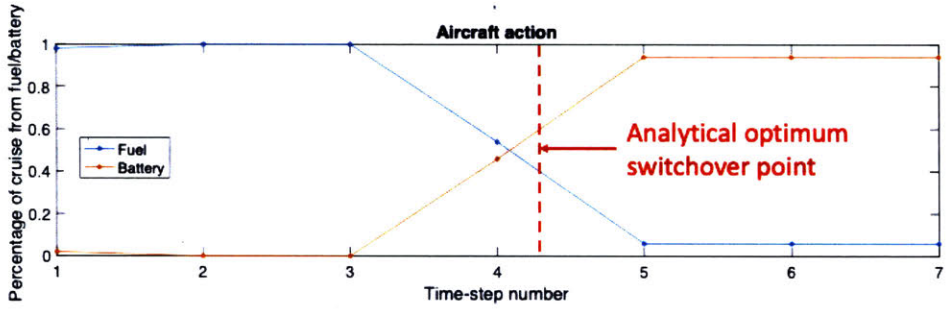
A unrealistically high (compared to present technology in 2018) battery specific energy value is used to increase the energy hybridization value without massively

increasing battery mass (relative to fuel and aircraft mass). Additionally, this ensures that the optimal solution can be captured by the DP framework. This choice is taken because if a small energy hybridization value is used, the usage of battery energy may not be apparent (the proportion of cruise time stems from battery energy would be small due to the relatively small amount of battery energy).

The results of the DP framework on the problem described previously are shown in Figure 5-2.



(a) Aircraft state during cruise derived from the DP framework



(b) Aircraft action during cruise derived from the DP framework

Figure 5-2: DP results for the cruise energy control management problem. The top plot indicates the fuel mass and battery energy levels while the bottom plot indicates the proportion of cruise time resulting from fuel or battery usage.

From Figure 5-2 it can be seen that the DP framework is able approximately reproduce the optimal energy management control policy, with the policy utilizing carbon fuel only for the first part of cruise before switching over to battery energy. Due to the state/action vector discretizations, the action choices are non-zero for the fuel/battery when they should be; this is purely a discretization effect. Furthermore, the switch over from fuel to battery energy is not a distinct step due to the time

discretization. For time step 4, the DP framework finds that a mix of battery and fuel energy is optimal since the time-steps are relativly large (compared to a continuous representation). As the time and state discretizations become infinitesimally small, the switch-over approaches a distinct step.

The cruise energy management example illustrates the potential of the DP framework. It has the ability to find the optimal energy management control policy when considering the entire flight profile and has the capability to account for any operational constraints that exist in the profile. With the general framework in place, there are several extensions that can be implemented to improve framework accuracy/fidelity and generality. The next section illustrates several potential extensions related to MHPS component matching.

5.3 MHPS component matching

There are several component matching issues that exist for a MHPS. The two that are focused upon in this thesis are:

1. Efficiency map matching between the carbon-fuel engine and EM for a parallel hybrid propulsion system.

2. Dynamic characteristic component matching between the electric and CF subsystems.

Efficiency map matching refers to how "well" the EM and CF engine efficiency maps interact with each other to yield the total system efficiency during propulsion system operation. Specifically, given a range of possible system-level operating points (power output), matching "goodness" can be quantified by the average total efficiency achievable across this range. The idea of efficiency map matching is illustrated in Figure 5-3 (reproduction of Figure 2-5).

Dynamic characteristic component matching refers to how the dynamic characteristics of the components interact with each other to produce the system-level dynamic characteristics. Specifically, how acceleration and inertia component characteristics

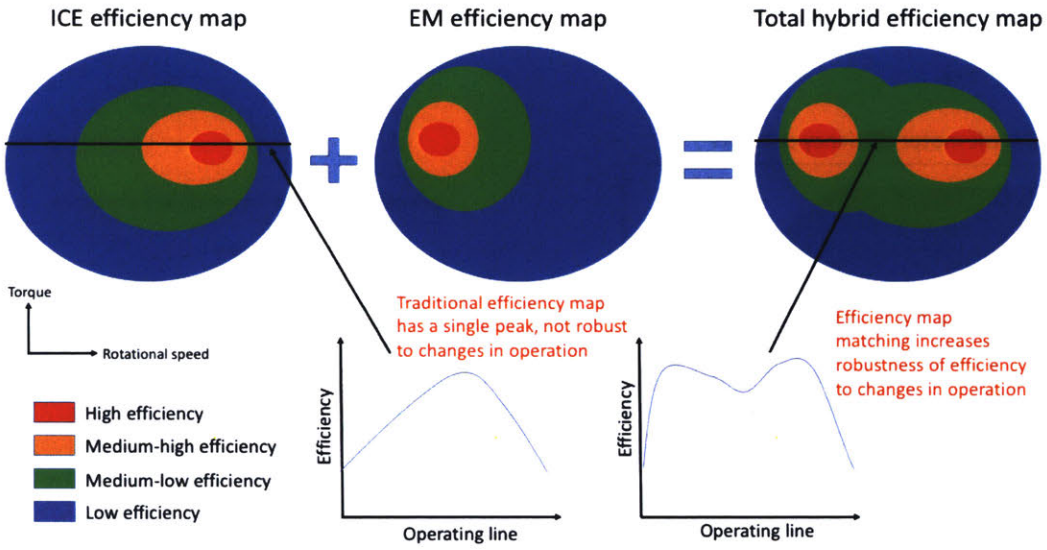


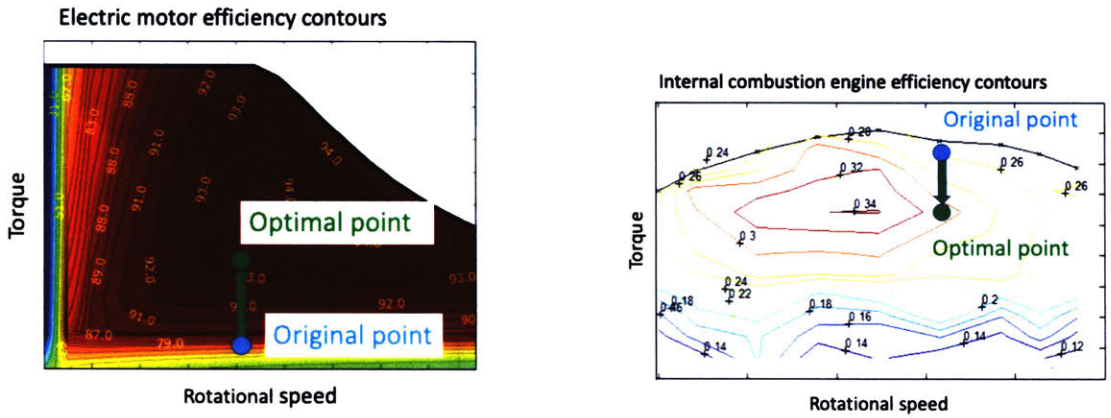
Figure 5-3: Total efficiency map of a hybrid propulsion system is a linear combination of the EM and ICE efficiency maps, when the ICE and EM are attached to a single shaft with no gearing.

affect the time-rate of change of system-level performance characteristics such as output power and power-split.

5.3.1 Efficiency map matching

As previously mentioned, a parallel hybrid propulsion system enables the total efficiency map to be a superposition of the efficiency maps of the EM and CF engine. This is because power can be supplied in different proportions from the CF engine and EM interchangeably. This effect can be illustrated by considering an EM and CF engine supplying power to a single shaft, with no gearing in the system. Therefore the EM and CF engine must have the same rotational velocity, with power from each component therefore proportional to each component's torque load. The torque load can be increased or decreased on each component as necessary, unless a constant power requirement is in place. In this case, an increase of torque on one component results in an equal decrease on the other. If an arbitrary torque split is set between the EM and CF engine, then the efficiency of each component could be low; there is an opportunity to choose a torque split value such that the efficiency of each compo-

nent increases, resulting in an increase in total efficiency. This scenario is illustrated in Figure 5-4.



(a) EM operating map

(b) ICE operating map

Figure 5-4: Illustration of the optimization opportunity for a parallel propulsion system. The torque split can be set to optimize the efficiency of the components and thus total system efficiency.

Utilizing representative CF engine and EM efficiency maps, the scenario illustrated in Figure 5-4 is investigated across a range of rotational velocities for two cases. The first case is for when the EM and CF engine provide power to the same shaft with no gearing. As mentioned, in this case, the rotational velocities of the EM and CF engine must be equal and power split is equal to torque split. The second case is for when the EM and CF engine provide power to different shafts, each with a propeller attached.

Parallel configuration on a single shaft

For the single shaft configuration, the following scenario is investigated. The optimal total efficiency of the system is determined on a constant total torque line across the operating speed range of the EM and CF engine. The optimal efficiency at each operating speed is found through a direct search on the torque split, with the total efficiency defined as in Equation 5.14.

$$\eta_{total} = \frac{\eta_{prop}\eta_{EM}\eta_{gen}\eta_{batt}\eta_{CF}}{\frac{P_{ICE}}{P_{total}}\eta_{EM}\eta_{gen}\eta_{batt} + \frac{P_{EM}}{P_{total}}} \tag{5.14}$$

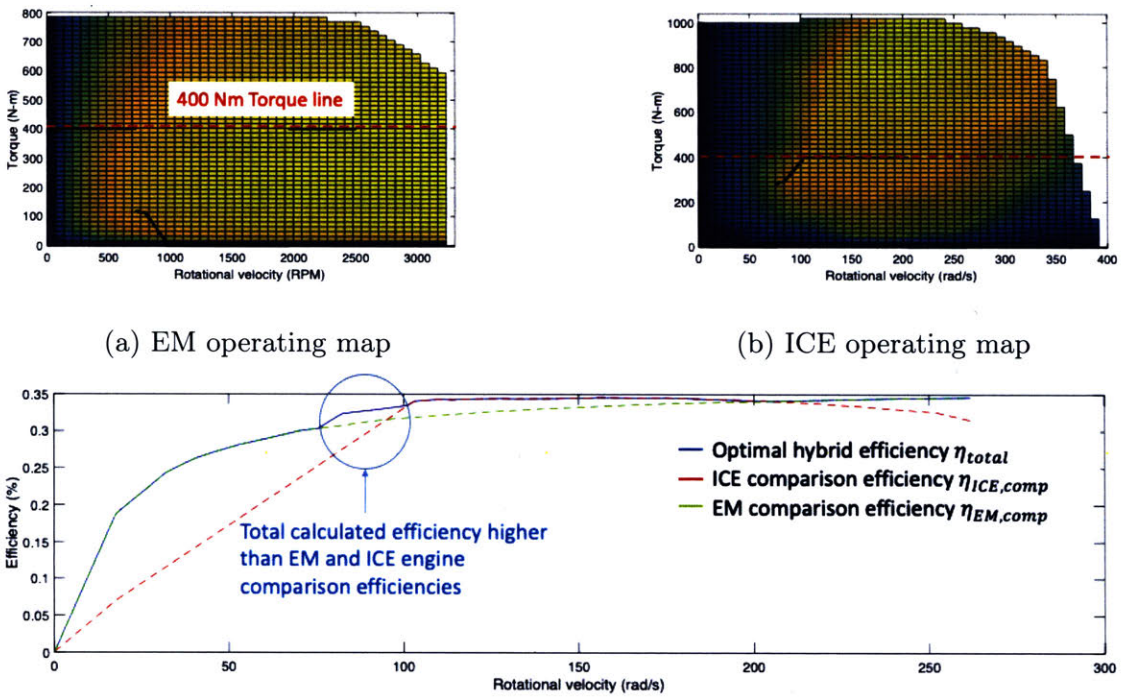
As a point of comparison, the efficiencies of the EM $\eta_{EM,compare}$ (EM comparison efficiency) and CF $\eta_{CF,compare}$ (CF engine comparison efficiency) at the same operating speed and torque are used (ie. $\eta_{EM,compare}$ when EM torque and speed are equal to the torque and speed used to calculate the optimal efficiency ($T_{EM,compare} = T_{total}$ and $\omega_{EM,compare} = \omega_{total}$) and $\eta_{CF,compare}$ when CF engine torque and speed are equal to the optimal efficiency torque and speed ($T_{CF,compare} = T_{total}$ and $\omega_{CF,compare} = \omega_{total}$)). Performance parameters used are tabulated in Table 5.2. The rotational velocity range considered is similar to most propeller aircraft and the torque value is representative of EM and CF engine torques in the power range of large UAVs. The electric motor efficiency is modified by what is referred to as the "Fuel-electricity conversion efficiency", which represents the efficiency of conversion between the CF stores and battery energy that is used by the EM. This value is representative of the CF engine efficiency while charging the batteries. It is employed in the total efficiency calculation because it is assumed that most of the battery energy that is used is sourced from the CF stores due to relatively low battery specific energy (e.g. the battery is continually charged by the generator in-flight) . Additionally, it ensures that the direct search at each rotational speed is not biased toward using the EM exclusively, which naturally has a higher efficiency relative to the CF engine.

Total torque output	400 N-m
Speed range	0-2500 RPM
Fuel-electricity conversion efficiency	0.3

Table 5.2: Primary hybrid propulsion system performance parameter values used in the DP framework example.

The optimal total efficiency, CF engine (considered as an ICE in this case) comparison efficiency $\eta_{ICE,comp}$, EM comparison efficiency $\eta_{EM,comp}$, efficiency maps, and constant torque line are shown in Figure 5-5.

From Figure 5-5 it can be seen that the optimal torque split strategy is to use the EM only for low rotational velocities between 0 and 600 RPM and high velocities between 2000 and 2500 RPM. In these regimes the total efficiency η_{total} is equal to



(a) EM operating map

(b) ICE operating map

(c) Total, ICE comparison, and EM comparison efficiencies

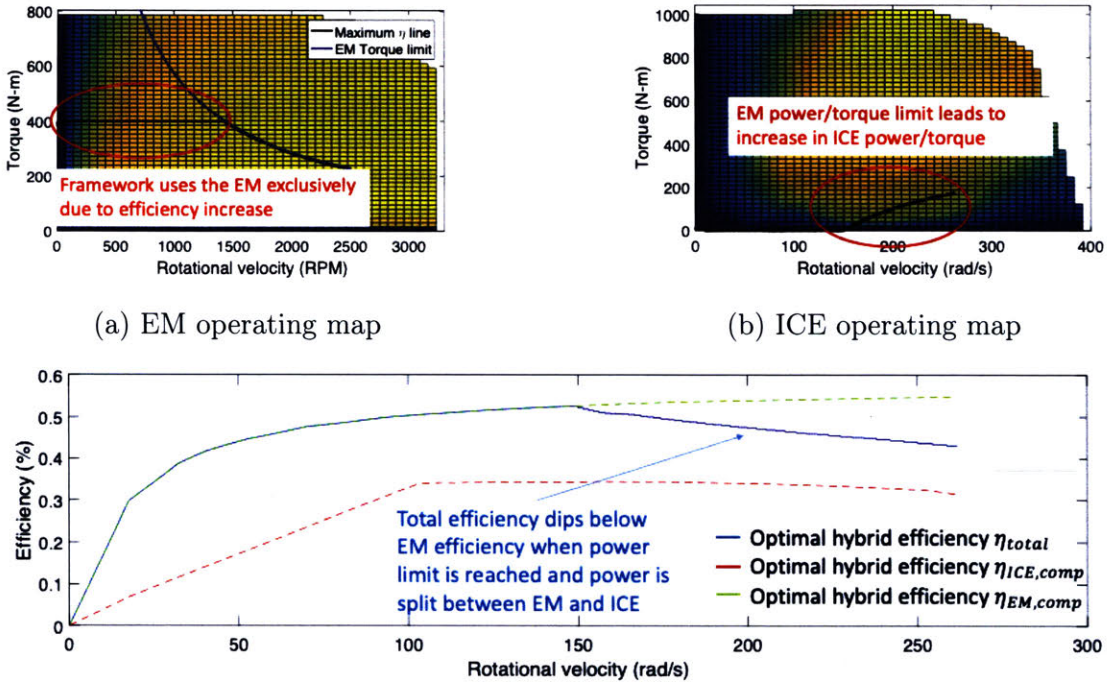
Figure 5-5: Efficiencies for the single shaft, parallel hybrid efficiency comparison. The efficiencies along a constant total torque line are considered.

that of the EM comparison efficiency $\eta_{EM,comp}$. For intermediate speeds between 1000 and 2000 RPM, the optimal MHPS split is to use the ICE only, resulting in the total efficiency η_{total} becoming equal to the ICE comparison efficiency $\eta_{ICE,comp}$. For a small range in between 600 and 1000 RPM, the optimal MHPS torque split is between 0 and 1 (power is provided by the EM and ICE in some proportion). This results in a total efficiency that is higher than that of the EM or ICE comparison efficiencies ($\eta_{EM,comp}$ and $\eta_{ICE,comp}$ respectively).

These results suggest that a MHPS's efficiency can be potentially higher than the efficiency of an individual EM/CF engine propulsion system. This is because of two reasons. First, the MHPS has the ability to leverage the torque split value at any operating point to achieve the best mix of efficiency between the components. Second, the MHPS has the ability to convert fuel energy to battery energy when it is efficient to do so (represented by the fuel-electricity conversion efficiency), utilizing the battery energy at a later time. As seen above, the fuel-electricity conversion efficiency

is essential for determining the optimal torque split and in practice is determined through simulations or operational data.

In the previous scenario, the total power output increases as the rotational velocity increases along the constant torque line for situations where sufficient battery energy is available to drive the EM. Now, consider a situation where either the battery energy or battery power capacity limits the EM power output along the constant torque line. By increasing the fuel-electricity conversion efficiency from 0.3 to 0.5 to bias the optimal torque split towards the EM, the effect of an EM power limitation can be illustrated. Again, a constant total torque line is traversed across a range of rotational velocities, except now the total EM power output is constrained to a preset value. The results for this scenario are shown in Figure 5-7.



(a) EM operating map

(b) ICE operating map

(c) Total, ICE comparison, and EM comparison efficiencies

Figure 5-6: Efficiencies for the single shaft, constrained parallel hybrid efficiency comparison. The efficiencies along a constant total torque line are considered. Furthermore, the EM has a maximum power constraint that manifests as a torque constraint dependent on the rotational speed.

From Figure 5-6, it can be seen that the bias towards EM usage works as intended, with the optimal split indicating EM usage only until the EM power constraint comes

into effect. Once the EM power alone cannot satisfy the total power requirement (due to EM power constraint), the ICE is utilized to make up the difference between the power requirement and maximum EM power output for the remainder of the velocity range. The total system efficiency reflects this behavior, with the total efficiency matching the EM comparison efficiency (ie. $\eta_{total} = \eta_{EM,comp}$) until the EM power constraint limit, at which point the total efficiency decreases below the EM comparison efficiency as ICE usage is forced (ie. $\eta_{total} = \eta_{ICE,comp} < \eta_{EM,comp}$).

The above example illustrates how a power constraint may affect the single-shaft efficiency map matching. Considering such a constraint may directly affect the total efficiency of the system, they need to be taken into account during any matching analysis.

Parallel configuration with separate shafts

For the separate shaft configuration, the EM and CF engine drive their own propellers and thus are not constrained to operate at the same speed as in the single shaft configuration. Instead, the operation of the EM-propeller and CF engine-propeller sub-systems are only constrained by the total thrust or power requirement at any point in time.

The following scenario is considered to illustrate the coupling between the EM and CF engine efficiency maps in this case. First, the power output of the propulsion system is required to be a certain value. The sum of the EM and CF engine propeller powers is equal to this required power value. Second, the EM derives its power from the electric generator, so the CF engine drives both its own propeller and the generator. The generator is assumed to be able to operate at any rotational speed and thus acts as a torque load on the CF engine. Torque load magnitude is the power required by the generator divided by the rotational velocity of the CF engine. Finally, the propellers are assumed to be fixed pitch, and the EM/CF engine are constrained to operate on the propeller operating curves.

For this scenario, the coupling between the EM and ICE efficiency maps is illustrated in Figure 5-7.

The interaction between the component efficiency maps for the separate shaft configuration can be summarized as follows:

1. For a given CF engine propeller power output, the torque/speed of the CF engine is set to the corresponding operating point on the CF engine operating map. This is the red point shown in Figure 5-7.

2. The remaining power/thrust requirement must be met by the EM propeller, which sets the operating point on the EM operating map according to the propeller characteristic.

3. The power used by the EM must be provided by the generator, and therefore the generator adds the corresponding torque load to the CF engine-propeller operating point. This new, final operating point on both efficiency maps is represented by the green-colored point. The torque load is the generator power divided by the rotational speed of the CF engine, set by the propeller and shown in Equation 5.15.

$$T_{generator} = \frac{P_{generator}}{\omega_{CF,prop}} \tag{5.15}$$

Based on the interaction between the CF engine and the EM in the separate shaft configuration, it can be seen that the CF engine has to be able to accommodate a higher torque load than it would with just a propeller attached due to the generator load. This phenomenon changes the design process in one important way. Due to the presence of the generator, the propeller and CF engine matching process is potentially different from the traditional matching process. In the traditional matching process, the propeller operating curve and CF engine map are aligned such that the propeller curve intersects the highest efficiency and/or maximum power point. In contrast, now the propeller must be smaller such that the additional torque from the generator pushes the operating point to the maximum power or efficiency region. The choice of how much to undersize the propeller is up to the designer. A smaller propeller would ensure that the generator and EM are able to access their full operating range, while a larger propeller will be more efficient, but at the cost of potentially limiting the EM

operating range. Bias toward either side is dependent on how valuable accessing the full EM operating range is during battery-empty flight.

5.3.2 Dynamic characteristic component matching

In the previous sections, various steady-state matching characteristics of the MHPS are examined. In this section, the dynamic time-varying matching characteristics of the MHPS and their effects on MHPS operation are investigated. Specifically, the dynamics on the rotating shafts and their effect on system operation are the focus of this section.

On any rotational shaft, the rotational acceleration is governed by Newton's Second Law for rotation (equation 5.16):

$$I\dot{\omega} = \sum_{i=1}^{N} T_i \tag{5.16}$$

where I is the rotational inertia of the shaft and all components attached, $\dot{\omega}$ is the rotational acceleration and T_i is the torque load of component i attached to the shaft, with N indicating the total number of components attached on the shaft. Equation 5.16 neglects the effect of shaft friction which may be significant in some cases but varies on a case-by-case basis. As in the previous section, the single shaft and separate shaft configurations are considered.

The rotational dynamics of the system limit system operation by constraining the time rate of change of key performance parameters such as shaft torque. This has the effect of potentially limiting the energy management control policy. For example, for an unconstrained system, the system can meet all the operating points that the energy management control policy may specify, even if they shift rapidly. With a dynamically-constrained system, if nearby required torque values are too far apart, the operation path will not be able to go through them due to the dynamic limitations. This would penalize the fuel consumption characteristics of the operation path since it is hitting operation points that are non-optimal. The above example is illustrated in Figure 5-8.

5.3.3 Single-shaft configuration dynamics

For the single-shaft configuration, the EM, generator, CF engine, and propeller are attached to a singular shaft. Newton's Second Law in this case is shown in Equation 5.17, with positive values corresponding to parameters in the propeller's design direction of rotation.

$$I_{total}\dot{\omega} = T_{CF} + T_{EM} - T_{gen} - T_{propeller} \tag{5.17}$$

In Equation 5.17, the CF engine, EM, and generator torques are dependent on how the corresponding components are operated at any point in time. The propeller torque can be rewritten as:

$$T_{propeller} = \frac{P_{propeller}}{\omega_{shaft}} \tag{5.18}$$

Utilizing the rotational acceleration from Equation 5.17 along with the definitions of propeller coefficient of torque and power, the rate of propeller thrust change can be derived (full details in Appendix D):

$$\frac{\frac{d(Th_{propeller})}{dt}}{Th_{propeller}} = \frac{2}{\omega_{shaft}}\left(\frac{T_{CF} + T_{EM} - T_{gen} - c_P D_{prop}^5 \omega_{shaft}^2 \rho}{I_{total}}\right) \tag{5.19}$$

Equation 5.19 sets the thrust rate of change at any point in time. When the generator torque is equal to zero with CF engine and EM torque at their maximum, the maximum thrust rate of change can be determined. This acts as a constraint on the thrust rate of change for any energy management control policy. For example, in the DP framework described previously, the thrust rate of change constraint would limit the operation points accessible from one time point to the next (since thrust changes do not occur immediately).

5.3.4 Separate-shaft configuration dynamics

In the separate-shaft configuration, the EM and CF engine propellers are mechanically decoupled and thus have independent dynamics. In this case, one shaft has the EM

and a propeller attached while the other shaft has the CF engine, generator, and a propeller attached. Utilizing a similar approach the thrust rate of change for the two shafts can be found. The CF engine sub-system shaft is shown in Equation 5.20, while the EM sub-system shaft is shown in Equation 5.21.

$$\frac{\frac{d\left(Th_{propeller,CF}\right)}{dt}}{Th_{propeller,CF}} = \frac{2}{\omega_{shaft,CF}}\left(\frac{T_{CF} - T_{gen} - c_P D^5_{prop,CF}\omega^2_{shaft,CF}\rho}{I_{total,CF}}\right) \tag{5.20}$$

$$\frac{\frac{d\left(Th_{propeller,EM}\right)}{dt}}{Th_{propeller,EM}} = \frac{2}{\omega_{shaft,EM}}\left(\frac{T_{EM} - c_P D^5_{prop,EM}\omega^2_{shaft,EM}\rho}{I_{total,EM}}\right) \tag{5.21}$$

The dynamics of each shaft limit the maximum thrust rate of change at any point in time to the sum of Equations 5.20 and 5.21 when the EM and CF engine are run at maximum torque.

For the separate shaft case, the shaft dynamics also limit the rate of change in the thrust/power split between the CF engine and EM propellers. For a constant total thrust/power requirement, changes in thrust/power in one shaft must be accompanied by an equal and opposite change in thrust/power in the other shaft. Therefore, the maximum rate of change of the thrust/power split is constrained by the shaft with the lower thrust rate of change at any given operating point. This suggests that if the thrust change dynamics are limiting the energy management control policy when compared to the dynamic limitation-free case, then focus should be placed on improving the dynamic response of the limiting shaft.

5.4 Design implications

From the resource optimization and matching results presented in this Chapter, several design implications can be articulated.

First, the availability of multiple energy sources in a hybrid propulsion system necessitates hybrid propulsion systems to have a energy management policy that takes into account the entire mission profile. Otherwise it is not guaranteed that the system

will be able to meet all operational requirements with an arbitrary energy management policy. Furthermore, a time-coupled policy ensures that the energy resources are utilized optimally and ensures that performance can be accurately estimated apriori. Dynamic programming (DP) is one framework that is able to determine an optimal, time-coupled, energy management policy.

The second design implication is that the carbon-fuel engine and EM efficiency maps can be matched such that they interact with each other to improve the total efficiency of the system. This enables the hybrid propulsion system to optimally utilize the EM and CF engine such that the best possible total efficiency value is achieved through the entire operating range. In general for a parallel configuration, matching may be achieved with efficiency maps that are efficient at different operating points (since the efficiency maps superimpose on each other for a parallel system).

The third design implication, which holds for a parallel configuration and when the EM derives its power from the CF stores, is that the CF engine must be able to accommodate the generator load for the EM to access its full operating range. The need for the full EM operating range must be evaluated on a case-by-case basis. Accommodating the generator load can either be accomplished by having a CF engine with a large torque range or by undersizing the propeller attached to the CF engine.

The final design implication is related to the dynamic matching between propulsion system components. For all configurations, the system dynamics determine the ability of the system to respond to changes in the required operating point or thrust/power output. Dynamic response could affect the ability of the propulsion system to meet the optimal operating points for fuel consumption or meet the operational requirements. Whether or not the dynamic response of a hybrid system is sufficient must be evaluated on a case-by-case basis.

5.5 Summary

This section focuses on several operational aspects of modular hybrid propulsion system usage in aircraft. First, a DP framework was implemented to determine the

hybrid energy management policy. The energy management policy determined by the DP framework is shown to be match the theoretical optimum policy in minimizing fuel consumption over cruise with a simple example. Furthermore the DP framework enables the stakeholder to set operational constraints throughout the flight profile; the DP framework has the ability to account for all constraints during determination of the optimal energy management policy.

The second operational aspect focused on is the static matching of hybrid components and corresponding effect on hybrid propulsion system performance. Efficiency map matching between an ICE and EM for a single-shaft parallel hybrid is demonstrated, with the total efficiency shown to be greater than the efficiency achievable with either the EM or ICE alone across the entire operating range. For a separate shaft configuration, it was shown that to enable the EM to access its full operating range when it derives energy from the generator, the CF engine must have enough torque to accommodate the generator load. One method to ensure enough torque is to size the propeller attached to the CF engine such that the propeller torque load is lower than it would otherwise be if sized without regard for the generator. Whether or not it is necessary for the EM to access its full operating range must be evaluated on a case-by-case basis. Factors to consider include whether or not limiting EM range affects the optimal energy management scheme and other practical requirements.

The final operational aspect is the dynamic matching characteristics of a parallel hybrid propulsion system. Single-shaft and separate shaft configurations are explored; for both configurations, dynamic performance limits the propulsion system's rate of thrust/power change. Whether or not the rate limitation constrains the energy management policy or ability to meet operational requirements should be evaluated on a case-by-case basis. For a single shaft configuration, the rate is set by the relationship between driving torque (from the EM and CF engine) and loads. With the separate shaft configuration, the thrust/power split is limited by the slower of the two shafts, when the thrust is constrained to remain constant. This is because as one shaft's thrust/power increases, the other one must decrease to keep the thrust/power constant.

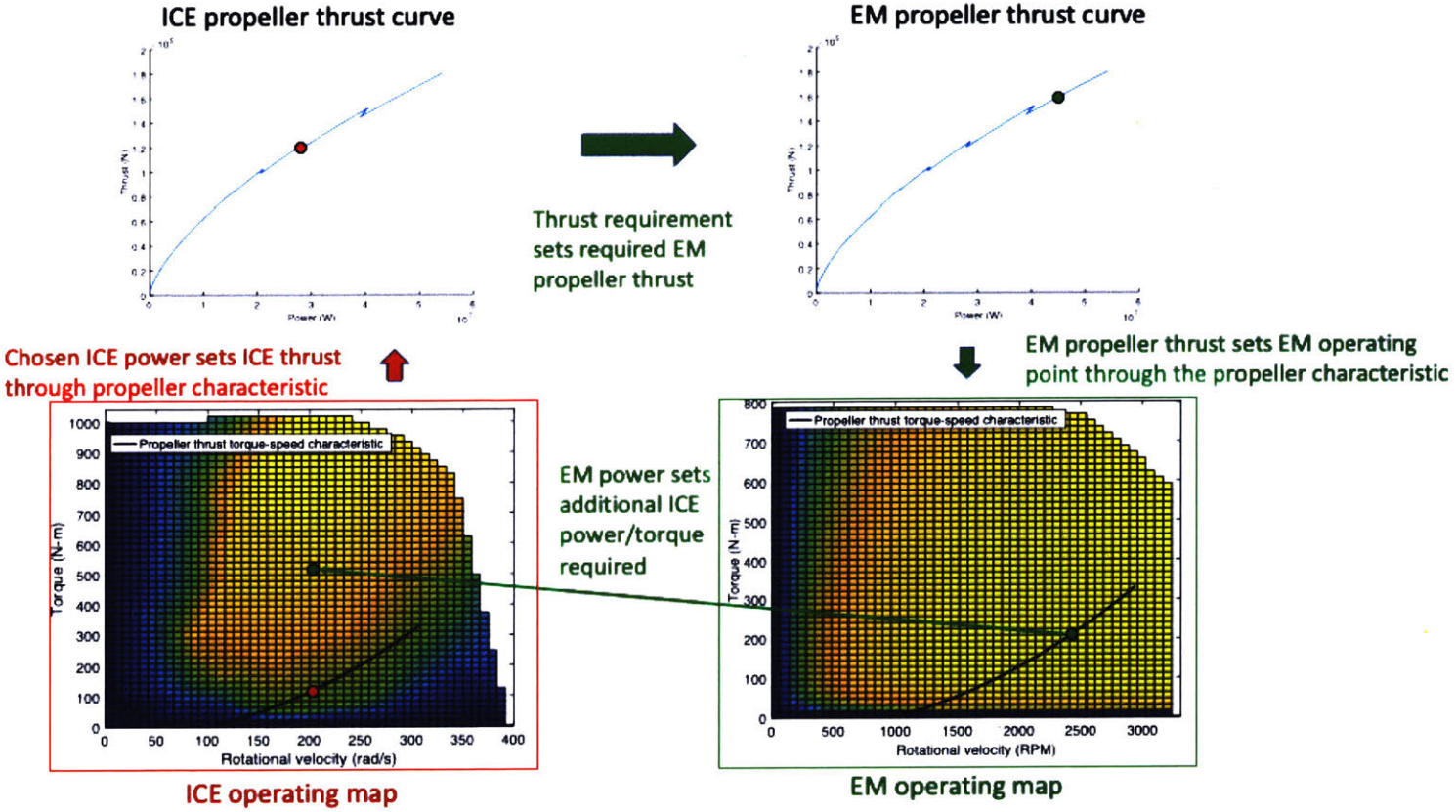


Figure 5-7: Efficiencies for the separate shaft, parallel hybrid efficiency comparison. Setting a power split value sets the CF engine/propeller operating point. The EM must provide the remaining power to meet the total power requirement; the power is derived from the generator, which adds an additional torque load to the CF engine.

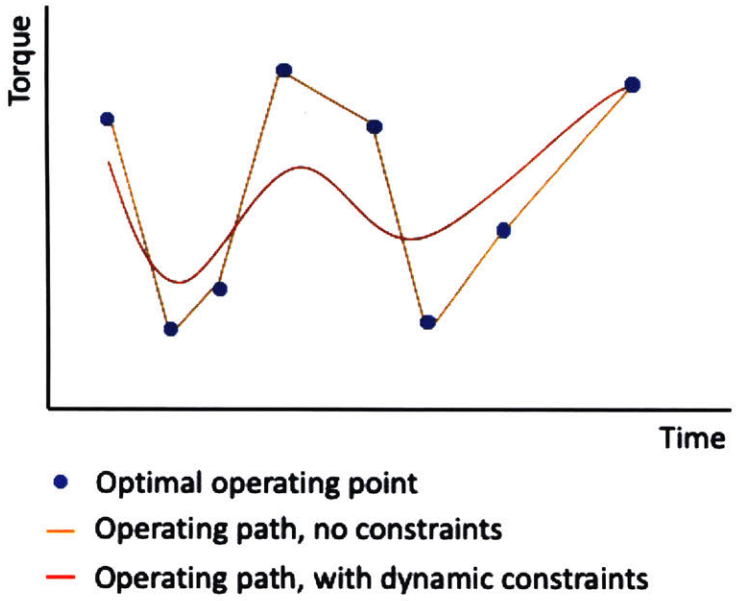


Figure 5-8: Effect of dynamic constraints on the optimal operation path of a system. The blue points represents the optimal operating points, with the orange line indicating the unconstrained operation path and the red line indicating the dynamically constrained operation path.

Chapter 6

Summary and conclusion

6.1 Summary

This thesis presents the concept of a novel Modular Hybrid Propulsion System (MHPS) for use in aircraft to enhance performance and flexibility. The MHPS considered here refers to a propulsion system consisting of a carbon-fuel subsystem and electrical subsystem, in either a parallel or series hybrid configuration, with the electrical components and carbon-fuel tank interchangeable between missions. With modular electrical components, the propulsion system's performance can be tailored to each mission, maximizing mission-specific performance or payload.

To illustrate the performance and flexibility benefits of the MHPS, a large UAV with a traditional propulsion system is assessed against a corresponding UAV with a MHPS. Assessment is carried out with a performance modeling framework detailed in Chapter 3, which determines aircraft performance as a function of hybrid propulsion system performance metrics and design choices. For system constituent components, the traditional propulsion system contains two turbo-diesel carbon-fuel engines, while the MHPS replaces one of the diesel engines with an EM, generator, battery pack, and controllers. A tradeoff study between the parallel and series hybrid configurations was conducted to determine the hybrid configuration considered for the large UAV. Based on the aspects of system mass, efficiency, integration flexibility and mechanical transmission requirements, a parallel hybrid configuration was chosen for the

UAV with the MHPS. For performance assessment, off-the-shelf components and a reconnaissance flight profile were considered for the traditional and modular hybrid propulsion systems. With the components considered, the large UAV with a MHPS was 1.2% heavier, had a 65.8% lower takeoff distance, 6.5% lower cruise time, and 69.6% lower climb rate. The reasons for the differences in performance between the MHPS and traditional propulsion system can be summarized as follows:

- Takeoff distance improvement results from the greater power output (>100%) of the EM when compared to the diesel engine it replaced.
- Mass increase is due to the slightly heavier electrical components compared to the diesel engine they replace.
- Cruise time reduction is due to the slight reduction in total efficiency and increase in aircraft mass.
- Climb rate reduction is due to the limited battery capacity. The diesel engine does not have the capacity to run the generator during climb and so the EM must draw energy from the battery pack for the duration of climb. Therefore battery capacity limits EM power output and by extension, climb rate.

To generalize the MHPS performance estimates for the large UAV retro-fit to other aircraft scales and designs, a set of performance relationships are presented. These performance relationships represent a functional relationship between aircraft performance and high-level propulsion system metrics (such as hybridization levels and specific powers/energies), for various flight segments. The effect of power and energy hybridization values on aircraft performance can be articulated from the performance relationships. Trends related to the power hybridization value are (assuming EM specific power is greater than CF engine specific power):

- Increasing the power hybridization value while maintaining hybrid engine mass proportion reduces the takeoff distance. This is because increasing the power hybridization value will increase the total power output during takeoff of the

propulsion system. For each unit increase in power hybridization, the unit reduction in takeoff distance is dependent on the ratio of specific power between the EM and CF engine π_{EM}/π_{CF}. Higher values result in greater unit reductions in takeoff distance.

- Increasing the power hybridization value while maintaining total aircraft specific power increases the available payload mass ratio $m_{payload}/m_{total}$. This is because the power output of the system is maintained while the engine mass is reduced. The reduction in engine mass directly increases the available payload mass ratio.

The effect of energy hybridization on MHPS performance is dependent on the product of the ratio of battery to CF specific energies $\frac{e_{batt}}{e_{fuel}}$ and the ratio of EM to CF flow efficiencies $\frac{\eta_{EM,flow}}{\eta_{CF,flow}}$. When the product is less than 1, increasing the energy hybridization value while maintaining total energy storage system (ESS) mass decreases the cruise time. This is because the fuel mass is replaced by battery mass, for which less energy can be extracted from on a per unit mass basis. When the product is above 1, increasing the energy hybridization value can have either of two effects, depending on the energy storage system mass ratio $\frac{m_{ESS}}{m_{total}}$. When the product is high enough (quantified in Section 4.2.3), increasing the energy hybridization value increases the cruise time. At this point, utilizing battery energy is more efficient on a per mass basis than carbon-fuel. Therefore increasing battery proportion increases available propulsive energy and cruise time. When the product is an intermediate value (quantified in Section 4.2.3), there is an optimal energy hybridization value that maximizes cruise time. Similar trends are also determined for cruise range and articulated in Section 4.2.4.

To extend the hybrid performance relationship findings to account for modularity, additional performance relationships were determined. In this thesis, modularity is quantified by the amount of mass that is available for modular components, referred to as free mass m_{free}. Performance relationships are formulated to indicate the flight segment performance spread achievable with modularity as a function of design parameters, technological parameters, and free mass. Performance spread is defined

as the difference between best segment performance achievable and baseline segment performance. Baseline segment performance is defined as the performance attained with the CF engine and some chosen fuel mass. For takeoff, free mass is assumed to be utilized by additional EM as EMs typically have superior specific power to CF engines. For cruise, free mass is assumed to be utilized by additional CF due to CF projected to possess superior specific energy to batteries for the next 20+ years. Specific findings are as follows:

- The functional relationship between takeoff performance spread and free mass is dependent on the ratio of EM to CF engine specific powers. When free mass is equal to the baseline engine mass, the takeoff distance can potentially be reduced by approximately 45% for equal EM and CF engine specific power and approximately 90% when the EM specific power is 9 times greater than CF engine specific power.

- The functional relationship between the free mass and cruise time spread is dependent on the ratio of free mass and baseline fuel mass. When free mass is equal to the baseline fuel mass, the cruise time spread is approximately 90% of the baseline cruise time. This is due to the logarithmic nature of the Breguet range equation.

To assess the applicability of the hybrid performance relationships to all aircraft scales, performance estimates from the performance relationships were assessed for 1) a set of hybrid aircraft of which the overall performance features are publicly available and 2) a set of virtual aircraft. For the hybrid aircraft that are in the open literature, performance values are provided for comparison. For the set of virtual aircraft, performance relationship performance estimates were compared against the performance calculated from the modeling framework developed in Section 3.3. The comparisons show that for both sets of aircraft, the magnitude of the performance relationship discrepancies are independent of aircraft scale.

For carbon-fuel and battery energy management in the MHPS, a dynamic programming (DP) framework is proposed. A DP framework was chosen due to its capa-

bility to account for the entire mission profile when determining the optimal energy management policy. This ability ensures that operational requirements throughout the flight profile are met while also ensuring that the resulting energy management policy is optimal. Furthermore, the framework easily enables the stakeholder to control model precision through the discretization scheme used.

The DP framework was implemented for a general cruise scenario, utilizing the modified Breguet range equation (equation 4.16) as the energy consumption model. An optimal energy management policy was found with the DP framework. For the optimal policy, only CF is utilized at first, followed by only battery energy being utilized to complete cruise. This result is in accordance with the theoretical optimum energy management policy.

Key matching characteristics for the MHPS are evaluated:

1. *Matching between the efficiency maps of the EM and CF engine in a parallel hybrid configuration.* For the configuration for which the CF engine and EM are attached to the same shaft, it is shown that the efficiency maps can collaborate to enable the total system efficiency to be higher than what could achievable with just the CF engine or EM. For a configuration with the CF engine and EM on separate shafts, the CF engine must have excess torque available to accommodate the generator load to enable the EM to access its full operating range. Whether or not the full operating range is required must be evaluated on a case-by-case basis.

2. *Collaboration of the propulsion component dynamics and effect on the total propulsion system dynamic performance.* For both the single and separate shaft parallel hybrid configurations, the dynamics primarily affect how quickly the system can respond to changes in required operating point. This has the potential to limit the energy management policy but must be evaluated on a case-by-case basis.

6.2 New findings and conclusion

6.2.1 System-level findings

Overall, the Modular Hybrid Propulsion System has shown the potential to enable a step-change in aircraft propulsion system performance and flexibility. The step-change is accomplished through combining the benefits of hybridization with the concept electrical component and fuel tank modularity.

The primary benefit of hybridization is enabling the use of electric motors (EMs), which hold several distinct advantages over traditional CF engines.

1. In many cases EMs have a higher specific power than CF engines. This can either enable the total hybrid engine size/mass to be reduced while maintaining power output or increasing total power output while maintaining engine size/mass. Correspondingly, either the payload capacity can be increased or the takeoff distance can be reduced. The performance relationships quantify these relationships and can be applied for performance estimation of a MHPS for all scale of aircraft.

2. Propulsive drivers (such as propellers) are easier matched to EMs when compared to CF engines. This is largely a consequence of EMs having a constant power output over a wide operating range, while CF engines reach maximum power at a specific operating point.

3. In a parallel hybrid configuration, the efficiency maps of the EM and CF engine can collaborate. Collaboration enables high system efficiency over a wide operating range if the efficiency maps are matched well.

In addition to holding advantages over CF engines, hybrid engines are also projected to enable superior cruise times/ranges over pure-electric propulsion systems for many years (20+). This is due to the inferior specific energy of batteries compared to carbon-fuel in the present and near future. Optimal battery sizing rules were derived that are a function of the product of the ratio of CF to battery specific energies and

ratio of EM to CF engine efficiencies. Overall, hybrid propulsion systems offer performance improvements over traditional propulsion systems while minimizing energy storage capability reductions.

With modularity, the MHPS enables maximum performance or payload capacity mission-to-mission. This is accomplished by ensuring that the propulsion system is properly sized, such that there is no "dead" mass and ensuring operational requirements are met. Significant changes in propulsion system performance when the free mass ratio magnitude is similar to the magnitudes of the baseline fuel or engine mass ratios. For example, if the engine mass ratio, fuel mass ratio, and free mass ratio are all equal, for an EM to CF engine specific power ratio of 9 and current battery technology, modularity enables the takeoff range to be reduced by up to 90% or the cruise endurance to be increased by up to 90%. With a large range of performance potential, a MHPS has the ability to enable a single airframe to meet a diverse set of mission requirements and accomplish a wide variety of missions. This concept is illustrated for a general aviation aircraft in Figure 6-1.

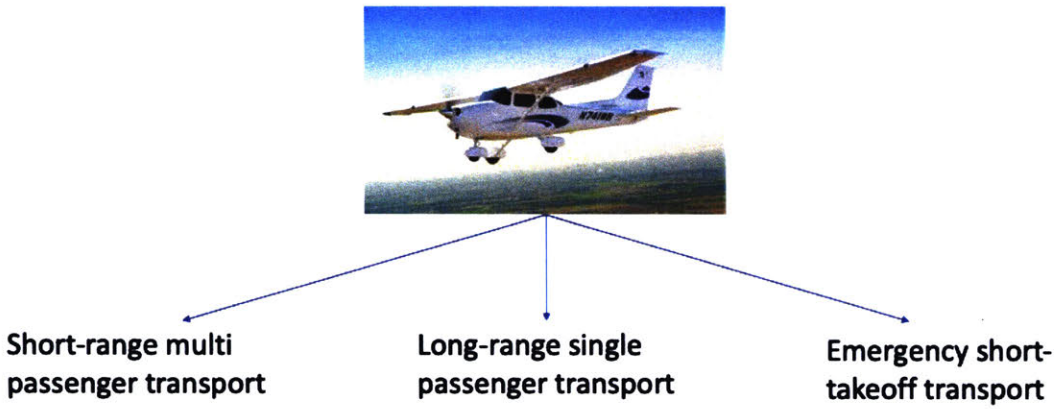


Figure 6-1: A single airframe for a GA aircraft could potentially take on several diverse roles with a MHPS

For energy management, a DP framework has the capability to optimize energy usage while ensuring operational requirements are met. Furthermore, it can be used to evaluate how well components match together on a mission-by-mission basis. The need for this ability is clear when considering the matching characteristics of the MHPS. Within the MHPS, component efficiency maps can collaborate to increase

the high-efficiency range of the propulsion system. The need for this expansion of the high efficiency region of the system is dependent on the mission; some missions may require the propulsion system to operate at many operating points while some may only require operation at a few operating points. A DP framework can be used to evaluate how efficiency map collaboration affects total fuel consumption for a mission. Similarly, the dynamic matching characteristics of the MHPS limit its rate of operation point change, but whether or not this affects fuel consumption can be determined by the DP framework.

While there are practical issues to be solved and several of the present models must be extended, the novel MHPS concept shows promise in enabling a step-change in aircraft propulsion system performance and flexibility.

6.2.2 Performance relationship design implications

The hybrid and modular performance performance relationships determine the conditions for which it is beneficial to utilize a MHPS over a traditional carbon-fuel propulsion system.

For a parallel hybrid propulsion system, the hybrid performance performance relationships indicate that hybridization of the propulsion system increases aircraft performance under the following conditions:

1. Payload capacity and takeoff performance are improved with hybridization if the electric motor specific power π_{EM} is greater than the specific power of the carbon-fuel engine π_{CF} it is replacing ($\pi_{EM} > \pi_{CF}$). In this case, the greater the power hybridization value, the lower the takeoff distance and greater the payload capacity for an equivalent aircraft.

2. Cruise time can be improved with hybridization if $e_{batt}\eta_{EM,flow} > e_{fuel}\eta_{CF,flow}$. Otherwise, hybridization will decrease cruise time; if still hybridized, battery proportion should be minimized to ensure maximal cruise time. If $e_{batt}\eta_{EM,flow} \geq e_{fuel}\eta_{CF,flow}$, then the optimal battery size is dependent on the value of $\frac{e_{batt}\eta_{EM,flow}}{e_{fuel}\eta_{CF,flow}}\left(\frac{2m_{fixed}}{m_{ESS}} - 1\right) - \frac{2m_{fixed}}{m_{ESS}} - 2$. This term quantifies the cruise time ben-

efit from burning fuel (reducing aircraft mass in the process). If less than 1, battery proportion r_m should be set to $r_m = \frac{2m_{fixed}\left(\frac{e_{batt}\eta_{EM,flow}}{e_{fuel}\eta_{CF,flow}}-1\right)}{m_{ESS}\left(\frac{e_{batt}\eta_{EM,flow}}{e_{fuel}\eta_{CF,flow}}+2\right)}$ to maximize cruise time. If greater than 1, energy hybridization should be maximized for maximum cruise time. Similar battery sizing rules exist for maximal cruise range and are articulated in Section 4.2.4.

Based on current technology (2018), the specific energy of batteries is well below that of carbon-fuel (battery specific energy is approximately 2% of carbon-fuel specific energy). As a result hybridization will result in reductions in cruise time and range if carbon-fuel is directly replaced with batteries. The peak specific power of typical state-of-the-art electric motors is above (about 9 times) the specific power of typical turbo-diesel engines, (about 6 times) the specific power of gasoline engines and (about 3 times) the specific power of typical small turbines. For turbofans and large turboshafts, the specific power of EMs are roughly equal (large turboshafts) or lower (turbofans). Based on these technology comparisons from a pure-performance viewpoint, hybridization is most beneficial for smaller GA-level aircraft for takeoff enhancement because these typically utilize internal combustion engines. Hybridization is not recommended for larger aircraft (such as commercial airliners) that typically utilize larger turboshafts or turbofans because hybridization will result in equivalent or worse takeoff performance with reduced cruise performance. Two exceptions exist: 1) if hybridization enables the use of unique propulsion architectures (such as boundary layer ingestion or distributed propulsion) that may provide efficiency or other operational benefits and 2) if propulsion system modularity is desired.

The modular performance performance relationships indicate that aircraft flight performance can be altered significantly (>50%) through electrical component and carbon-fuel tank modularity. In general, performance swings are dependent on the amount of mass that is available for modularity m_{free}. Takeoff performance spread magnitude is dependent on the ratio of electric motor specific power to the baseline propulsion system specific power (typically the CF engine), $\frac{\pi_{EM}}{\pi_{CF}}$. Cruise performance range magnitude is dependent on whether carbon-fuel or battery is utilized (the op-

timal choice depends on level of battery vs. carbon-fuel specific energy). Modularity is primarily recommended for aircraft that are required to meet a broad set of mission requirements such as large UAVs, as modularity would enable these aircraft to maximize performance on a mission-to-mission basis.

Chapter 7

Recommendations for future work

Future work on the MHPS should focus in four areas. First, the hybrid and modular performance relationships should be extended to account for vertical takeoff and landing (VTOL) aircraft. VTOL aircraft are rapidly becoming prevalent in future aircraft designs due to vertical takeoff eliminating runway requirements. Furthermore, the use of electrical components in a MHPS makes practical implementation of a VTOL configuration more feasible. For a VTOL aircraft, the cruise and payload performance relationships remain applicable since these two are not affected by the VTOL capability. A vertical takeoff performance relationship and hover-time performance relationship would enable performance estimation for all scale of VTOL aircraft.

The second area of future work would be practical implementation of the MHPS on an aircraft. Currently the modular concept's performance benefits are articulated and quantified, without regard for practical implementation. Several issues related to implementation are:

1. Structural/mechanical design that enables modularity, propulsion system layout that ensures aircraft stability while considering modularity.

2. Propulsion system layout that ensures aircraft structural integrity and stability when considering modular componentry.

3. A proof-of-concept implementation of the MHPS concept on an existing airframe.

Each of these items would push the MHPS concept closer towards implementation on operating aircraft.

The third area of future work should be more detailed development and implementation of the DP framework for determining the optimal energy management policy. Additional flight operational constraints would include high-energy usage payloads (such as a radar), acceleration (dash) segments, and EM-only usage (for low acoustics). Further work could be focused on a proof-of-concept utilizing the DP framework to evaluate component choices and matching. For example, efficiency maps could be utilized in-place of constant efficiencies. In this case, the DP framework would find the optimal power-split at each time-point, analogous to what is done in Section 5.3.1. In this way, the effect of CF engine and EM efficiency map shape on mission fuel consumption could be quantified.

The fourth area of future work would be investigation of MHPS dynamics on a more holistic basis. Instead of focusing on shaft dynamics, focus would be placed on the interaction of the propulsion system with the rest of the aircraft. With each part of the aircraft having different dynamics, there is an open question on how propulsion system dynamics and placement affect overall aircraft dynamic characteristics. Furthermore, if a link between overall aircraft dynamic characteristics and component characteristics, traditional, all-electric, and hybrid propulsion system tradeoffs could be quantified in terms of system dynamics.

Appendix A

Derivation of Hybrid Performance Relationships

A.1 Takeoff distance performance relationship derivation

The takeoff distance performance relationship is derived from conservation of energy and definition of the conversion efficiency, assuming constant altitude during takeoff:

$$\frac{d(KE)}{dt} = mv\frac{dv}{dt} = P_{total}\eta_{convert} \tag{A.1}$$

To substitute takeoff distance into the above relationship, a first order approximation is used:

$$dR = vdt \tag{A.2}$$

Substitution of the above into the conservation of energy equation:

$$mvdv = \frac{P_{total}\eta_{convert}}{v}dR \tag{A.3}$$

Rearranging yields:

$$dR = \frac{mv^2}{P_{total}\eta_{convert}}dv \tag{A.4}$$

Integration of the above yields the following, assuming constant mass during the takeoff run. Takeoff is assumed to occur when aircraft velocity reaches the specified takeoff velocity:

$$\Delta R = \left(\frac{m_{total}}{P_{total}}\frac{1}{\eta_{convert}}\right)\left[\frac{v^3}{3}\right]_0^{v_{TO}} \tag{A.5}$$

With the takeoff velocity set to the aircraft stall velocity shown in equation 3.1 (using the takeoff lift coefficient), the takeoff range is found:

$$\Delta R = \frac{1}{3}\left(\frac{m_{total}}{P_{total}}\frac{1}{\eta_{convert}}\right)\left(\frac{m_{total}}{S}\right)^{3/2}\left(\frac{2g}{\rho}\right)^{3/2}\frac{1}{{c_L}^{3/2}} \tag{A.6}$$

The total aircraft specific power can be rewritten as a function of the EM and CF engine specific powers as follows. First conservation of energy:

$$P_{total} = P_{EM} + P_{CF} \tag{A.7}$$

Normalizing by total mass and multiplying/dividing the EM and CF power by EM and CF mass respectively yields:

$$\frac{P_{total}}{m_{total}} = \frac{P_{EM}}{m_{EM}}\frac{m_{EM}}{m_{total}} + \frac{P_{CF}}{m_{CF}}\frac{m_{CF}}{m_{total}} \tag{A.8}$$

Further, by defining $m_{propSystem} = m_{CF} + m_{EM}$ and substituting it into Equation A.8 yields:

$$\frac{P_{total}}{m_{total}} = \frac{m_{propSystem}}{m_{total}}\left(\frac{P_{EM}}{m_{EM}}\frac{m_{EM}}{m_{propSystem}} + \frac{P_{CF}}{m_{CF}}\frac{m_{CF}}{m_{propSystem}}\right) \tag{A.9}$$

Rearranging and substitution of the definition of power hybridization H_P and Equation A.9 yields the takeoff distance performance equation (Equation 4.2).

$$\frac{\Delta R\left(\frac{m_{propSystem}}{m_{total}}\right)}{\left(\frac{m_{total}}{S}\right)^{\frac{3}{2}}\left(\frac{2g}{\rho}\right)^{\frac{3}{2}}} = \frac{1}{3}\frac{1}{{c_L}^{\frac{3}{2}}}\frac{1}{\eta_{convert}}\left(\frac{(1-H_P)}{\pi_{ICE}} + \frac{H_P}{\pi_{EM}}\right) \tag{A.10}$$

A.2 Cruise time performance relationship derivation

The total cruise time of an aircraft with a hybrid propulsion system is taken as the sum of cruise times using the carbon-fuel and electric sub-systems independently. The implicit assumption is that each sub-system's power output is adequate to maintain steady cruise when used independently.

For carbon-fuel usage, the derivation begins with the definition of brake specific fuel consumption (BSFC), a common metric used to quantify carbon-fuel engine fuel consumption:

$$BSFC = \frac{-\frac{dm_{fuel}}{dt}}{P_{CF}} \tag{A.11}$$

Noting that to maintain steady cruise, the power output is equal to the momentum power dissipated:

$$P_{CF}\eta_{CF,prop} = \dot{A}^* \tag{A.12}$$

Substituting the above and rearranging the BSFC equation yields:

$$\frac{dm_{fuel}}{dt}\eta_{CF,prop} = -(BSFC)\dot{A}^* \tag{A.13}$$

Further noting that aircraft weight ($m_{aircraft}g$) is equal to lift for cruise, and that $\frac{dm_{fuel}}{dt}$ is equal to $\frac{dm_{aircraft}}{dt}$ (only source of aircraft mass change is due to fuel burn), Equation A.13 becomes:

$$\frac{dm_{aircraft}}{dt} = -(BSFC)\dot{A}^*\frac{(m_{aircraft}g)^{3/2}}{L^{3/2}}\frac{1}{\eta_{CF,prop}} \tag{A.14}$$

Further rearranging and multiplying the numerator and denominator of the right hand side (R.H.S) by $\sqrt{\rho S}$ yields:

$$\frac{dm}{m^{3/2}} = -(BSFC)\frac{\dot{A}^*\sqrt{\rho S}}{L^{3/2}}\frac{g^{3/2}}{\sqrt{\rho S}}\frac{1}{\eta_{CF,prop}}dt \tag{A.15}$$

Integrating both sides from the start of cruise to end of cruise, which is defined

as the time when fuel mass is equal to zero yields:

$$\left[-2m^{-1/2}\right]_{m_{fixed}+m_{fuel}}^{m_{fixed}} = -(BSFC)\frac{\dot{A}^*\sqrt{\rho S}}{L^{3/2}}\frac{g^{3/2}}{\sqrt{\rho S}}\frac{1}{\eta_{CF,prop}}\Delta t \tag{A.16}$$

Rearranging and noting that $BSFC = \frac{1}{\eta_{CF}e_{fuel}}$,

$$\Delta t = 2\eta_{CF}\eta_{CF,prop}e_{fuel}\frac{\sqrt{\rho S}}{g^{3/2}}\frac{L^{3/2}}{\dot{A}^*\sqrt{\rho S}}\left(\frac{1}{\sqrt{m_{fixed}}} - \frac{1}{\sqrt{m_{fixed}+m_{fuel}}}\right) \tag{A.17}$$

For the electric battery contribution to the cruise time, a similar approach is taken. The derivation is based on conservation of energy:

$$P_{EM} = \dot{A}^* \tag{A.18}$$

Utilizing the definition of EM and battery discharge efficiency (denoted η_{batt}):

$$P_{EM} = \frac{dE_{batt}}{dt}\eta_{EM}\eta_{batt}\eta_{EM,prop} = \dot{A}^*\frac{(m_{aircraft}g)^{3/2}}{L^{3/2}} \tag{A.19}$$

After rearranging:

$$dE_{batt}\eta_{EM}\eta_{batt}\eta_{EM,prop} = \frac{\dot{A}^*}{L^{3/2}}(m_{aircraft}g)^{3/2}\,dt \tag{A.20}$$

Integration of A.20 yields the following (note that aircraft mass is assumed constant during battery-supplied cruise):

$$E_{batt}\eta_{EM}\eta_{batt}\eta_{EM,prop} = \frac{\dot{A}^*}{L^{3/2}}(m_{aircraft}g)^{3/2}\,\Delta t \tag{A.21}$$

Combining equations A.17 and A.21 and noting the definitions of CF and EM flow efficiency yields the total cruise time of an aircraft with a hybrid propulsion system:

$$\Delta t = \frac{L^{3/2}}{\dot{A}^*}\frac{1}{g^{3/2}}\left[2\eta_{CF,flow}e_{fuel}\left(\frac{1}{\sqrt{m_{fixed}}} - \frac{1}{\sqrt{m_{fixed}+m_{fuel}}}\right) + \frac{m_{batt}e_{batt}\eta_{EM,flow}}{m_{fixed}^{3/2}}\right] \tag{A.22}$$

Rearranging yields the total cruise time performance relationship shown in Equation 4.16.

A.3 Cruise range performance relationship derivation

Derivation of the cruise range performance relationship is similar to the derivation of cruise time performance relationship with one key difference. For cruise range, it is assumed that the air density ρ is variable and equal to the value that would be required for the aircraft to maintain steady flight. For the cruise range contribution due to carbon-fuel, before Equation A.15 can be integrated, the variable air density must be taken into account. Noting that in this case air density ρ is equal to:

$$\rho = \frac{2m_{aircraft}g}{Sc_L v^2} \tag{A.23}$$

Equation A.15 becomes:

$$\frac{dm}{m^{3/2}} = -(BSFC)\frac{\dot{A}^*\sqrt{\rho S}}{L^{3/2}}\frac{gv}{\sqrt{\frac{2m}{c_L}}}\frac{1}{\eta_{CF,prop}}dt \tag{A.24}$$

Rearranging, noting that $dt = \frac{dR}{v}$ and $BSFC = \frac{1}{\eta_{CF}e_{fuel}}$ yields:

$$\frac{dm}{m} = -\frac{1}{\eta_{CF}e_{fuel}}\frac{\dot{A}^*\sqrt{\rho S}}{L^{3/2}}g\sqrt{\frac{c_L}{2}}\frac{1}{\eta_{CF,prop}}dR \tag{A.25}$$

Integration of A.25 from starting cruise mass to end cruise mass (zero fuel) yields:

$$\ln\left(\frac{m_{fixed+fuel}}{m_{fixed}}\right) = \frac{1}{\eta_{CF}e_{fuel}}\frac{\dot{A}^*\sqrt{\rho S}}{L^{3/2}}g\sqrt{\frac{c_L}{2}}\frac{1}{\eta_{CF,prop}}R_{cruise} \tag{A.26}$$

Further simplification yields the CF contribution to cruise range:

$$\frac{R_{cruise}g\sqrt{\frac{c_L}{2}}}{\left(\frac{L^{3/2}}{\dot{A}^*\sqrt{\rho S}}\right)e_{fuel}\eta_{CF,flow}} = \ln\left(1+\frac{m_{fuel}}{m_{fixed}}\right) \tag{A.27}$$

The derivation of the cruise range contribution due to battery usage begins with Equation A.20, and multiplying/dividing through by ρS to yield:

$$dE_{batt}\eta_{EM,flow} = \frac{\dot{A}^*\sqrt{\rho S}}{L^{3/2}}\frac{1}{\sqrt{\rho S}}\left(m_{aircraft}g\right)^{3/2}dt \tag{A.28}$$

Noting that $dt = \frac{dR}{v}$, Equation A.23, and that aircraft mass is the fixed mass (assuming battery usage is after fuel is expended), yields:

$$dE_{batt}\eta_{EM,flow} = \frac{\dot{A}^*\sqrt{\rho S}}{L^{3/2}}\sqrt{\frac{c_L}{2}}\left(m_{aircraft}g\right)dR \tag{A.29}$$

Integration yields:

$$E_{batt}\eta_{EM,flow} = \frac{\dot{A}^*\sqrt{\rho S}}{L^{3/2}}\sqrt{\frac{c_L}{2}}\left(m_{aircraft}g\right)R_{cruise} \tag{A.30}$$

After rearranging and noting $E_{batt} = m_{batt}e_{batt}$:

$$\frac{R_{cruise}g\sqrt{\frac{c_L}{2}}}{\left(\frac{L^{3/2}}{\dot{A}^*\sqrt{\rho S}}\right)} = \frac{m_{batt}}{m_{fixed}}e_{batt}\eta_{EM,flow} \tag{A.31}$$

Which is the contribution to cruise range due to battery usage.

Combination of Equations A.27 and A.31 yields the final cruise range performance relationship shown in Equation 4.17.

A.4 Payload performance relationship derivation

The payload performance relationship derivation is based on conservation of mass with the following component parts:

1. Payload capacity
2. Hybrid engine, consisting of the EM, generator, and CF engine.
3. Aircraft structure/airframe
4. Battery pack

5. Fuel tank and fuel mass

Conservation of mass then yields:

$$m_{total} = m_{payload} + m_{fuel} + m_{batt} + m_{struct} + m_{gen} + m_{CF} + m_{EM} \tag{A.32}$$

Normalizing by m_{total} and rearranging yields:

$$\frac{m_{payload}}{m_{total}} = 1 - \frac{m_{struct}}{m_{total}} - \frac{m_{batt}}{m_{total}} - \frac{m_{fuel}}{m_{total}} - \frac{m_{gen}}{m_{total}} - \frac{m_{CF}}{m_{total}} - \frac{m_{EM}}{m_{total}} \tag{A.33}$$

Substituting the generator, CF engine, and EM specific power values into Equation A.33 along with rearranging yields Equation A.34.

$$\frac{m_{payload}}{m_{total}} = 1 - \frac{m_{struct}}{m_{total}} - \frac{m_{batt}}{m_{total}} - \frac{m_{fuel}}{m_{total}} - \frac{1}{m_{total}} \left(P_{CF} \frac{m_{CF}}{P_{CF}} + P_{gen} \frac{m_{gen}}{P_{gen}} + P_{EM} \frac{m_{EM}}{P_{EM}} \right) \tag{A.34}$$

Multiplying and dividing the last term on the R.H.S by P_{total} in Equation A.34 yields Equation A.35.

$$\frac{m_{payload}}{m_{total}} = 1 - \frac{m_{struct}}{m_{total}} - \frac{m_{batt}}{m_{total}} - \frac{m_{fuel}}{m_{total}} - \frac{P_{total}}{m_{total}} \left(\frac{P_{CF}}{P_{total}} \frac{1}{\pi_{CF}} + \frac{P_{gen}}{P_{total}} \frac{1}{\pi_{gen}} + \frac{P_{EM}}{P_{total}} \frac{1}{\pi_{EM}} \right) \tag{A.35}$$

Finally, assuming that the generator capacity is equal to the CF engine power capacity ($P_{gen} = P_{CF}$) and noting the definition of power hybridization ($H_P = \frac{P_{EM}}{P_{total}}$ yields the payload scaling relationship (Equation 4.18).

$$\frac{m_{payload}}{m_{total}} = 1 - \frac{m_{struct}}{m_{total}} - \frac{m_{batt}}{m_{total}} - \frac{m_{fuel}}{m_{total}} - \frac{P_{total}}{m_{total}} \left[(1 - H_P) \left(\frac{1}{\pi_{CF}} + \frac{1}{\pi_{gen}} \right) + H_P \frac{1}{\pi_{EM}} \right] \tag{A.36}$$

A.5 Climb rate performance relationship derivation

Similar to the derivation for the cruise time performance relationship, the climb rate performance relationship derivation begins with conservation of energy. In this case for steady climb, the power output of the propulsion system must equal the change in potential energy of the aircraft and power dissipated due to aerodynamic losses:

$$(P_{EM} + P_{CF})\,\eta_{prop} = m_{aircraft} g \frac{dh}{dt} + P_{drag} \tag{A.37}$$

With the assumption that the CF system power output is equal to drag power, the EM system power output is then equal to the rate of aircraft potential energy change:

$$P_{EM}\eta_{EM,prop} = m_{aircraft} g \frac{dh}{dt} \tag{A.38}$$

Noting the definition of battery and EM efficiency and substituting those parameters into Equation A.38 yields:

$$\frac{dE_{batt}}{dt}\eta_{EM}\eta_{batt}\eta_{EM,prop} = m_{aircraft} g \frac{dh}{dt} \tag{A.39}$$

Integration of Equation A.39 with respect to time yields the battery energy used for climb:

$$E_{batt} = \frac{e_{batt} m_{batt}}{\eta_{EM}\eta_{batt}\eta_{EM,prop}} = \frac{m_{aircraft} g \Delta h}{\eta_{EM}\eta_{batt}\eta_{EM,prop}} \tag{A.40}$$

A.6 Modular takeoff distance spread derivation

For the modular takeoff distance spread performance relationship derivation, it is assumed that all of the free mass is utilized for increasing the EM size and/or adding additional EMs. This assumption is taken because in many cases, the specific power of the EM is greater than the CF engine, so a unit mass increase in EM will increase the total power output more than a unit mass increase in CF engine. Additionally, the baseline configuration is assumed to contain only a CF engine. Therefore the

takeoff distance achievable with the baseline is the following:

$$\Delta R_{baseline} = \frac{1}{3}\left(\frac{m_{total}}{m_{CF}}\frac{m_{CF}}{P_{CF}}\frac{1}{\eta_{convert}}\right)\left(\frac{m_{total}}{S}\right)^{3/2}\left(\frac{2g}{\rho}\right)^{3/2}\frac{1}{c_L^{3/2}} \tag{A.41}$$

The minimum takeoff distance is achieved when all the free mass is used for EM:

$$\Delta R_{min} = \frac{1}{3}\left(\frac{m_{total}}{m_{CF}+m_{free}}\frac{1}{\frac{P_{EM}}{m_{EM}}\frac{m_{free}}{m_{total}}+\frac{P_{CF}}{m_{CF}}\frac{m_{CF}}{m_{total}}}\frac{1}{\eta_{convert}}\right)\left(\frac{m_{total}}{S}\right)^{3/2}\left(\frac{2g}{\rho}\right)^{3/2}\frac{1}{c_L^{3/2}} \tag{A.42}$$

Normalizing the difference between Equations A.41 and A.42 by Equation A.41 yields the modular takeoff distance range spread performance relationship (Equation 4.19):

$$\frac{\Delta R_{min}-\Delta R_{baseline}}{\Delta R_{baseline}} = \frac{\frac{m_{free}}{m_{total}}\pi_{EM}}{\left(\frac{m_{prop,base}}{m_{total}}\pi_{prop,base}+\frac{m_{free}}{m_{total}}\pi_{EM}\right)} \tag{A.43}$$

A.7 Modular cruise time spread derivation

Similar to the modular takeoff distance range performance relationship, the modular cruise time performance relationship assumes that the free mass is utilized by filling it with fuel mass. This is because the specific energy of carbon-fuel is and will be much greater than battery specific energy for many years. The baseline configuration is assumed to consist of only some amount of fuel mass for energy storage as well. Therefore the baseline cruise time is the following:

$$\Delta t_{baseline} = 2\eta_{CF}\eta_{CF,prop}e_{fuel}\frac{\sqrt{\rho S}}{g^{3/2}}\frac{L^{3/2}}{\dot{A}^*\sqrt{\rho S}}\left(\frac{1}{\sqrt{m_{fixed}}}-\frac{1}{\sqrt{m_{fixed}+m_{fuel,baseline}}}\right) \tag{A.44}$$

The maximum cruise time is achieved when all of the free mass is utilized for carbon-fuel storage:

$$\Delta t_{baseline} = 2\eta_{CF}\eta_{CF,prop}e_{fuel}\frac{\sqrt{\rho S}}{g^{3/2}}\frac{L^{3/2}}{\dot{A}^*\sqrt{\rho S}}\left(\frac{1}{\sqrt{m_{fixed}}}-\frac{1}{\sqrt{m_{fixed}+m_{fuel,baseline}+m_{free}}}\right) \tag{A.45}$$

Normalizing the difference between Equations A.45 and A.44 by Equation A.44 yields the modular cruise time performance relationship (Equation 4.20):

$$\frac{\Delta t_{max} - \Delta t_{base}}{\Delta t_{base}} = \frac{\sqrt{\frac{m_{fixed}+m_{fuel,base}}{m_{fixed}}} - 1}{1 - \sqrt{\frac{m_{fixed}+m_{fuel,base}}{m_{fixed}+m_{fuel,base}+m_{free}}}} \tag{A.46}$$

A.8 Anergy scaling group derivation

In the context of aircraft, Anergy ($\dot{A}^*$) indicates the the amount of energy dissipated due to aerodynamic drag. In the traditional view, the amount of energy dissipated is equal to the drag force multiplied by velocity and therefore:

$$\dot{A}^* = P_{drag} = \frac{1}{2}\rho S c_D v^3 \tag{A.47}$$

Noting the cruise velocity (Equation B.7):

$$\dot{A}^* = \frac{1}{2}\rho S c_D \left(\frac{L}{\frac{1}{2}\rho S c_L}\right)^{3/2} \tag{A.48}$$

Further rearranging:

$$\frac{\dot{A}^*}{L^{3/2}} = \frac{c_D}{c_L^{3/2}} \frac{1}{\sqrt{\frac{1}{2}\rho S}} \tag{A.49}$$

A final set of rearranging yields the Anergy scaling group:

$$\frac{\dot{A}^*}{L^{3/2}}\sqrt{\rho S} = \sqrt{2}\frac{c_D}{c_L^{3/2}} \tag{A.50}$$

Appendix B

Flight segment performance modeling derivation

B.1 Takeoff performance modeling

Takeoff performance modeling is based upon Newton's Second Law for the aircraft:

$$m_{total}\frac{dv}{dt} = (Th) - D \tag{B.1}$$

Rearranging yields:

$$\frac{dv}{(Th) - D} = \frac{dt}{m_{total}} \tag{B.2}$$

Equation B.2 provides the relationship between time and velocity of the aircraft during takeoff. Additionally noting the first-order approximation of the relationship between distance traveled and velocity:

$$dR = (v)dt \tag{B.3}$$

yields the differential relationship between velocity and distance traveled during takeoff. Takeoff performance modeling is accomplished by numerically integrating Equations B.2 and B.3 simultaneously until the specified takeoff velocity is achieved.

B.2 Climb rate performance modeling

Climb rate performance modeling is achieved through an iterative procedure as follows:

1. An initial optimistic climb rate is assumed. This climb rate is used to calculate energy/power requirements in the succeeding steps.

2. The total climb is discretized into segments of constant altitude change dh.

3. From the FBD depicted in Figure 3-4, the aircraft angle of attack and flight velocity are calculated such that force balance is maintained for each discretized climb segment. Lift and drag coefficients are set apriori based on aircraft aerodynamic characteristics.

4. For each segment, the effective CF engine power is calculated based upon normalized pressure:

$$P_{CF,effective} = P_{CF,SL}\frac{p_h}{p_{SL}} \tag{B.4}$$

5. The required climb power is calculated based on rate of climb and aircraft velocity.

6. It is assumed that CF engine power contributes first to the required climb power, followed by EM/battery power if necessary. Therefore if required climb power is lower than CF engine effective power:

$$P_{CF} = P_{climb} \tag{B.5}$$

   And if the required climb power is greater than the CF engine effective power, then the CF power is set to its maximum and EM power is set to the difference between the two:

$$P_{EM} = P_{climb} - P_{CF,max} \tag{B.6}$$

7. Once the CF engine and EM power are set, the fuel and battery usage are calculated. The CF engine exclusively uses carbon-fuel and the EM exclusively

uses battery energy. Carbon-fuel usage is determined through Equation B.13 and battery usage is determined through Equation B.11.

8. Once the total energy requirements are found, the required battery mass is compared against the battery mass on-board. Fuel mass is assumed to be sufficient for climb. If battery mass on-board is insufficient, the climb rate is reduced and steps 2-7 are repeated until the required battery mass is less than or equal to the battery mass on-board.

B.3 Cruise time and range performance modeling

For the cruise time performance model, it is assumed that aircraft velocity is equal to the velocity required to maintain steady-level cruise:

$$v_{cruise} = \sqrt{\frac{2m_{aircraft}g}{\rho S c_{L,cruise}}} \tag{B.7}$$

The power dissipated from the aircraft due to drag losses is denoted as P_{drag}:

$$P_{drag} = \frac{1}{2}\rho S c_D v_{cruise}^3 \tag{B.8}$$

Additionally, the thrust power must be equal to the dissipated power at each point in time:

$$P_{thrust} = P_{drag} \tag{B.9}$$

For a series hybrid configuration, the entirety of the thrust power is provided by the EM:

$$P_{EM}\eta_{EM,prop} = P_{thrust} \tag{B.10}$$

During cruise, it is assumed that the energy for the EM can either come from the batteries or fuel tank. For battery usage, the rate of battery energy usage comes directly from the definition of battery and EM efficiencies.

$$\frac{dE_{batt}}{dt} = \frac{P_{EM}}{\eta_{EM}\eta_{batt}} \tag{B.11}$$

On the other hand, when the EM draws power from the generator and thus indirectly from the carbon-fuel tank, the rate of fuel usage can be found through the efficiency definitions of the components in the energy flow path:

$$\frac{dm_{fuel}}{dt} = \frac{P_{EM}}{e_{fuel}\eta_{EM}\eta_{batt}\eta_{gen}\eta_{CF}} \tag{B.12}$$

For a parallel configuration where the CF engine directly drives a propeller, the rate of fuel usage is:

$$\frac{dm_{fuel}}{dt} = \frac{P_{CF}}{e_{fuel}\eta_{CF}} \tag{B.13}$$

Once the power split scheme between the CF engine propeller and EM propeller and energy split scheme between the battery and carbon-fuel tank are determined, Equations B.11, B.12 and B.13 are numerically integrated until the battery energy and carbon-fuel mass equal to zero. The time at which this occurs is denoted the cruise time achievable.

The cruise range calculation is similar to the cruise time calculation except the velocity is set apriori and considered constant for cruise. The primary change is that the air density is assumed to change to enable this constant velocity cruise:

$$\rho_{cruise} = \frac{2m_{aircraft}g}{Sc_L v_{cruise}^2} \tag{B.14}$$

Fuel rate and battery energy usage are the same as for the cruise time calculation. The differential cruise range is equal to the velocity multiplied by the differential time-step:

$$dR = v_{cruise}dt \tag{B.15}$$

The total cruise range is achieved when battery and fuel stores are empty.

B.4 Total efficiency derivation for a parallel hybrid propulsion system

The total efficiency of a propulsion system is defined as the ratio of momentum power output to power of the fuel source:

$$\eta_{total} = \frac{(Th)v}{P_{fuel}} \tag{B.16}$$

In this case, it is assumed that energy comes from the carbon-fuel stores. For the energy flow chain from CF to the CF engine propeller, the efficiency is:

$$\eta_{CF,flow} = \frac{(Th)_{CF,prop}v}{P_{fuel_{CF}}} = \eta_{CF,prop}\eta_{CF} \tag{B.17}$$

While for the energy flow chain from CF to the EM engine propeller, the efficiency is:

$$\eta_{EM,flow} = \frac{(Th)_{EM,prop}v}{P_{fuel_{EM}}} = \eta_{EM,prop}\eta_{EM}\eta_{batt}\eta_{gen}\eta_{CF} \tag{B.18}$$

To derive the total efficiency, Equation B.16 is split up into contributions from the EM and CF engine:

$$\eta_{total} = \frac{(Th)_{EM,prop}v + (Th)_{CF,prop}v}{P_{fuel_{EM}} + P_{fuel_{CF}}} \tag{B.19}$$

Equation B.19 can be further manipulated to yield:

$$\eta_{total} = \frac{(Th)_{CF,prop}v}{P_{fuel_{CF}}}\frac{P_{fuel_{CF}}}{P_{fuel_{EM}} + P_{fuel_{CF}}} + \frac{(Th)_{EM,prop}v}{P_{fuel_{EM}}}\frac{P_{fuel_{EM}}}{P_{fuel_{EM}} + P_{fuel_{CF}}} \tag{B.20}$$

The flow efficiencies can be substituted into Equation B.20 to yield:

$$\eta_{total} = \eta_{CF,flow}\frac{P_{fuel_{CF}}}{P_{fuel_{EM}} + P_{fuel_{CF}}} + \eta_{EM,flow}\frac{P_{fuel_{EM}}}{P_{fuel_{EM}} + P_{fuel_{CF}}} \tag{B.21}$$

The fuel powers can be replaced by EM and CF engine power output by utilizing efficiency definitions:

$$P_{fuel,CF} = \frac{P_{CF}}{\eta_{CF}} \tag{B.22}$$

$$P_{fuel,EM} = \frac{P_{EM}}{\eta_{EM}\eta_{batt}\eta_{gen}\eta_{CF}} \tag{B.23}$$

Substituting the above into Equation B.21 yields:

$$\eta_{total} = \eta_{CF,flow}\frac{\frac{P_{CF}}{\eta_{CF}}}{\frac{P_{CF}}{\eta_{CF}} + \frac{P_{EM}}{\eta_{EM}\eta_{batt}\eta_{gen}\eta_{CF}}} + \eta_{EM,flow}\frac{\frac{P_{EM}}{\eta_{EM}\eta_{batt}\eta_{gen}\eta_{CF}}}{\frac{P_{CF}}{\eta_{CF}} + \frac{P_{EM}}{\eta_{EM}\eta_{batt}\eta_{gen}\eta_{CF}}} \tag{B.24}$$

Simplification of Equation B.24 yields:

$$\eta_{total} = \eta_{CF,flow}\frac{P_{CF}\eta_{EM}\eta_{batt}\eta_{gen}}{P_{CF}\eta_{EM}\eta_{batt}\eta_{gen} + P_{EM}} + \eta_{EM,flow}\frac{P_{EM}}{P_{CF}\eta_{EM}\eta_{batt}\eta_{gen} + P_{EM}} \tag{B.25}$$

Substitution of the flow efficiencies back into Equation B.25 yields if propeller efficiencies are equal:

$$\eta_{total} = \frac{(P_{EM} + P_{CF})\,(\eta_{EM}\eta_{gen}\eta_{batt}\eta_{CF})}{P_{CF}\eta_{EM}\eta_{batt}\eta_{gen} + P_{EM}} \tag{B.26}$$

Dividing the numerator and denominator by the total power (sum of CF and EM powers), yields the final total efficiency relationship:

$$\eta_{total} = \frac{\eta_{prop}\eta_{EM}\eta_{gen}\eta_{batt}\eta_{CF}}{\frac{P_{ICE}}{P_{total}}\eta_{EM}\eta_{gen}\eta_{batt} + \frac{P_{EM}}{P_{total}}} \tag{B.27}$$

Appendix C

Hybrid configuration component tradeoff study for large UAV retro-fit

C.1 Carbon-fuel engine selection

To select the carbon-fuel engine, several criteria are used:

- Specific power
- Thermal efficiency or fuel consumption
- Size and how well the power rating matches up with the required cruise power. For the large UAV retrofit, cruise power is estimated to be 30-40 kW.

Furthermore, the carbon-fuel engines must accept diesel fuel due to fuel-availability concerns. Based upon an extensive search, several diesel engine options are considered:

Model/Manufacturer	Power output	Specific power	Fuel consumption
Deltahawk V4 series	120 kW	0.852 kW/kg	246 g/kWh
Safran SR305	171.5 kW	0.831 kW/kg	219 g/kWh
Contindental CD-135	99 kW	0.765 kW/kg	214 g/kWh
Mercedes OM660	40 kW	0.468 kW/kg	216 g/kWh

Table C.1: Carbon-fuel engines considered for the large UAV MHPS retrofit

The first three options are aviation diesel engines which have specific power values around 0.8 kW/kg, while the Mercedes OM660 is a automobile engine with a lower specific power value of 0.468 kW/kg. The fuel consumption of the engines are similar at around 215 g/kWh with the exception of the Deltahawk V4 series, which has a fuel consumption 14.4% higher. Finally, out of the chosen diesel engines, only the power rating of the OM660 is similar to the cruise power required, with other options more than doubling the required power.

Due to the above factors, the OM660 was chosen as the carbon-fuel engine for the large UAV MHPS retro-fit. The primary differentiating factor of the OM660 is the size and how well the power matches the power requirement; all other engines are over-sized and add unused mass to the aircraft.

C.2 Electric motor selection

The selection criteria for electric motors are similar to those for the carbon-fuel engine:

- Specific power
- Thermal efficiency or fuel consumption
- Gross power rating, which should be of similar magnitude as the CF engine. This is to ensure that the propellers are similarly sized between the CF engine and EM.

The following electric motors are considered (note that efficiencies are not shown because the peak efficiencies for all options are similar with around 95% peak efficiency):

From Table C.2, it is clear there are two main classes of EMs considered. The first are small EMs (Thin-gap, Aerotech) that would be connected in series to provide enough power to drive a propeller. The second class are the YASA motors, which are larger size EMs that only require a single module to drive the propeller.

For the small EMs, the total power output can be tuned exactly to what is required since power output can be modified in small increments. While this feature is

Model/Manufacturer	Power output (continuous)	Specific power
Thin-gap TG71xx	4.03 kW	2.55 kW/kg
YASA 750	70.0 kW	1.89 kW/kg
YASA P400	60.0 kW	2.2 kW/kg
Aerotech S series	1.0 kW	0.52 kW/kg

Table C.2: Electric motors considered for the large UAV MHPS retrofit

desirable, the main downside is that even when connected in such a way, the propeller must be matched to the rotational velocity of a single EM, which at the scale shown is in the 10000 RPM range. This rotational velocity is typically too high for a large UAV propeller and would require some gearing.

For the large EMs, the power output cannot be tuned and the EM must have a power rating close to what is required. While large EMs have this drawback, they have rotational velocities around 3000 RPM at the scale shown, which is much better suited to drive a large UAV propeller. For this reason, only the large EMs are considered for the large UAV retro-fit.

Out of the two YASA EMs, the YASA P400 is chosen for the large UAV retro-fit due to a higher specific power. In both cases the power output is of similar magnitude as the Mercedes OM660 and sufficient to provide a significant improvement in takeoff distance.

The YASA P400 has a controller that is specifically designed for it and as an added bonus, the YASA P400 can be utilized as a generator. Therefore it is also chosen as the generator in the large UAV retro-fit

C.3 Battery selection

The main choice for battery selection in the large UAV retro-fit is the battery chemistry and manufacturer. Each chemistry has specific advantages and disadvantages, typically trading off specific energy, reliability, cost, and specific power.

For battery selection, the primary factors for evaluation were:

- Specific energy

- A manufacturer with aviation experience

Due to aviation experience criteria, Kokam was chosen as the battery manufacturer as Kokam has battery packs specifically formulated for aviation applications and restrictions.

Out of the lithium-ion battery chemistry's available, a Nickel-Manganese-Cobalt (NMC) cell was chosen for the retro-fit due to its high specific energy. Kokam packs of this chemistry have a specific energy of around 190 Wh/kg, which is the highest that they offer. Several of these packs are combined together to form the total battery pack for the large UAV retro-fit.

Appendix D

Propulsion system dynamic performance relationship derivation

Dynamics are first considered for the separate shaft case. For the CF subsystem shaft, Newton's Second Law dictates (Note that no gearing is considered):

$$I_{shaft,CF}\frac{d\omega_{CF}}{dt} = T_{CF} - T_{CF,prop} - T_{gen} \tag{D.1}$$

For the EM subsystem shaft:

$$I_{shaft,EM}\frac{d\omega_{EM}}{dt} = T_{EM} - T_{EM.prop} \tag{D.2}$$

Noting the definition of propeller coefficient of thrust:

$$c_{Th} = \frac{(Th)}{\rho D^4 \left(\frac{\omega}{2\pi}\right)^2} \tag{D.3}$$

The rate of thrust change with respect to shaft rotational acceleration can be found by rearranging and taking the derivative of with respect to time:

$$\frac{d(Th)}{dt} = 2c_{Th}\rho D^4 \left(\frac{\omega}{(2\pi)^2}\right)\frac{d\omega}{dt} \tag{D.4}$$

Along with the definition of propeller coefficient of power:

$$c_P = \frac{P}{\rho D^5 \left(\frac{\omega}{2\pi}\right)^3} \tag{D.5}$$

The coefficient of power shown in Equation D.5 can be substituted into Equation D.1 and D.2 by noting the relationship between propeller shaft power and torque:

$$P = T\omega \tag{D.6}$$

For the CF subsystem shaft, Equation D.1 then becomes:

$$I_{shaft,CF}\frac{d\omega_{CF}}{dt} = T_{CF} - \frac{c_{PCF,prop}\rho D^5 \left(\frac{\omega_{CF}}{2\pi}\right)^3}{\omega_{CF}} - T_{gen} \tag{D.7}$$

While for the EM subsystem shaft, Equation D.2 becomes:

$$I_{shaft,EM}\frac{d\omega_{EM}}{dt} = T_{EM} - \frac{c_{PEM,prop}\rho D^5 \left(\frac{\omega_{EM}}{2\pi}\right)^3}{\omega_{EM}} \tag{D.8}$$

Substitution of Equation D.4 into Equations D.7 and D.8 yields Equations D.9 and D.10 respectively.

$$I_{shaft,CF}\frac{\frac{d(Th)_{CF,prop}}{dt}}{2c_{Th}\rho D^4 \left(\frac{\omega_{CF}}{(2\pi)^2}\right)} = T_{CF} - \frac{c_{PCF,prop}\rho D^5 \left(\frac{\omega_{CF}}{2\pi}\right)^3}{\omega_{CF}} - T_{gen} \tag{D.9}$$

$$I_{shaft,EM}\frac{\frac{d(Th)_{EM,prop}}{dt}}{2c_{Th}\rho D^4 \left(\frac{\omega_{EM}}{(2\pi)^2}\right)} = T_{EM} - \frac{c_{PEM,prop}\rho D^5 \left(\frac{\omega_{EM}}{2\pi}\right)^3}{\omega_{EM}} \tag{D.10}$$

Rearranging Equations D.9 and D.10 and dividing through by propeller thrust yields Equations D.11 and D.12 respectively.

$$I_{shaft,CF}\frac{\frac{d(Th)_{CF,prop}}{dt}}{((Th)_{CF,prop})} = \left(\frac{2}{\omega_{CF}}\right)\left(T_{CF} - c_{PCF,prop}\rho D^5 \left(\frac{\omega_{CF}^2}{8\pi^3}\right) - T_{gen}\right) \tag{D.11}$$

$$I_{shaft,EM}\frac{\frac{d(Th)_{EM,prop}}{dt}}{((Th)_{EM,prop})} = \left(\frac{2}{\omega_{EM}}\right)\left(T_{EM} - c_{PEM,prop}\rho D^5\left(\frac{\omega_{EM}^2}{8\pi^3}\right)\right) \quad \text{(D.12)}$$

Dividing Equations D.11 and D.12 through by the CF shaft and EM shaft rotational inertia respectively yields the rate of thrust change achievable on each drive shaft.

The single shaft case is similar as the separate shaft case, except all components are on a single shaft. The dynamic performance relationship is simply Equation D.11 with the addition of the torque contribution from the EM:

$$I_{shaft,total}\frac{\frac{d(Th)_{total,prop}}{dt}}{((Th)_{total,prop})} = \left(\frac{2}{\omega_{shaft}}\right)\left(T_{CF} + T_{EM} - c_{Pprop}\rho D^5\left(\frac{\omega_{shaft}^2}{8\pi^3}\right)\right) \quad \text{(D.13)}$$

Appendix E

Example of MHPS design

An example of MHPS design for a general-use large UAV is detailed here to illustrate the beneficial aspects of the MHPS and how to utilize the findings in this thesis.

For this example, components and aircraft are considered "rubber", or that their sizing can be considered continuous. This means that components can be any size and are not limited to discrete choices.

E.1 Large UAV design scenario

Suppose we are interested in designing a large UAV to accomplish these distinct tasks:

1. Transport a total payload of 200 kg (either 2 passengers or cargo) a range of 600 km (roughly the distance between San Francisco, CA and Los Angeles, CA).

2. Survey a region for a time period of 16 hours, with a camera system that weighs 10 kg.

3. Transfer between airports a distance of 2000 km apart with no payload.

In all cases, it is assumed that runways are guaranteed to allow for a 200 m takeoff distance. However, in few cases, the aircraft must be able to achieve takeoff from a distance of 75 m, while maintaining a 200 km cruise range. Therefore there are a total of four UAV usage-scenarios that must be considered. Cruise altitude is assumed to occur at 5000 m altitude.

Furthermore, the technology considered in this scenario is represented by the following parameters:

- Battery pack specific energy e_{batt} of 200 Wh/kg (720 kJ/kg).
- Battery pack specific power π_{batt} of 750 W/kg.
- EM peak specific power π_{EM} of 9 kW/kg.
- Diesel engine specific power π_{CF} of 1 kW/kg.
- EM thermal efficiency η_{EM} of 0.95 and diesel engine thermal efficiency η_{CF} of 0.4.
- Carbon-fuel specific energy e_{fuel} of 42.6 MJ/kg.

The above values are considered constant no matter the size of each component. Mechanical, electrical, and battery efficiencies are considered to be unity (ideal). A diesel engine is assumed because of expected aircraft scale and need for wider fuel availability compared to airplane gasoline.

For aircraft design parameters, propellers are considered to generate thrust with an efficiency of 0.8 and wing loading is assumed to be 90 kg/m^2 due to the expectation that the cruise velocity will be similar to a general aviation aircraft. The takeoff lift coefficient is taken as 1.5, with a conversion efficiency $\eta_{convert}$ of 0.3. Furthermore, due to external constraints (such as cost, material, and design), the structural mass of the aircraft is assumed to be 40% of the total aircraft mass. Finally, an additional 10% of the total aircraft mass is allocated for miscellaneous system componentry such as drive shaft(s), electrical wires, controllers, and actuators.

For aerodynamics, maximum cruise lift-to-drag ratio is assumed to be 15, with a corresponding lift coefficient of 0.4 (and therefore corresponding drag coefficient of 0.027). For this example, a traditional separation between thrust and drag accounting is assumed, and therefore the lift-anergy ratio $\frac{L^{3/2}}{A^*\sqrt{\rho S}}$ is taken to be equal to $\frac{c_L^{3/2}}{c_D\sqrt{2}}$. In this case, the value is equal to 6.71.

E.2 Component sizing

E.2.1 Determining propulsion system type

To start, the optimal battery sizing rule must be determined through the performance relationships described in Chapter 4. This is based upon the the product of the specific energy ratio e_{batt}/e_{fuel} and efficiency ratio $\eta_{EM,flow}/\eta_{CF,flow}$. Based on the technology parameters assumed, the specific energy ratio is equal to 0.0169 and efficiency ratio is 2.5, resulting in a total product of 0.0422. This value of 0.0422 is much lower than the cruise time threshold of 1, indicating that a minimum battery mass is optimal for cruise time. For cruise range, the group $\left(1+\frac{m_{ESS}}{m_{fixed}}\right)\frac{e_{batt}\eta_{EM,flow}}{e_{fuel}\eta_{CF,flow}}$ must be greater than 1 for the optimum battery sizing rule to be different than the cruise time case. For cruise range, the energy storage system mass ratio m_{ESS}/m_{fixed} must be at least 22.6 for the rule to be different. Based on most conventional aircraft design, this value is infeasible and therefore the optimum battery sizing rule is equivalent for optimal cruise time and range.

From here, there are two design options:

1. A large UAV with a MHPS. This is the choice if one of the cruise time/range requirements cannot be achieved with a pure-electric propulsion system.

2. A large UAV with a modular electric-only propulsion system. This would be the choice if all the cruise and payload requirements are achievable with only battery usage.

To determine whether or not an electric-only propulsion system is feasible, the required battery mass ratio $\frac{m_{batt}}{m_{fixed}}$ for the cruise range/time requirements are calculated through the performance relationships and shown in Table E.1.

From Table E.1, it can be seen that the most stringent requirement from a battery mass standpoint is the cruise time operational requirement. The battery mass ratio must be over 4 times greater than the fixed aircraft mass for an all-electric aircraft to be viable. This is impossible given that the maximum battery mass ratio possible is equal to 1 because the structural mass ratio and miscellaneous mass ratio must total

Operational requirement	Battery mass ratio requirement $\frac{m_{batt}}{m_{fixed}}$
200 kg payload, 600 km cruise range	0.55
10 kg payload, 16 hour cruise time	4.06
0 payload, .2000 km cruise range	1.82

Table E.1: Battery mass ratio requirements for a pure-electric aircraft to meet

0.5 (aircraft is only structure and battery, with no propulsion). Therefore a hybrid propulsion system is necessary.

With the propulsion system type established, initial component size estimates are required to start the iterative process of component sizing.

E.2.2 Sizing of fixed and baseline components

The first initial sizing estimate is of the battery. Since we know that the battery should be minimized for optimal cruise performance, equations 4.9 and 4.3 can be utilized. The specific power requirement requires initial performance/mass estimates of other components while the specific energy requirement only requires the cruise altitude to specify minimum battery size. Therefore the battery specific energy requirement is utilized as it will provide a minimum battery size requirement regardless of other component specifications. From equation 4.9, the minimum battery mass ratio $\frac{m_{batt}}{m_{total}}$ is found to be 0.0681, when considering a cruise altitude of 5000 m and the battery technology considered. At this point a maximum of 63.2% (taking into account required structure, miscellaneous, and battery mass ratios) UAV mass is available for the CF engine, EM(s), generator(s), fuel and payload. For this scenario, we consider the EM(s), payload, additional battery and some amount of fuel as the modular componentry in the MHPS. For the baseline componentry, we need to determine the CF engine size and baseline fuel mass.

To determine the CF engine size the minimum CF engine power needs to be determined. Since the CF engine is required to provide the majority of power/energy for cruise, it must be large enough to overcome drag power. By equating the power dissipated by drag to CF engine power output modified by a propeller efficiency

($P_{drag} = P_{CF}\eta_{prop}$), setting the cruise velocity to that shown in Equation B.7, dividing through by CF engine mass and rearranging, a formulation for the CF engine mass ratio $\frac{m_{CF}}{m_{total}}$ can be found:

$$\frac{m_{CF}}{m_{total}} = \sqrt{\frac{m_{total}}{S}}\sqrt{\frac{2}{\rho}}\frac{g^{3/2}\frac{c_D}{c_L^{3/2}}}{\pi_{CF}\eta_{prop}} \tag{E.1}$$

From equation E.1 and utilizing the UAV design/aerodynamic parameters, the CF engine mass ratio is found to be equal to 0.063. The generator mass ratio m_{gen}/m_{total} is the CF engine mass ratio modified by the ratio of CF engine to generator specific power:

$$\frac{m_{gen}}{m_{total}} = \frac{\pi_{CF}}{\pi_{gen}}\frac{m_{CF}}{m_{total}} \tag{E.2}$$

Noting that the generator specific power value π_{gen} is equal to the EM specific power value of 5, the generator mass ratio is found to be 0.0127.

To determine the baseline fuel mass ratio, the least stringent cruise requirement is used. In this scenario, the least stringent requirement is from the short takeoff case (200 km cruise). Utilizing the cruise range performance equation (equation 4.17), the fuel-to-fixed mass ratio m_{fuel}/m_{fixed} is found to be 0.0078. Since $m_{total} \geq m_{fixed}$, $\frac{m_{fuel}}{m_{total}} \leq \frac{m_{fuel}}{m_{fixed}}$, a first approximation for fuel mass ratio $m_{fuel,baseline}/m_{total}$ can be taken to be 0.0078.

With the required structure mass ratio $m_{structure}/m_{total}$, battery mass ratio m_{batt}/m_{total}, CF engine mass ratio m_{CF}/m_{total}, generator mass ratio m_{gen}/m_{total}, and baseline fuel mass ratio $m_{fuel,baseline}/m_{total}$, the total accounted-for mass ratio is found to be 65.2%. This leaves 34.8% of UAV mass available for modular componentry (EM(s), additional fuel/batt and payload).

E.3 Sizing of modular components to meet operational requirements

With the fixed componentry in place, we need to ensure that the remaining modular component mass budget is sufficient to meet the other operational requirements.

The process can be described as follows:

1. Utilize equation 4.16 or 4.17 to determine the required fuel mass ratio to meet the cruise time or range requirement.

2. Utilize equation 4.2 to determine the required power hybridization factor H_P to meet the takeoff requirement. Use the required power hybridization factor to find the required EM mass ratio m_{EM}/m_{total}.

3. Find the additional (total minus battery in-place for the baseline) battery required to meet the battery specific power requirement. This is accomplished by multiplying the EM mass ratio m_{EM}/m_{total} by the ratio of specific powers between the EM and battery π_{EM}/π_{batt}, which in this case has a value of 12.

4. Find the remaining mass ratio available for payload.

The resulting modular component mass ratios are seen in Table E.2.

From the payload mass ratios $\frac{m_{payload}}{m_{total}}$ shown in Table E.2, it can be seen that the battery mass ratio required for the short takeoff scenario is not feasible. This is because the battery specific power is insufficient and illustrates the fact that the MHPS is still limited by battery technology. To overcome this limitation, changes in aircraft design outside of the propulsion system (altering the wing loading or increasing the takeoff lift coefficient or conversion efficiency) are required.

Ignoring the short-takeoff scenario, the total required aircraft mass can be calculated. The maximum total mass sets the required aircraft size. In this case, the 200 kg payload, 600 km cruise range requirement is the most stringent scenario considered, resulting in a total aircraft mass of 862.07 kg. The resulting fixed component and free mass available calculated from the mass ratios are tabulated in Table E.3.

Operational requirement	Fuel mass ratio requirement $\frac{m_{fuel}}{m_{fixed}}$	EM mass ratio requirement $\frac{m_{EM}}{m_{total}}$	Additional battery mass ratio required $\frac{m_{batt}}{m_{total}}$	Payload mass ratio available $\frac{m_{payload}}{m_{total}}$
200 kg payload, 600 km cruise range	0.0233	0.012	0.076	0.232
10 kg payload, 16 hour cruise time	0.1515	0.012	0.076	0.102
0 payload, 2000 km cruise range	0.0798	0.012	0.076	0.172
75 m takeoff, 0 payload, 200 km cruise range	0.0078	0.042	0.50	-0.202

Table E.2: Modular component mass ratios required to meet operational mission requirements

With the UAV mass breakdown shown in Table E.3, the UAV is able to accomplish the missions outlined at the beginning of this Appendix chapter. While the short-takeoff scenario of 75 m is in-feasible with the battery technology considered, a takeoff distance of 100 m is achievable when utilizing all of the free mass for additional battery.

E.4 Choosing specific components

In the previous section, the findings of Chapter 4 are utilized to size a large UAV to meet several sets of mission requirements. In this section, the findings of Chapter 5 are utilized to further illustrate how to choose between components with similar high-level performance parameter values.

The scenario used for this illustration is as follows.

E.4.1 Component selection scenario

With the desired component sizes calculated in the previous section, consider the scenario where we now have to choose between two component sets with the char-

Component	Mass ratio requirement	Mass $\frac{m_{payload}}{m_{total}}$
Structure	0.40	344.82 kg
Misc.	0.10	86.20 kg
CF engine	0.063	54.31 kg
Generator	0.013	10.94 kg
Battery, baseline	0.068	58.70 kg
Fuel, baseline	0.008	6.72 kg
Free	0.348	300.00 kg

Table E.3: Modular component mass ratios required to meet operational mission requirements

acteristics tabulated in Table E.4. It is assumed that the high-level performance characteristics (power, efficiency, etc) are identical.

Performance characteristic	Component set 1	Component set 2
Maximum thrust rate of change	10 kN/s	3 kN/s
Maximum power split rate of change	0.5/s	0.1/s
EM peak efficiency operating point	400 Nm, 3000 RPM	200 Nm, 6000 RPM
CF engine peak efficiency operating point	300 Nm, 3000 RPM	500 Nm, 1000 RPM

Table E.4: Considered component sets for the MHPS component selection scenario

From Table E.4, it can be seen that the two component sets offer quite different performance characteristics despite identical high-level performance. Component set 1 has superior dynamic performance (thrust and power split rates of change) to component set 2. On the other hand, component set 2 has a CF engine and EM whose peak efficiency points are far from each other, while component set 1's peak efficiency points are close to one another. Therefore component set 1 can respond to operating point changes quicker than component set 2 while component set 2 has greater potential for efficiency map collaboration.

To determine which component set to integrate into the sized large UAV, each of the component sets have to be input into the framework for energy management policy determination. In this case, the component set characteristics would be input into the DP framework along with the mission of interest, as described in Chapter

5 individually and the energy management policies would be compared. The policy with the lowest fuel consumption (or other performance metric of interest) would be chosen for integration with the corresponding component set. For example, if the energy management policy for component set 1 consumes 50 kg of fuel while the policy for component set 2 consumes 45 kg of fuel, then component set 2 would be chosen for integration. Additionally, it could be assumed that dynamic performance is not as important as efficiency map collaboration for the mission considered. A similar and opposite conclusion could be reached if the results were reversed.

Bibliography

[1] http://i385.photobucket.com/albums/oo291/tkaald/Cdi%20Engine%20and%20Gearbox/cutcdi.jpg. Accessed: 2018-10-03.

[2] Vahana. https://www.airbus-sv.com/projects/1. Accessed: 2018-10-03.

[3] Zunum aero aircraft, 2018.

[4] Aaron D. Anderson, Nathaniel J. Renner, Yuyao Wang, Shivang Agrawal, Samith Sirimanna, Dongsu Lee, Arijit Banerjee, Kiruba Haran, and James L. Felder. System weight comparison of electric machine topologies for electric aircraft propulsion. *2018 AIAA/IEEE Electric Aircraft Topologies Symposium*, 2018.

[5] Dimitri P. Bertsekas. *Dynamic Programming and Optimal Control.* Athena Scientific, 4th edition, 2017.

[6] Marty K. Bradley and Christopher K. Droney. Subsonic ultra green aircraft research. 2015.

[7] Benjamin J. Brelje and Joaquim R.R.A. Martins. Electric, hybrid, and turboelectric fixed-wing aircraft: A review of concepts, models, and design approaches. *Progress in Aerospace Sciences*, 2018.

[8] Peter G. Bruce, Stefan A. Freunberger, Laurence J. Hardwick, and Jean-Marie Tarascon. Li–o2 and li–s batteries with high energy storage. *Nature Materials*, 11:19 EP –, 12 2011.

[9] Nicholas Cumpsty. *Jet Propulsion: A Simple Guide to the Aerodynamic and Thermodynamic Design and Performance of Jet Engines.* Cambridge University Press, 2 edition, 2003.

[10] Kristen P. Duffy and Ralph H. Jansen. Turboelectric and hybrid electric aircraft drive key performance parameters. *2018 AIAA/IEEE Electric Aircraft Technologies Symposium*, 2018.

[11] Mehrdad Ehsani, Yimin Gao, Stefano Longo, and Kambiz Ebrahimi. *Modern Electric, Hybrid Electric, and Fuel Cell Vehicles.* CRC Press, 3 edition, 2018.

[12] D. Felix Finger, Carsten Braun, and Cees Bil. An initial sizing methodology for hybrid-electric light aircraft. *2018 Aviation Technology, Integration, and Operations Conference*, 2018.

[13] Steven Fletcher, Marie-Claire Flynn, Catherine E. Jones, and Patrick J. Norman. Hybrid electric aircraft: state of the art and key electrical system challenges. *The Transportation Electrification eNewsletter*, 2016.

[14] William J. Fredericks, Mark D. Moore, and Ronald C. Busan. Benefits of hybrid-electric propulsion to achieve 4x increase in cruise efficiency for a vtol aircraft. 2014.

[15] Airbus Group. E-fan: The new way to fly. Brochure, 2015.

[16] D.K. Hall, E.M. Greitzer, A.P. Dowdle, J.J. Gonzalez, W.W. Hoburg, J.H. Lang, J.S. Sabnis, Z.S. Spakovszky, B. Yutko, C. Courtin, W. Thalheimer, L. Trollinger, J. Tylko, N. Varney, A. Uranga, S. Byahut, and M. Kruger. Feasibility of electrified propulsion for ultra-efficient commercial aircraft. 2018.

[17] Frederick G. Harmon, Andrew A. Frank, and Jean-Jacques Chattot. Conceptual design and simulation of a small hybrid-electric unmanned aerial vehicle. *Journal of Aircraft*, 43:1490–1498, 2006.

[18] Philip Hill and Carl Peterson. *Mechanics and Thermodynamics of Propulsion.* Addison-Wesley Publishing Company, 2 edition, 1992.

[19] T. Hutchinson, S. Burgess, and G. Herrmann. Conceptual hybrid-electric powertrain architectures: Applying empirical design data to life cycle assessment and whole-life cost analysis. *Applied Energy*, 119:314–329, 2014.

[20] Ralph H. Jansen, Cheryl Bowman, Jankovsky Amy, Rodger Dyson, and James Felder. Overview of nasa electrified aircraft propulsion research for large subsonic transports. *53rd AIAA/SAE/ASEE Joint Propulsion Conference*, 2017.

[21] Kokam. Kokam aviation/uav battery pack. http://kokam.com/module-aviation-uav/. Accessed: 2018-10-03.

[22] Jonas Ludowicy, René Rings, Dominik Felix Finger, and Carsten Braun. Sizing studies of light aircraft with serial hybrid propulsion systems. Presented at DLRK 2018, 2018.

[23] John M. Miller. Electric motor research and development. 2013 U.S. DOE Hydrogen and Fuel Cells Program and Vehicle Technologies Program Annual Merit Review and Peer Evaluation Meeting, 2013.

[24] Ajay Misra. Technical challenges and barriers affecting turbo-electric and hybrid electric aircraft propulsion. Keynote presentation at ENERGYTECH 2017 conference, 2017.

[25] U.S Department of Defense. Unmanned aircraft system airspace integration plan. 2011.

[26] P. Panagiotou, I. Tsavlidis, and K. Yakinthos. Conceptual design of a hybrid solar MALE UAV. *Aerospace Science and Technology*, 53:207–219, 2016.

[27] Clément Pornet. *Conceptual Design Methods for Sizing and Performance of Hybrid-Electric Transport Aircraft.* PhD thesis, Tèchnical University of Munich, 2018.

[28] Clement Pornet, C. Gologan, P.C. Vratny, A. Seitz, O. Schmitz, A. T. Isikveren, and M. Hornung. Methodology for sizing and performance assessment of hybrid energy aircraft. *Journal of Aircraft*, 52:1–12, 2014.

[29] Clement Pornet and A. T. Isikveren. Conceptual design of hybrid-electric transport aircraft. *Progress in Aerospace Science Technology*, 79:114–135, 2015.

[30] Martin L. Puterman. *Markov Decision Processes: Discrete Stochastic Dynamic Programming.* John Wiley & Sons, Inc., New York, NY, USA, 1st edition, 1994.

[31] Carlo E.D. Riboldi. An optimal approach to the preliminary design of small hybrid-electric aircraft. *Aerospace Science and Technology*, 81:14–31, 2018.

[32] A.G. Siemens. Extra 330le. https://www.siemens.com/press/pool/de/events/2016/corporate/2016-12-innovation/inno2016-aerobatic-airplane-e.pdf, 2016.

[33] Jacob Sliwinski, Alessandro Gardi, Matthew Marino, and Roberto Sabatini. Hybrid-electric propulsion integration in unmanned aircraft. *Energy*, 140:1407–1416, 2017.

[34] Alex M. Stoll, JoeBen Bevirt, Mark D. Moore, William J. Fredericks, and Nicholas K. Borer. Drag reduction through distributed propulsion. *14th AIAA Aviation Technology, Integration, and Operations Conference*, 2014.

[35] Mark Voskuijl, Joris van Bogaert, and Arvind G. Rao. Analysis and design of hybrid electric regional turboprop aircraft. *CEAS Aeronaut Journal*, 2017.

[36] YASA. Yasa p400 r series. https://www.yasa.com/yasa-p400/. Accessed: 2018-10-03.

[37] YASA. Yasa p400 r series. https://www.yasa.com/controllers/. Accessed: 2018-10-03.